Chair of Astronautics
Prof. Prof. h.c. Dr. Dr. h.c.
Ulrich Walter

Semesterarbeit

Examination of Interference between Hypersen HPS-3D160 LiDAR and Intel RealSense D435 Stereo Depth Camera in the RACOON-Laboratory

SA-2020-06

Author:
Daniel Faust

Supervisor: Dipl.-Ing. Martin Dziura
Chair of Astronautics
Technische Universität München

Acknowledgments

First of all, I want to thank my supervisor, Dipl.-Ing. Martin Dziura for his help and support throughout my working on this thesis. I want to thank him for all the feedback during the experiments and writing process.

Additionally, I want to thank my friends and family, who supported me during the months it took to work on this thesis. Thank you for listening, giving constructive feedback and all your comments on the content composition and phrasing.

Abstract

In this thesis the interferences between two depth cameras used in the RACOON-Laboratory, located at the Technical University in Munich are examined. The Intel RealSense D435 stereo camera and the Hypersen HPS-3D160 solid state LiDAR.

An analytical, followed by an experimental examination is done. The focus is put on the effects resulting from the laser pattern projector in the stereo camera and laser flash from the LiDAR system, both working with the same wavelength.

The experimental part examines multiple combinations of the camera's parameters. Therefore, the operating modes of the two cameras as well as different ambient conditions inside the laboratory are varied. The main focus is laid on the RealSense projector power and the LiDAR's operating modes. With each combination a short recording is done. The fill rate of the recordings, as well as the standard deviation are used as metrics that help to quantify the interferences. Additionally, recordings are done with a polarization filter in front of the cameras.

The results show that for both cameras interferences are present. The influence on the RealSense is of a supporting character, negative effects cannot be seen. The influence on the LiDAR is more difficult to classify, but very small, presumably negligible. The filter mainly reduces the performance of the LiDAR and is therefore not considered useful.

As a side effect the influences of the different parameters on the recordings can be seen from the created figures as well and therefore help to understand both systems.

Contents

List of Figures

List of Tables

Acronyms

3-D three dimensional

ADR Active Debris Removal

API Application Programming Interface

ASIC Application-specific Integrated Circuit

CMOS Complementary metal-oxide semiconductor

DoF Degrees of Freedom

FMCW Frequency Modulated Continous Wave

FOV Field of View

fps Frames per Second

GEO Geostationary Orbit

GPIO General Pupose Input Output

GUI Graphical User Interface

HD High Definition

HDR High Dynamic Range

IR infrared

LEO Low Earth Orbit

LiDAR Light Detection And Ranging

MEMS Microelectromechanical Systems

MLI Multi Layer Insulation

OOS On-Orbit Servicing

OPA Optical Phased Arrays

PIC Photonics Integrated Circuits

RACOON-Lab Real-Time Attitude Control and On-Orbit Navigation Laboratory

RADAR Radio detection and ranging

ROI Region of Interest

SDK System Development Kit

ToF Time of Flight

TUM Technical University of Munich

USB Universal Standard Bus

VCSEL Vertical Cavity Surface Emitting Laser

VGA Video Graphics Array

1 Introduction

1.1 Motivation

With the start of the first space flights, the first artificial objects began to stay in space. New rocket launches bring new satellites, but also discarded rocket stages or fairing. And over time, the satellites reach their end of service. Now they are either disposed, Geostationary Orbit (GEO) satellites in a satellite graveyard orbit which is higher than the GEO, Low Earth Orbit (LEO) satellites get lowered in an orbit where they burn up in the atmosphere. Or, especially early launched and damaged satellites, they stay where they are. But the latter, together with discarded rocket parts, altogether called space debris, bear a rising risk. They can collide and thereby produce new, smaller debris which in turn can hit other operational satellites. But also functioning satellites can collide and produce debris. So, by now, about 25 000 objects, cataloged by space surveillance networks are up in space, endangering satellites [1]. Estimations by statistical models even come to almost 129 million objects between 1 mm and 10 cm [2]. And their number is rising, which can be seen in figure 1–1, showing the evolution since 1960.

This increasing number of operational satellites on the one hand and space debris on the other lead to the task, to think about possibilities and solutions for Active Debris Removal (ADR). One concept is to send special Servicer satellites in space that can connect to damaged satellites. As these damaged satellites often have no working control link to the ground anymore, one of the challenges is, to dock the Servicer to the target in order to be able to move or collect the damaged satellite. Another idea are service missions, called On-Orbit Servicing (OOS), that can repair damaged satellites or refill consumables like fuel or cooling liquids to extend their lifetime.

Both applications have in common, that they need the satellite to navigate by itself in space and perform proximity operations, that can't be controlled by the ground station in real time due to the signal delay. The Real-Time Attitude Control and On-Orbit Navigation Laboratory (RACOON-Lab), located at the chair of astronautics at the Technical University of Munich (TUM) simulates this scenario and offers a hardware in the loop simulator to test sensors for proximity operations in space and simulate various aspects.

Target of the thesis

In order to be able to determine the exact attitude of the target satellite, sensors for depth measurements are required and they need to work constantly accurate and precise. The target of this thesis is to examine the interference between the two depth measurement sensors Hypersen HPS-3D160 and Intel RealSense D435, which were already implemented in the Servicer structure of the RACOON-Lab in a preceding work [3]. In recordings of the RealSense, collected during this thesis, a flickering light could

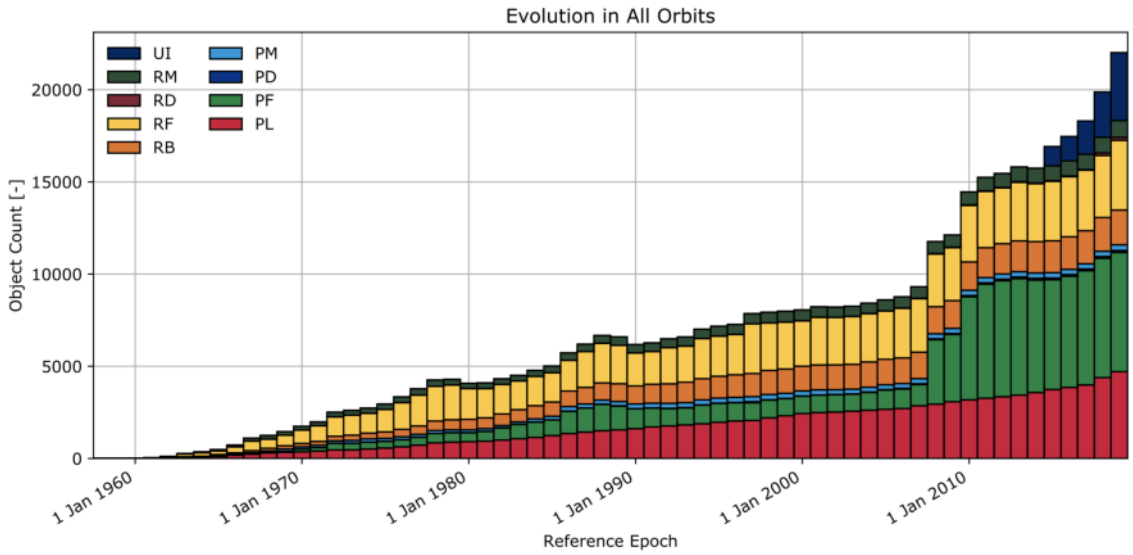

Fig. 1–1: Evolution of space debris since 1960 in all geocentric orbits [1]

be observed. The observation led to this thesis, as an examination and classification of the interference between the two sensors is important for the optimization of the path tracking capabilities. As the algorithms that are used for visual odometry use the depth pictures calculated by the cameras and do not calculate them by themselves from the recorded pictures, the general attention is on the produced depth pictures. The objective is to identify interference and their effects on the quality of the depth images. It does not consist in determining the effects on path tracking. Additionally, approaches are presented to minimize the effects of interference on the depth images.

1.2 Methodology

In order to have a red line in this work, the most promising theories for interference are collected at this place. In the following, first an overview about the used technology is given in chapter 2, followed by an analytical examination of the theories in chapter 3. In chapter 4 experiments are made, based on this theories and the theoretical examination.

1. The RealSense has influence on the LiDAR
   (a) The LiDAR recognizes the pattern of the RealSense
      i. The LiDAR sensor misinterprets the pattern of the RealSense as reflected light
2. The LiDAR has influence on the RealSense
   (a) The visibility of the supporting pattern of the RealSense decreases because of the bright flashes of the LiDAR
   (b) The performance of the RealSense improves due to the additional light from the Light Detection And Ranging (LiDAR) flash
   (c) The performance of the RealSense algorithm decreases

2 State of Technology

In order to receive depth information of a scene, a range of potential technologies are available. A general distinction can be made between contact and contactless techniques. Another possibility for classification is to differentiate between active and passive sensors [4]. Both of the two sensor technologies used for depth measurements in the RACOON-Lab and examined in this thesis are contactless measurement methods, so they are in no mechanical contact with the probe during measurements.

The first sensor, the D435 is a stereo infrared camera produced by Intel. It uses triangulation to calculate the depth information of the target. With one limitation, the RealSense can be classified as a passive sensor. Further information to the technology can be found in section 2.1. The second sensor, a Hypersen HPS-3D160, uses the flash LiDAR technology according to the manufacturer. In general LiDAR sensors are active sensor technologies, that use light to measure distances and either the Time of Flight (ToF) or the Frequency Modulated Continous Wave (FMCW) principle is used. Further information to this technology can be found in section 2.2.

2.1 Stereo Vision

Stereo Cameras produce depth pictures using triangulation. A stereo vision system consists of 2 identical cameras with a known baseline. As an object or a point on a structure in some distance to the camera has different positions on the two imagers, separated by the disparity d, the depth c can be calculated by Eq. 2–1 using the baseline b and the focal length f[5].

$$c = \frac{f * b}{d} \tag{2–1}$$

Benefit of the technology is its passive nature. No active element is needed, as long as the object of interest is illuminated. In order to be able to measure the disparity of a point on the two pictures, the system has to compare both pictures and identify matching points[5]. Cameras are usually in the visible color spectrum, but systems with infrared cameras, as used in this thesis, exist as well. Drawbacks occur, when objects contain texture-less surfaces. In this case, issues may emerge in the matching process. Further difficulties arise from the necessary processor power needed for the matching process while real time requirements must be met, and the necessary illumination. In order to improve the matching, in some cases pattern projectors are used, that can create a pattern on texture-less surfaces and thus help the algorithms to find corresponding points[5, 6].

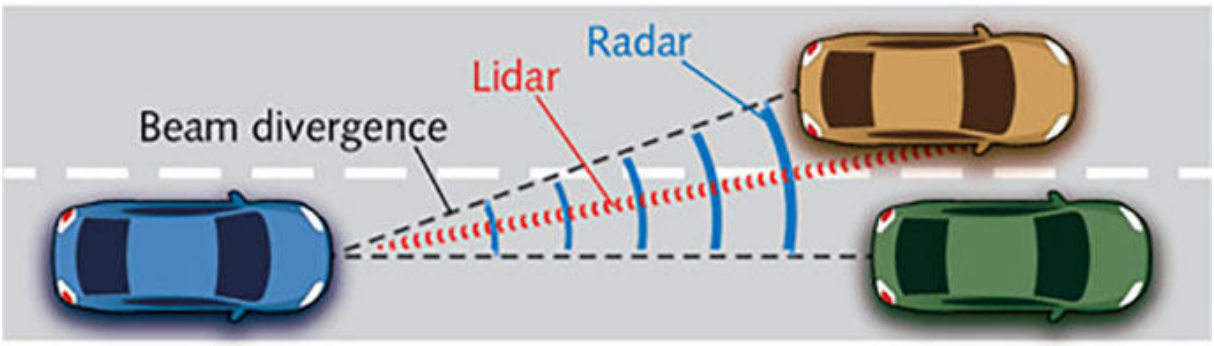

Fig. 2–1: Differences in the beam width between LiDAR and RADAR. Due to the shorter wave lengths of electromagnetic waves in the visible light spectrum, compared to the ones in the radio spectrum, the beam divergence is smaller and thus can display more details of an object [7].

2.2 Light Detection and Ranging (LiDAR)

LiDAR is the name for a group of technologies, including pulsed, flash and FMCW LiDAR. They have in common, to use light to measure the distance to an object, the first two using the ToF principle. In recent years, the further and new development of LiDAR technologies has been strongly promoted, as there is a great demand for solid state LiDAR especially in the automotive market. LiDAR is popular, as it provides a way to receive more detailed depth pictures in contrast to the widely used Radio detection and ranging (RADAR), since the shorter wavelengths allow more detailed measurements[7]. Please also see figure 2–1 for further explanation. And as LiDAR emits the measurement signal by itself, it also needs no foreign illumination of the scene, in contrast to Stereo Vision approaches.

2.2.1 Time of flight (ToF) LiDAR

The most popular form today is the pulsed LiDAR, using the ToF principle, where the time between emitting a laser pulse and recognizing its reflection at the sensor is measured. When combined with the speed of light, the distance between the sensor and the reflecting object can be calculated with Eq. 2–2, where d is the distance between the sensor and the object, t, the time between emission and detection and c the speed of light.

$$d = \frac{t * c}{2} \tag{2–2}$$

LiDAR technology has several advantages over stereo cameras. They include a lower computational effort, better scalability and less artifacts. Drawbacks are its deteriorating performance under some ambient light conditions[4]. If the laser uses a wave

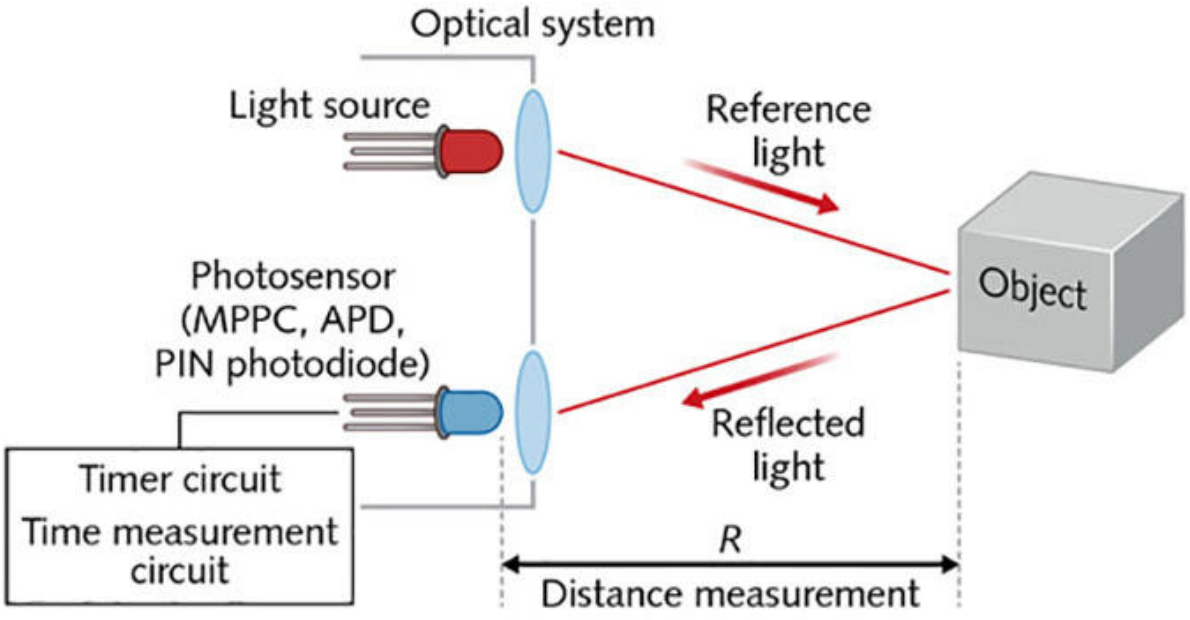

Fig. 2–2: The basic setup for a ToF LiDAR system [7]

length, also present in the ambient light, the sensor can't determine if the recognized light is originating from the LiDAR or the environment. In figure 2–2 the basic working principle of a ToF LiDAR can be seen.

The technology alone is one dimensional, as it can only emit the pulse in one direction. To receive a three dimensional (3-D) depth picture, multiple approaches exist. In the following a brief overview over the technologies available is given.

Mechanical Beam Steering

The by now most used form to generate a 3-D picture is a mechanical beam steering. The laser beam is sequentially moved to multiple positions by a mirror, to gain a grid of depth points that can together build a depth picture. In order to speed up this process, a structure of multiple sensors working together can be used [8]. Since the mechanics are physically limited in their speed and additionally prone to defects, alternatives are researched.

Solid State Beam Steering

Recently, research on distance sensors has increasingly focused on solid state LiDAR systems, as these are considered indispensable for autonomous driving. This is especially due to the ability of LiDAR to produce accurate and detailed depth images without ambient light. Only the poor robustness, the size, the high cost and low scanning speed of mechanical ToF LiDAR systems are a problem, as such sensors are difficult to install in automobiles. Solid state systems should solve these problems. Without mechanical

parts, the robustness is increased, the size and costs can be reduced and scanning frequencies increased[9, 10]. Among others, approaches with Photonics Integrated Circuits (PIC) include Optical Phased Arrays (OPA) [11] and Microelectromechanical Systems (MEMS) [12]. Another solid state solution is the Flash LiDAR, which does not use beam steering, but a single laser flash. More details about this technology can be found in section 2.2.2.

2.2.2 Flash LiDAR

While most LiDAR sensors, whether ToF or FMCW, use beam steering to create a point cloud, the flash LiDAR uses a single strong pulse of light to illuminate the entire scene of interest. The reflected light is then detected by a sensor that contains numerous pixels. This way the whole depth image can be obtained at once. The achievable Field of View (FOV) and resolution depends, comparable to common digital photo sensors in digital cameras, on the number of pixels in the sensor and the optics in front of it. Although with flash LiDAR the maximum illumination time per pixel is higher at the same frame rate because all pixels are illuminated at once, beam steering LiDAR sensors are more common at larger distances. This is due to the fact that here the whole available power of the laser can be used for each measurement point, whereas a Flash LiDAR splits it up to all points and thus a safe data set can be obtained.[10].

2.2.3 Frequency Modulated Continuous Wave (FMCW) LiDAR

Another LiDAR PIC technology, the FMCW doesn't rely on the intensity of light pulses, but instead on the wave length of the light. Light is emitted with a linear changing frequency and the reflected signals are combined with the ones emitted at this time. The frequency difference can than be deduced from the resulting pattern [10]. The beam can be moved with the same technologies described for ToF sensors.

2.3 State of Research

In this chapter the RACOON-Lab is described in detail, including the implemented depth sensors used in this thesis. Further, research in LiDAR and stereo camera sensors is presented, to give a short overview over technology and available sensors apart from the ones used in this thesis.

2.3.1 RACOON-Laboratory

The RACOON-Lab was developed, in order to be able to simulate the complete link between the operator on earth and the satellite with its sensors in space. To simulate the human-machine interface, a control station is available.

The orbit simulator mainly consists of three main parts. The Servicer, Target and Light source simulator. Black curtains are attached to the walls, to reduce background illumination through reflections. The light source simulator is made out of a sun simulator and a earth albedo simulator. Both use a metal halide lamp, that can widely simulate the original light spectrum [13, 14]. The light sources are placed on a rail, that encloses the two satellites in its center, visible in fig. 2–3.

The **Servicer satellite** is a structure, that can hold multiple instruments. The main objective of the RACOON-Lab is the development and evaluation of the sensors mounted here in a space environment [15]. It provides 6 Degrees of Freedom (DoF).

The **Target satellite** simulates a damaged or uncontrollable satellite. It is a model of a satellite, covered with reflective material, simulating Multi Layer Insulation (MLI). It has 5 DoF [15].

The depth sensors in the RACOON-Lab are used for visual odometry. Different types of sensors are tested and compared. In previous works multiple sensors, including the Microsoft Kinect, LIDAR Hokuyo UST-2, Flir Bumblebee 2 or Stereo Labs ZED were installed [3, 15]. The two sensors installed at the time of this thesis are the Intel RealSense D435 and Hypersen HPS-3D160. Both were installed in the master thesis from Lucio Franceschini [3]. In this work a complete implementation in the local system was carried out. Both sensors can be controlled via a single configuration file in conjunction with applications performing the recording, transmission, storage and evaluation of the data. The collected data is stored in a HDF5 file format.

2.3.2 Intel RealSense D435 Stereo Infrared Camera

The RealSense D435 Stereo Camera, developed by Intel uses two OmniVision OV9282 infrared sensors and a OmniVision OV2740 color sensor. To improve the depth picture quality, an optional infrared Vertical Cavity Surface Emitting Laser (VCSEL) laser pattern projector can be switched on when required [16]. The intensity of the projector can be changed, in order to avoid problems as saturated laser points or bad depth pictures caused by weak laser points [17]. Its pattern scheme is shown in figure 2–4.

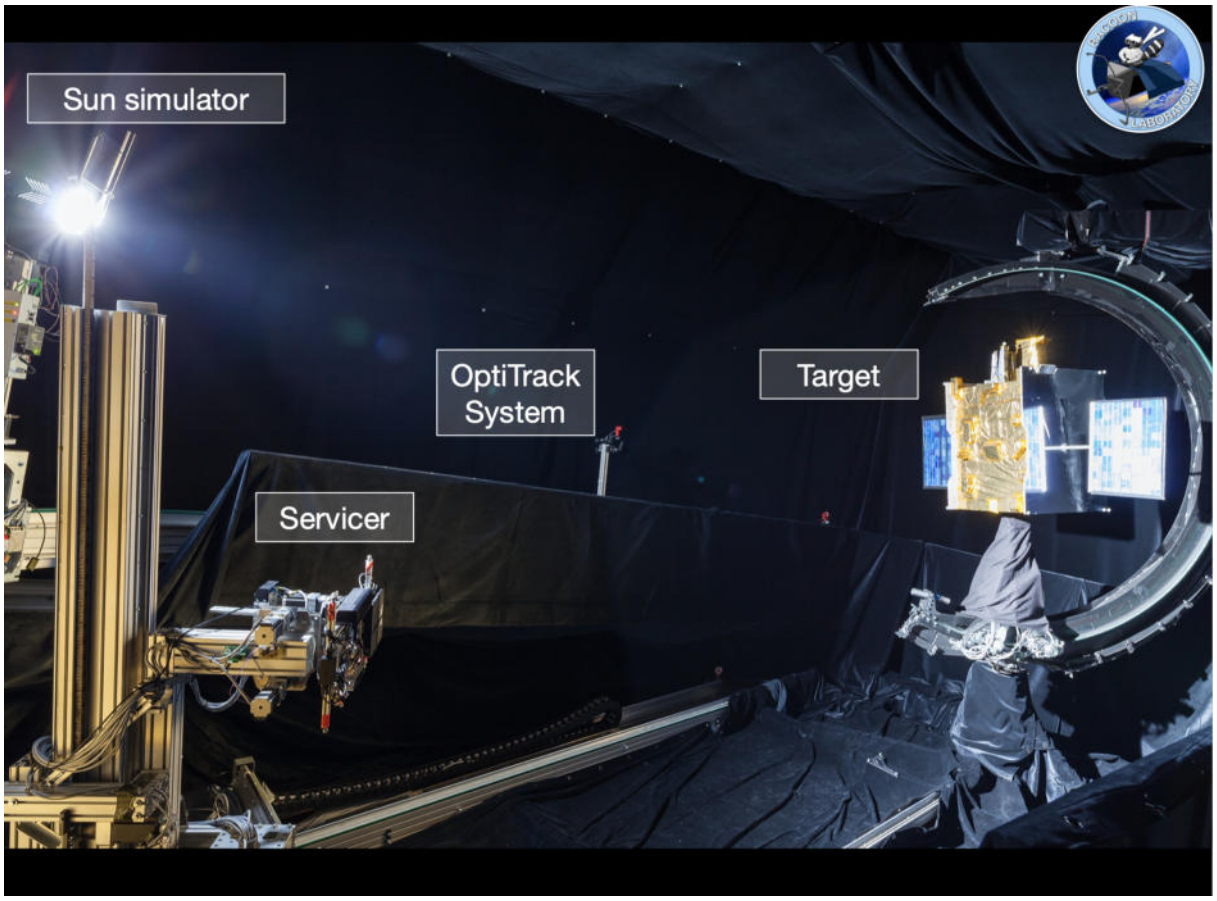

Fig. 2–3: Picture of the RACOON-Lab. On the left the Servicer can be seen, including the mounted sensors. On the right the Target is located, covered with highly reflective foil. In the left upper corner, the sun simulator is located, which can be moved on a rail system around the two satellites. Additionally an optical tracking system is installed, that uses white ball markers for tracking [15].

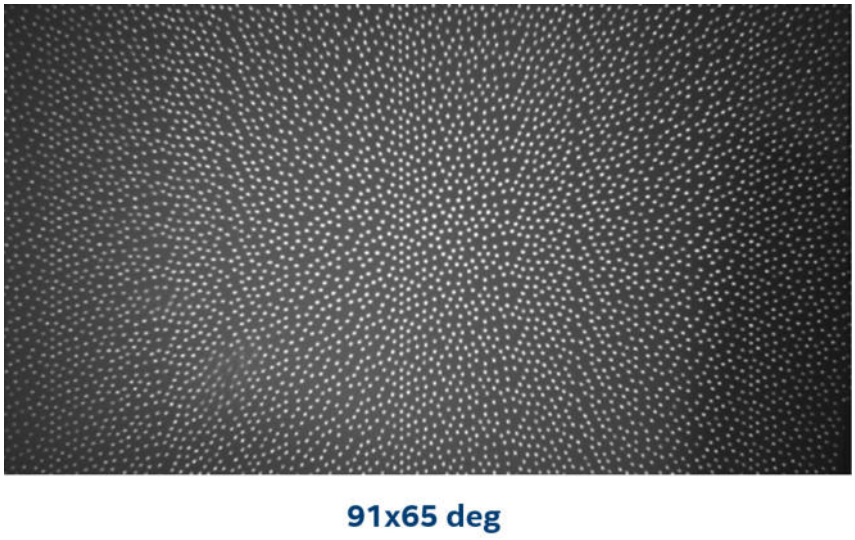

Fig. 2–4: Shape of the pattern of the RealSense D435 camera [17]

Tab. 2–1: Selected properties of the RealSense D435[16]

Parameter	Property
IR Projector Wave Length	850 nm ± 10 nm @ 20 degree Celsius
IR Projector Power	360 mW average 4.25 W peak
IR Projector Pattern Type	Static
Imager Shutter Type	Global Shutter
Maximum FPS	90 FPS
Maximum FOV (H/V/D) at 2 m with HD	86/57/94
Minimum measurebale depth (Resolution: 424x240)	105 mm

The design of the sensor is shown in figure 2–5, which displays the front view. In table 2–1 selected properties of the Camera are collected. A full list can be found in the datasheet. The FOV depends on weather Video Graphics Array (VGA) or High Definition (HD) output is used, while HD provides a bigger one. The minimum measurable depth on the resolution setting, increasing with the resolution. The Frames per Second (fps) decrease with the resolution [16].

During the recording, the D430 module with its D4 vision processor unit, processes the collected infrared pictures in real time and calculates the depth map. In the following, all data, including the pictures of the infrared and color sensors, as well as the calculated depth picture are transferred via a Universal Standard Bus (USB) 3.1 Gen. 1 port with a USB Type-C connector and cable. Using the provided System Development Kit (SDK), various parameters for the depth module can be set. Among others the exposure time,

Fig. 2–5: Front view of the Intel RealSense D435 Stereo Camera. In the very left of the picture, the 'right' infrared sensor, as seen from the sight of the camera is located, followed by the infrared pattern projector, the 'left' infrared sensor and on the very right the RGB module. The center of the reference system used in the depth map is located at left infrared sensor [18].

power of the infrared (IR) pattern projector, digital gain and a Region of Interest (ROI). Instead of setting this parameters manually, automatic modes can be used. Additionally parameters for the color module can be set as well. Multiple RealSense cameras can be used together and be synchronized via a hardware interface [16, 19]. With the available software, the video stream with all collected images can be reviewed.

2.3.3 Hypersen HPS-3D160 Infrared LiDAR

The HPS-3D160 uses a flash[1] infrared LiDAR developed by the Chinese company Hypersen. It uses a 850 nm VCSEL emitter and a Complementary metal-oxide semiconductor (CMOS) photosensitive sensor[20]. It can be seen in figure 2–6, it's most important parameters are given in table 2–2. The maximum fps can be increased when a ROI is set. Multiple ROI can be set in parallel. A SDK is available, that provides an Application Programming Interface (API) and Graphical User Interface (GUI). Besides a standard operating mode, where the integration time can be set manually, various High Dynamic Range (HDR) modes are available. The AUTO-HDR mode, where the integration time is adjusted automatically, "based on the amplitude of the signal in the current measurement environment" [21], the SUPER-HDR mode, that combines a specified number of frames while minding a set maximum total integration time and a SIMPLE-HDR mode, that combines two frames with different integration times that can be set [21]. Similar to the RealSense system, a synchronized measurement can be performed via General Pupose Input Output (GPIO) pins.

[1] According to mail correspondence with the manufacturer Hypersen

Fig. 2–6: Lateral front view of the Hypersen HPS-3D160 [22].

Tab. 2–2: Selected properties of the HPS-3D160[20]

Parameter	Property
Infrared VCSEL emitter	850 nm
Power consumption of the IR emitter	4 W
Maximum Power Consumption	6 W
Quiescent Power Consumption	0.7 W peak
Measurable Distance Range	0.25-12 m on a 90% reflective white target
Maximum FPS	35 fps
Resolution	160 $\times$ 60 px
FOV	76 $\times$ 32°

2.3.4 Research in Stereo Vision

In the field of Stereo Vision the main research at the moment focuses on the development of new algorithms. Especially the matching process is difficult and algorithms with good performance are an important part of the product. Thus, a lot of effort is spend on developing better performing matching processes [23]. Other problems occurring with Stereo Vision are falsely interpreted images. This includes false boundaries, reflection issues and identification of obstacles [23]. False boundaries occur, when the real boundaries can't be seen from the view point of the sensors. Alternatively reflection issues can lead to false boundaries as well, when a reflection over a flat surface is interpreted as a boundary by the algorithm. In this case a pattern projector can be helpful. The identification of obstacles can lead to problems, when a shadow is falsely interpreted as an obstacle or the other way round [23].

Common manufacturers for Stereo Vision sensors are Stereolabs, Intel or FLIR.

2.3.5 Research in LiDARs

Apart from improving the performance of existing cameras, the main focus on research in the LiDAR field at this time lays on the development of a solid state camera, that is cheap, fast and robust enough, to be used in cars as a standard.

As the potential market for LiDAR sensors is big, a couple of companies develop new approaches. The company Ouster in the USA develops solutions using their own Multi-Beam Flash LiDAR technology. It works with the 850 nm wavelength, despite the high amount of ambient light with this wavelength [24].

The L515 LiDAR is a camera developed by Intel. It is a solid state LiDAR , working with a MEMS. It is compatible with the same SDK, as the RealSense D435, used in this thesis [25].

2.3.6 Research in depth sensor interference

Research in the development of new sensors, especially LiDAR , and of new data processing algorithms, especially matching algorithms, has been done a lot in the past and present. But compared to this, little research has been done in the examination of interference between multiple depth sensors. Some authors analyze the accuracy of single sensors, but mutual influence is still little researched.

2.3.6.1 Interference between multiple Kinect 1 cameras

The Kinect cameras in their first edition use structured light sensors for depth measurement. The Kinect combines a infrared light emitter, that sends out a pattern and a infrared and RGB image sensor. As the pattern is known exactly, changes caused by the examined scene are used for a depth calculation. This principle leads to problems

with the use of multiple cameras in parallel, as the cameras can no longer identify their pattern between the others.

Martín et al. [26] examined interference between two Microsoft Kinect cameras. Additionally, Berger et al. [27] tried to combine multiple Kinect cameras and therefore tried to reduce interference between them. In order to achieve this, mechanical shutters are mounted in front of the cameras.

3 Analytical Examination

This chapter discusses in an analytical manner the influences of the two depth sensors on each other on the basis of the previously defined hypotheses. Different aspects important for interference and their influence on the hypotheses from section 1.2 are discussed. First general aspects of interest for interference are analyzed in section 3.1, followed by the individual hypothesis in section 3.2.

3.1 General aspects

3.1.1 Laser wave length

If one wants to suppress light from another source in order to provide influences one could use different filters that only let pass the light originating itself. One of these filters is a spectral filter, that only lets pass a small spectrum of wave lengths.

The wave length of both the two lasers used in the sensors, the pattern projector of the RealSense stereo depth camera and the flash diodes of the HPS-3D160 however work with the same wave length. Therefore, both sensors are theoretically able to detect the emitted laser light of the respective other.

And this also makes it impossible to use a spectral filter, as this would suppress the own emissions as well.

3.1.2 Laser polarization

Another idea to prevent interference is the polarization of the laser sources. In general, laser light is polarized, so this approach seems promising. The polarization direction of each laser emitter could be identified and a polarization filter could be mounted in front of the respective image sensors. This way, only the associated sensors could detect the light emitted by its own laser.

But two problems occur with this approach. First, VCSEL laser diodes, as they are used in both laser emitters, have no specific polarization direction. They only have two preferred but not exclusive ones. The polarization state is changing over time [28]. Regarding this, a single polarization direction can not be determined for both lasers. And furthermore the polarization state can change, when the laser is reflected at the examined object. This process is dependent on the angle of incidence.

However, a polarization could help, that is placed in front of both cameras. As well the emitter section as the sensors would have to be covered. The emitted light of one sensor would get polarized in one direction and the light of the other one orthogonal to that. This way only the light with the same polarization of the emitted one could be detected. External sources would get suppressed and especially no light from the

respective other camera would be recognized. However some problems occur. When the light gets reflected its polarization direction can change and therefore reduce its effectiveness.

3.1.3 Light intensity

In order to quantify the influence of one light emitter on the other, it is important to know the intensity of the light. It can be assumed, that the higher the intensity of an emitter, the bigger is its impact on a sensor. The about ten times higher laser power together with a smaller emitting FOV of the HPS-3D160 is leading to the assumption that the irradiance of the LiDAR laser is significantly higher, than the RealSense one. However, as the RealSense laser emits a structured pattern with about 5000 concentrated light dots [29], while the LiDAR is emitting a diffuse flash, a clear assumption is more difficult to make.

3.2 Analysis of the specific hypotheses

3.2.1 Hyp. 1: The RealSense has influence on the LiDAR

Both cameras use the same wave length for their emitting lasers, which leads to the assumption, that the LiDAR can theoretically be influenced by the RealSense. But this potential influence is only present, if the RealSense emits light. And this is only the case if the pattern projector of the RealSense is activated. In order to have an influence on the LiDAR however, the latter now also has to recognize the pattern at all. This in turn, leads to the hypothesis 1a.

3.2.1.1 Hyp. 1a: The LiDAR recognizes the pattern of the RealSense

A recognition of the pattern of the RealSense or parts of it by the CMOS sensor of the LiDAR is generally possible. The LiDAR sensor can recognize the pattern, if its light waves are first of all reflected by the examined object or surroundings. As both sensors are placed at the same place and aligned in the same direction, a direct projection of the pattern inside the LiDAR sensor is not possible. A reflection however can be considered as being very likely. To be recognized however, the light has to be strong enough even if it is reflected.

As it is not completely clear how the LiDAR works, an prediction if this scenario is likely is difficult to make.

3.2.2 Hyp. 2: The LiDAR has influence on the RealSense

Similar to Hyp. 1, an influence of the LiDAR on the RealSense is possible, due to the same operating wave length of the laser used. As the flash is active as long as the

LiDAR records depth data, influence in general is possible. And due to the non static nature of the flash an influence of the LiDAR on the RealSense is more likely than vice versa.

3.2.2.1 Hyp. 2a: The visibility of the supporting pattern of the RealSense decreases because of the bright flashes of the LiDAR

If the flash, emitted by the HPS-3D160, is strong enough to thin out the pattern of the RealSense or at least reduce its visibility, this can affect the matching improvements achieved with the pattern. But in order to thin out the pattern, the flash needs to be brighter than the latter. As stated above, this should only be the case, if the pattern is operated at a low intensity. Looking at the recordings from [3], especially in the ones without additional earth albedo light, a decreasing visibility of single laser dots on the satellite can be observed when the flash is emitted at the same time of the recorded image. This process is especially visible at the highly reflective parts of the satellite, covered with a MLI demonstrator. Parts with lower reflectivity show less various intensities of the pattern. An effect on the depth calculation can not be identified however without having a reference recording without the flashes of the LiDAR .

Additionally the polarization of the lasers can have an effect on the visibility of the pattern. If the two emitters and the corresponding image sensors are equipped with corresponding polarizing filters, the corresponding other camera's lasers could be suppressed.

3.2.2.2 Hyp. 2b: The performance of the RealSense improves due to the additional light from the LiDAR flash

As a stereo camera system needs ambient light to work the additional light of the LiDAR could also help the camera instead of having negative effects. Even though the RealSense can project a pattern when the conditions are bad, this can not really lighten the scene. Therefore the flashes of the LiDAR could especially be helpful in badly illuminated scenarios. This effect should increase with the relative amount of time the LiDAR flash is active. Therefore the SUPER-HDR mode with a high maximum integration time should have the biggest effect.

3.2.2.3 Hyp. 2c: The performance of the RealSense algorithm decreases

Having in mind the exposure setting of the RealSense, a varying illumination of the scene caused by the LiDAR flash could lead to a decrease in depth picture quality. To be able to perform the pixel matching process, the Application-specific Integrated Circuit (ASIC) running the matching algorithm needs sufficient image quality. The auto exposure mode tries to find the best exposure time in order to get an image with as much details and structure identifiable as possible. But with the flash occurring on single recorded pictures of the RealSense but not continuously due to different frame rates and drift between the recording times the exposure time can not be adapted

to meet the varying light conditions. This could lead to decreasing quality in at least some depth images. Using auto exposure settings the RealSense will try to meet both conditions by adapting the exposure to a value between the optimums of the two conditions. A manually set exposure time could at least prevent the latter problem, but not the main one.

4 Experimental Examination

In this chapter, a experimental examination of interferences is performed. First, in section 4.1 the used metric is introduced, followed by the experimental setup, which is presented in section 4.2. Multiple sequences with different camera settings are recorded, whereas both cameras are used within different ambient conditions and as well alone and together. How these recordings are executed is presented in section 4.3, followed by the processing of the received data in section 4.4.

After the main experiment, a brief examination of the LiDAR behavior is done in section 4.5 as the data of the main experiment showed unexpected results.

4.1 Metric

In order to be able to measure interference, a metric is needed. Therefore the Fill-Rate, Deviation from a mean value and the standard deviation is used.

4.1.1 Fill rate

The fill rate represents the number of valid pixels in a recorded and processed frame. Valid in this case means, that the pixels depth value is unequal to 0 in the RealSense recordings. In the LiDAR recordings, a value of 65500 or 65300 seem to mark invalid pixels. This however is only an assumption, as the datasheet and documentation do not provide further information to that topic.

Invalid pixels can be the result of numerous reasons, which prevent the camera system from calculating a depth value. This can be the missing ability for matching points in the RealSense or a insufficient light reflection for the LiDAR . Different settings can influence the fill rate directly, since they determine the confidence with which a pixel must be considered valid by the cameras algorithms.

However, the fill rate only provides information about the amount of collected data, not about its quality. To gain a brief overview about the quality of the data, the standard deviation is used as a second metric.

4.1.2 Standard Deviation

The standard deviation is used, to receive an overview over the variance of the depth values. The mean value used for its calculation is calculated from all recordings done for each camera.

It can show at which spots deviations occur and how many pixels have a deviation from the mean value and how big this is.

Tab. 4–1: Available Presets for the RealSense D435 [30]

Preset	Recommended Use Cases
High Density	Higher fill factor, sees more objects
Medium Density	Balance between Fill factor and accuracy
High Accuracy	High confidence threshold value of depth, lower fill factor
Hand	Good for hand tracking, gesture recognition, good edges
Default	Best visual appeal, clean edges, reduced point cloud spraying

4.2 Setup

4.2.1 Selection of parameters

Both cameras offer the possibility to individually set a number of parameters in order to adapt them to different application scenarios. In order to be able to identify and quantify influences of individual parameters on possible interferences afterwards, several parameters of both cameras are now selected. They are varied during the experiment. The remaining parameters remain constant during the whole experiment and are selected in a way that interferences are favored. A list of all selected parameters for both cameras can be found in table 4–2 and 4–3 at the end of the section.

RealSense

For the RealSense, there is principally a large number of different parameters available to configure its individual components, including the IR and color sensors, the depth calculation processor and the pattern projector. Only some of these parameters are described sufficiently in the documentation and intended to be modified by the end user. The remaining ones are not supposed to be set individually, rather than through a set of presets. For these presets, the values of the parameters are selected by Intel by machine learning in order to perform best under special conditions. A list of these presets can be found in 4–1. JSON-Files with the corresponding parameters are provided by Intel in order to allow further independent development and following an open source approach [30]. For this experiment however, only the $HighAccuracy$ and $HighDensity$ preset are used. The former provides a depth image with values that are as accurate and reliable as possible. The algorithm provides only those values for which it can prove the correctness of the calculation with high confidence. Data points, during whose calculation uncertainties occurred, are removed from the point cloud. The result is a depth picture with less data points than usual. The $HighDensity$ preset however, aims for a point cloud that includes as many data points as possible. The confidence threshold is therefore lower than for other presets.

Parameters, that can be set individually include the projector power, resolution of both depth and color sensors individually and frame rates. These parameters are described

in the documentation, intended to be modified by the user and are independent from the presets.

A second parameter, which is to be changed during the experiment besides the preset, is the power of the pattern projector. As mentioned before, the presence and intensity of the laser could have an influence on possible interferences. Therefore the power, which can be set to values between 0 and 360 mW is set to 0, 180 and 360 mW throughout the experiment. This allows to examine a principle influence and its extent.

As can be seen in the camera tests in [3], a resolution of 848 x 480 px provides the best performance in general, including the highest fill rate. A high fill rate in general is useful for a later examination as it can be an indicator for interference. This resolution setting also suits the recommendation from Intel in order to receive the best results for general purposes [30]. Therefore, this value is also used in this experiment. The exposure time is set automatically by the camera in order to allow adaptation to changing environmental conditions. Furthermore, to be representative the settings should represent a configuration that can be used for regular applications in the laboratory as well.The depth scale factor is set to a value of 0.0001 m^{-1}.

HPS-3D160

Unfortunately, the documentation of the Hypersen HPS-3D160 is not as detailed and comprehensive as the RealSense one. Therefore it is difficult to perform a proper selection of available parameters. The documentation is extended throughout the releases and new information is added from time to time. Parameters may thus be available in the future, even if this is not the case at the time this thesis is written.

Two of the available recording modes, the SUPER-HDR and SIMPLE-HDR mode combine multiple sequentially recorded frames. The first one to improve the depth quality of the background and the latter to set a range of measurement by setting a minimum and maximum integration time. A good depth quality of the background, however, is not important, actually even unwanted in this setup as the focus lays on the target and the background is designed to be as discrete as possible. On the other hand, a combination of multiple sequentially recorded frames could enlarge the effect of a potential interference. The possibility to set a minimum and maximum integration time though can help to eliminate false signal. But as a proof of interference is searched this is considered as not helpful for this experiment.

Having this in mind, the experiments are performed with two different recording modes: HDR Disabled and SUPER-HDR. The HDR Disabled mode is selected because it is the most comprehensible setting. It allows to set a fixed integration time. Therefore a fixed period of illumination of the laser can be expected here. The SUPER-HDR mode is selected, because it should provide a more varying illumination time of the laser. This is due to its working principle, as described in chapter 2.3.3.

However, as the documentation does not provide a clear description of neither the general working principle of the camera nor the meaning of the parameters, an addi-

Tab. 4–2: Chosen parameters for variation during the experiment

	Parameter	Value
RealSense:		
	Laser projector power	0/180/360 mW
	Preset	High Accuracy & High Density
HPS-3D160:		
	Integration time setting	SUPER-HDR/HDR Disable with 5 000 & 10 000 μs

Tab. 4–3: Chosen fixed parameters throughout the experiment

	Parameter	Value
RealSense:		
	Resolution (IR and color)	848 x 480
	Frame rate (IR and color)	30 fps
	Depth scale factor	0.0001 m^{-1}
	Exposure	Auto
HPS-3D160:		
	ROI	-
	Distance filter	Off

tional small experiment is done in section 4.5 in order to receive a brief overview of the camera's behavior in the two selected recording modes. A ROI is not set.

4.2.2 Laboratory

The position and orientation of the satellites are chosen in order to examine interference on different surfaces. Therefore the satellite is positioned in a way showing all kind of surfaces at once to the cameras, as can be seen in figure 4–1. The mounting of the cameras itself on the chaser satellite can be seen in figure 4–2.

The axes values of the laboratory are shown in table 4–4. The chaser and target satellite are kept in the same position throughout the whole experiment. As an interference of the cameras is most likely to occur without the sun or earth albedo simulator active, both are turned off for the first experiment. However, in order to improve the working conditions of the RealSense, the general lightning of the RACOON-Lab is activated, providing an ambient light.

Throughout the experiment the laboratory is set to three different states in order to examine the cameras in different ambient conditions. Therefore the lightning is varied

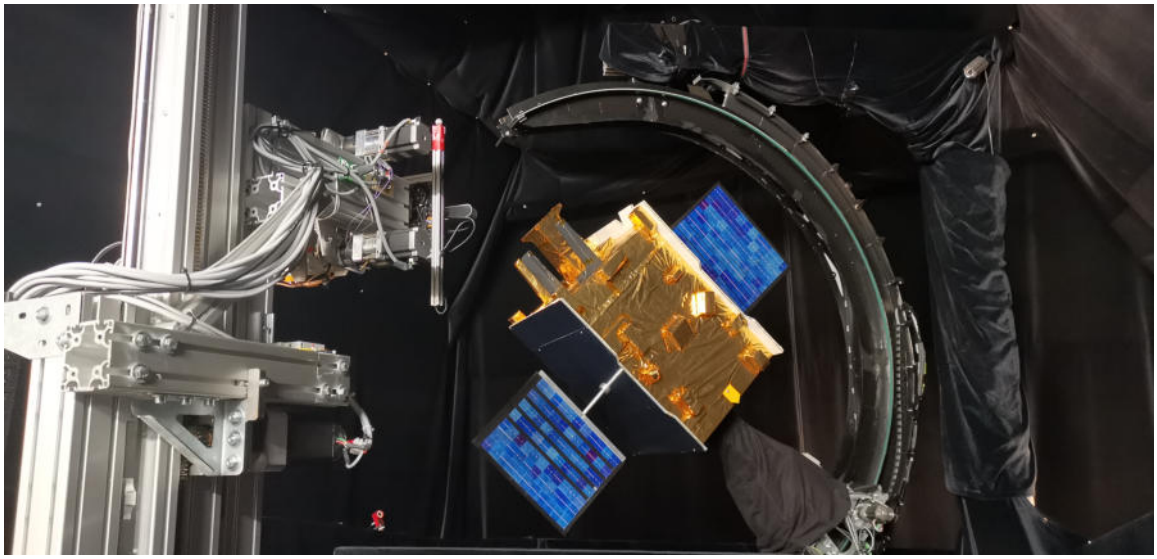

Fig. 4–1: **Position and orientation of the target and chaser satellite relative to each other. On the left the chaser structure with its cameras can be seen. The cameras point in direction of the target. The targets orientation is of a kind, that its different surface coatings are all pointing in the direction of the cameras at the same time.**

Fig. 4–2: **Mounting of the cameras on the chaser structure. Three cameras can be seen, including the RealSense at the bottom and the LiDAR at the right of the picture.**

Tab. 4–4: Axis settings of the laboratory

Axis	Designation	Value	Conversation Factor
0	Servicer Linear X	180 000 steps	85 600 steps/m
1	Servicer Linear Y	14 000 steps	85 600 steps/m
2	Servicer Rotation Z	-200 steps	24 430 steps/m
3	Servicer Linear Z	-190 000 steps	226 250 steps/m
4	Servicer Rotation Y	0 steps	24 430 steps/m
5	Servicer Rotation X	-000 steps	24 430 steps/m
6	Target C Arc Rotation Z	-19 548 steps	24 890 steps/rad
7	Target C Sled Y	150 000 steps	190 986 steps/rad
8	Target Head Rotation X	-5 500 steps	144 000 steps/m
9	Target Head Rotation Y	300 steps	24 430 steps/m
10	Target Head Rotation Z	77 000 steps	24 430 steps/m
11 & 12	Sun Movement & Rotation	Not available	Not available
13	Albedo Linear	37 620 steps	159 949 steps/m
14	Albedo Rotation	93.1	88.944 steps/deg

Tab. 4–5: Laboratory states used throughout the experiment

State	Lights	Additional Settings
1	None	None
2	Albedo On	None
3	Laboratory Facility Lights On	None
4	None	Polarization Filter applied to both cameras

and, in order to briefly examine the influence of a polarizing filter in front of the cameras, one gets attached to both cameras in one of the recording series. An overview is given in table 4–5.

4.3 Recording Procedure

For each of the laboratory states from table 4–5 one series of recordings is done. Throughout one series some of the cameras parameters are varied and the cameras are active both alone and together. With the different parameter and camera combinations a short recording is done with either one camera alone or both together. The different combinations can be seen in table 4–6. First, the two cameras are tested alone in recording 1-6 and 7-10 to obtain a data basis without interference. In the recordings 11-16 especially the influence of the LiDAR on the RealSense is examined.

Therefore the LiDAR is operated in the SUPER-HDR mode with an integration time of $5\,000\,\mu s$ and frame count of 4. The RealSense with the $HighAccuracy$ mode first, followed by the $HighDensity$ mode. And last, in recording 17-22 the influence of the RealSense on the LiDAR is the main suspect of the examination. Therefore the LiDAR is operated in the HDR Disabled mode with both $5\,000$ and $10\,000\,\mu s$ integration time and the RealSense with its $HighAccuracy$ mode. Each parameter combination which includes the RealSense is done with the three different laser projector values.

Both cameras are controlled manually via their corresponding GUI. Hence a small delay can be seen in the recorded data of the RealSense. This delay however can be easily removed during the data processing. However, in order to receive a sufficient long recording the recording sequences last at least 10 seconds. During the data procession one quarter of the frames is removed as well at the beginning and the end of the recording. However, both the reduced and the complete data set is saved for later analysis.

Tab. 4–6: Recording settings and camera combinations for each series of recordings. An exception is made for the "Lablight" recording sequences, where only the combinations 1-10 are recorded.

Recording	Camera	Preset/Mode	Laser Setting	(Max.) Exposure time setting and frame count
1	RealSense	High Accuracy	0 mW	Auto
2	RealSense	High Accuracy	180 mW	Auto
3	RealSense	High Accuracy	360 mW	Auto
4	RealSense	High Density	0 mW	Auto
5	RealSense	High Density	180 mW	Auto
6	RealSense	High Density	360 mW	Auto
7	HPS-3D160	HDR-Disable	-	5 000 μs
8	HPS-3D160	HDR-Disable	-	10 000 μs
9	HPS-3D160	SUPER HDR	-	5 000 μs / 4
10	HPS-3D160	SUPER HDR	-	10 000 μs / 4
11	RealSense	High Accuracy	0 mW	Auto
	HPS-3D160	SUPER HDR	-	5 000 μs / 4
12	RealSense	High Accuracy	180 mW	Auto
	HPS-3D160	SUPER HDR	-	5 000 μs / 4
13	RealSense	High Accuracy	360 mW	Auto
	HPS-3D160	SUPER HDR	-	5 000 μs / 4
14	RealSense	High Density	0 mW	Auto
	HPS-3D160	SUPER HDR	-	5 000 μs / 4
15	RealSense	High Density	180 mW	Auto

	HPS-3D160	SUPER HDR	-	5 000 μs / 4
16	RealSense	High Density	360 mW	Auto
	HPS-3D160	SUPER HDR	-	5 000 μs / 4
17	RealSense	High Accuracy	0 mW	Auto
	HPS-3D160	HDR-Disable	-	5 000 μs
18	RealSense	High Accuracy	180 mW	Auto
	HPS-3D160	HDR-Disable	-	5 000 μs
19	RealSense	High Accuracy	360 mW	Auto
	HPS-3D160	HDR-Disable	-	5 000 μs
20	RealSense	High Accuracy	0 mW	Auto
	HPS-3D160	HDR-Disable	-	10 000 μs
21	RealSense	High Accuracy	180 mW	Auto
	HPS-3D160	HDR-Disable	-	10 000 μs
22	RealSense	High Accuracy	360 mW	Auto
	HPS-3D160	HDR-Disable	-	10 000 μs

4.4 Data Processing

4.4.1 Import to MATLAB

After the collection of the data, it has to be processed. This is done via MATLAB. Therefore it has to be imported from its different file formats first. While the RealSense exports one $.bag$ file per recording, the LiDAR exports one $.csv$ file. In this $.csv$ file all frames are included and separated by metadata information between each frame. To import them into MATLAB, the $.csv$ format is easy to handle.

The $.bag$ format however has to be converted first. With the tool $rs - convert$, provided in the SDK this can be done easily. The converted data consists of one $.csv$ file per frame, which in turn can be easily imported into MATLAB again.

The imported data is than combined and stored in a cell array for further analyzing.

4.4.2 Conversion of the LiDAR data

In order to calculate metrics uniformly for both sensors, the data of the HPS-3D160 is slightly converted. The RealSense data uses the value 0 for invalid pixels inside of a frame, whereas the LiDAR uses a value of 65300 or 65500 to indicate invalid pixels. The behavior to indicate invalid pixels with these two values however is not documented. Therefore an official declaration of this values is not available and in this

case only an assumption. Besides this the depth values of the RealSense are available in meter, whereas the LiDAR system uses millimeter.

Therefore, in order to unify the both data sets, the LiDAR data is converted to the notation of the RealSense system.

4.5 Additional Experiment: Examination of the recording behavior of the HPS-3D160

As mentioned before, the Hypersen camera does not provide sufficient information to fully understand its recording behavior. Additionally the observations of the main experiment do not correspond to what was expected in advance. In order to receive a better understanding of the LiDAR modes, the following section examines the recording behavior of the two used camera modes by using a consumer action camera.

4.5.1 Setup

To record the LiDAR during operation a Yi Technologies 4K Action Camera as it can be seen in figure 4–3 is used. Therefore it is placed opposite the LiDAR in a distance of 1 meter and at the same height. After turning off all illumination the recording is started manually via the smartphone application coming with the camera. In the following 2 single depth pictures are recorded by the LiDAR with the available software. After that the LiDAR is set to the recording mode for approximately 5 seconds and afterwards the recording of the action camera is terminated. This procedure is repeated with all settings the camera is operated with throughout the experiment. These settings can be found in table 4–6, Record 7 to 10. The separation in two single pictures and one video recording is done in order to be able to determine a potential deviating behavior.

4.5.2 Results

The recorded files are examined manually. Therefore the files are played back with QuickTime Player, which offers the feature to play a video frame by frame. Now the duration of one integration time can be calculated by counting the number of consecutive frames that show the four laser diodes in an active state. In figure 4–4 three frames with active diodes are shown. It can be seen that the diodes in all three frames have different intensities. It can be concluded that the intensities of the laser diodes varies throughout the recording of one frame. However they are all frames within one integration sequence with the HDR Disabled mode. While the SUPER-HDR mode combines multiple recorded frames to one final frame in the output, the HDR Disabled mode should only do one. The assumption however is that the LiDAR does multiple measurements for one frame in order ro reduce errors.During a recording with the SUPER-HDR mode the variations are even larger, including single frames. This pause presumably originates from the pause between the recordings of the later combined frames. With the known frame rate, the duration of one integration sequence can be

Fig. 4–3: **A Yi Technologies 4K Action Camera with 12 MP sensor resolution and up to 240 frames per second video recording [31]**

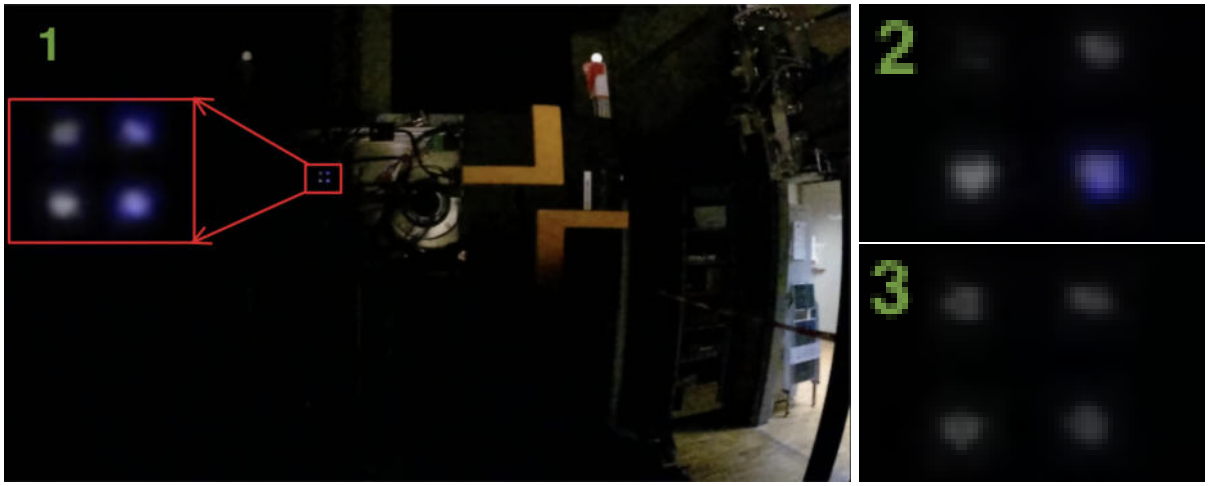

Fig. 4–4: **Recorded frames of the active LiDAR laser diodes. They show different states of the diodes, that occurred throughout the recordings. In figure 1 a frame from the Yi action camera can be seen. The part where the four active laser diodes of the LiDAR are visible is enlarged. All four diodes can be clearly seen in this frame. In the other two figures enlarged frames from the same recording can be seen. Figure 2 however only shows three of the diodes. Figure 3 shows the diodes in a significantly weaker state.**

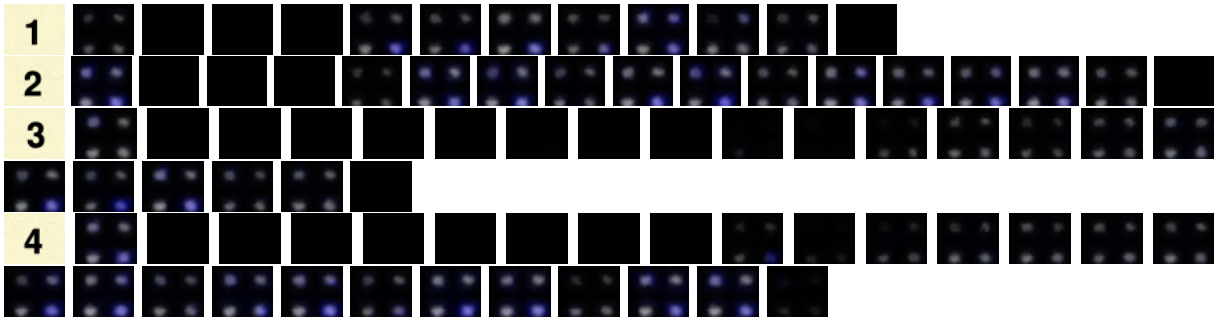

Fig. 4–5: Recorded sequences of the LiDARs recording behavior. An additional frame is added to the beginning and end of each sequence as a boundary.

Tab. 4–7: Results of the LiDAR recording behavior

	Mode and integration time	#Frames on	#Frames off	Active time abs. [ms]	Active time rel.
1	HDR Diabled; 5 000μs	7	3	29.17	70%
2	HDR Diabled; 10 000μs	11.5	3.5	47.92	76.7%
3	SUPER-HDR; 5 000μs	9.5	10.5	39.58	47.5%
4	SUPER-HDR; 10 000μs	16	10	66.67	61.54%

calculated via Eq. 4–1 with n_{Frames} being the number of consecutive frames with active laser diodes and $t_{Laser,\ active}$ the calculated integration time.

$$t_{Laser,\ active} = \frac{n_{Frames}}{f_{FPS}} = \frac{n_{Frames}}{240\,s^{-1}} \tag{4–1}$$

The results of this calculation can be seen in table 4–7. For each mode and integration time, 10 consecutive sequences with active diodes were analyzed and a mean value calculated. Besides the number of frames with active diodes the number of frames with inactive diodes are counted as well. With this information the relative time can be calculated in which the diodes are active throughout a recording. As can be seen in figure 4–5, the determination if the frame shows the active or inactive mode is not always clearly identifiable. Therefore the data is not to be seen as very reliable, but it can give a qualitative overview.

As it can be seen, the relative time with active diodes is not bigger for the SUPER-HDR mode as some would expect. This presumably is caused by the bigger computational effort, which is needed to calculate a final frame from the multiple ones recorded within the SUPER-HDR mode. Besides that it can be seen, that the real integration time in all cases is significantly different from the indicated one. An explanation could be, that the LiDAR presumably does a series of multiple records during the integration time and compares them to find reliable results. These sub records could have the indicated integration time, though it is not possible to validate this theory with the available action camera.

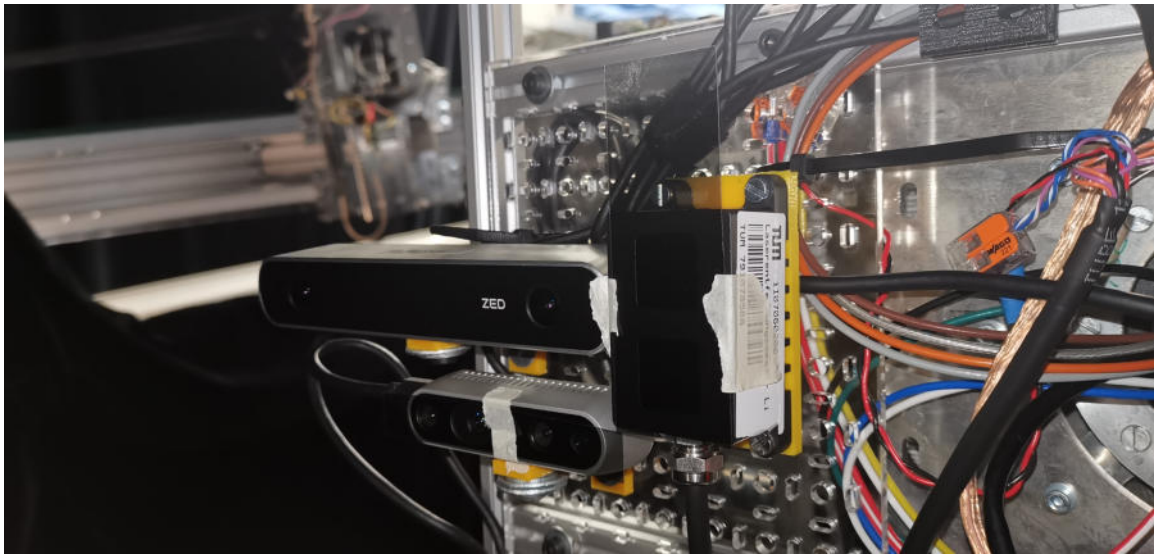

Fig. 4–6: Cameras with attached polarizing filter

4.6 Additional experiment: Minimizing interference with polarization filters

Due to its simple setup, an additional experiment is done, which examines the reduction of interference with an polarizing filter in front of the cameras. It is included into the main experiment as the laboratory state 4 in table 4–5. The recording procedures and data processing is exactly the same as for the first two lab states.

The filter is a simple polarizing filter in home user quality. It is cut in halves and attached to both cameras in a way, that the two pieces cover the emitter as well as the sensor section of each camera. They are attached perpendicular to each other and should therefore block the laser light of the respective other. In figure 4–6 both cameras can be seen while the filter segments are attached to them.

5 Results

In this chapter, the results of the experiment are shown. Therefore, the data is processed with Matlab and illustrated in multiple figures. An analysis of the shown data is done that provides the basis for the discussion in chapter 6.

The chapter is divided into the results indicating influences on the RealSense in section 5.1 and on the LiDAR in section 5.2.

5.1 Influence on the RealSense

5.1.1 Fill Rate

5.1.1.1 Mean fill rates

The fill rate is calculated for both, separately for every recorded frame and the average over each recording. The latter can give an overview about the general occurrence of interference, as the recordings with every camera alone can easily be compared with the data where both were run together. Figure 5–1 shows how the fill rate of the RealSense camera changes with the LiDAR turned on and how it correlates with the projector power of the RealSense. In every figure, the blue line, representing the fill rate of the RealSense operating alone, is lower than the other lines, except on the top right figure, where it becomes slightly higher with the projector turned on.

Additionally it can be recognized, that the fill rates of the RealSense are higher when the LiDAR is operating in the HDR-Disabled mode, than with it operating in the SUPER-HDR mode. That correlates with the observations of the behavior of the LiDAR in section 4.5. They showed that the HDR Disabled mode results in a higher relative time of the laser diodes of the LiDAR being active than the SUPER-HDR mode, though it was expected otherwise.

Another observation is the higher impact on the fill rate when the RealSense is operated with the High Density preset. In the Dark and Filter recordings, the increase is bigger with the H.D. preset than with the H.A. preset, in the Albedo recordings it is about the same. As expected the fill rate with the H.D. preset is generally higher than with the H.A. one.

One can also observe that the filter seems to have a negative effect on the fill rate, as with both presets and with every operating mode of the LiDAR the fill rates are lower than in the Dark recording series. Here one has to keep in mind, that the Filter recordings were done without illumination as well.

However, even though the LiDAR seems to have an influence on the RealSense fill rate, the influence of the projector seems to be higher.

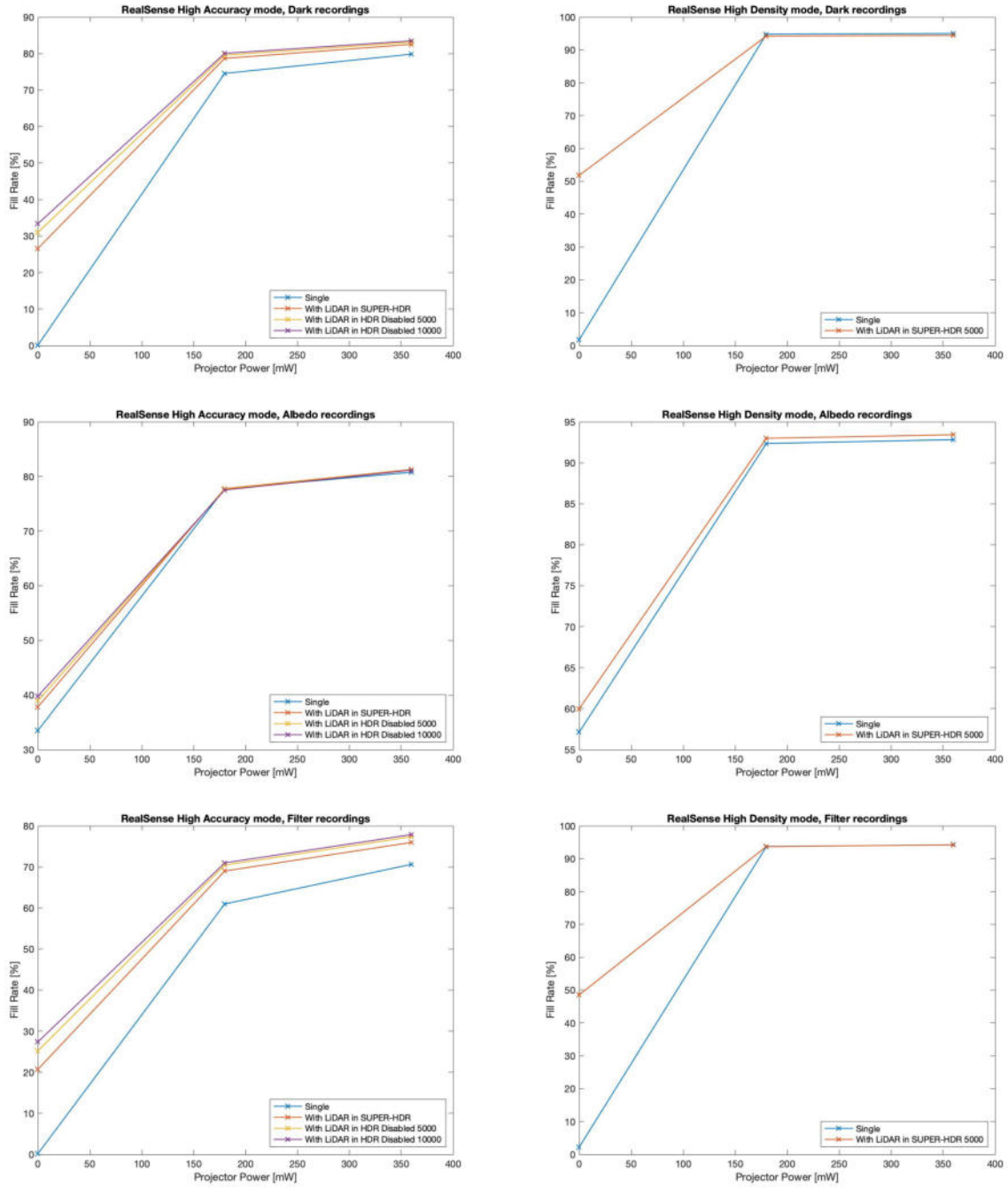

Fig. 5–1: Mean fill rates of the RealSense. The figures on the left show the recordings with the High Accuracy preset, on the right with the High Density preset. The top row shows the recordings without light, the middle with albedo lightning and the bottom with attached polarizing filter. Each figure shows the development of the fill rate with increasing laser projector power of the RealSense. Please note the different scale ranges on the y-axis.

5.1.1.2 Fill rates over time

Besides the general influence on the fill rates, the fill rate over time is of interest as well. In figures 5–2, 5–3 and 5–4 the behavior of all recordings can be seen. Each sub diagram shows the development of the fill rate for one recording configuration, with all four cases (or three for the Lablight case) shown in the same sub diagram. Therefore the influence of the different illuminations can easily be seen. In 5–2 the recordings 1-6, that are the ones of the RealSense alone are displayed and grouped after preset and projector power. 5–3 has the same layout and shows recording 11-16. Here the LiDAR was operated in SUPER-HDR mode. 5–4 shows recording 17-22. As the RealSense was only operated with the High Accuracy preset in these recordings but the LiDAR with two different integration times in the HDR Disabled mode, the layout differs slightly from the two preceding ones.

One has to keep in mind, that the recording intervals of the two cameras are not completely identical. The first frames include a time where the LiDAR is inactive, while the RealSense is already recording. These frames could have been removed from the figure, but as they clearly show the general influence they were considered as well.

It can be seen that without the LiDAR being active the fill rate is an erratic noise in all cases and configurations. But in figure 5–3 one can see that with both cameras being active most of the recordings have a repeating pattern, which is similar for all shown cases and configurations. However the pattern is not visible in the recordings of the Albedo case, except in the H.A. one with no projector operating (top left). The level of the amplitudes also decreases the higher the fill rate is.

One can also see that in recording 16 and 17 the fill rate is slightly decreasing in the Dark case as soon as the LiDAR becomes active. Looking at 5–4 this isn't the case for the HDR Disabled mode.

In record 20-22 one can see a distinct pattern especially in the first one. For the recordings with an integration time of 5 000 μs in the HDR Disabled case (record 17-19) the oscillation is more uniform. Again, the Albedo case recordings seem to be the least influenced.

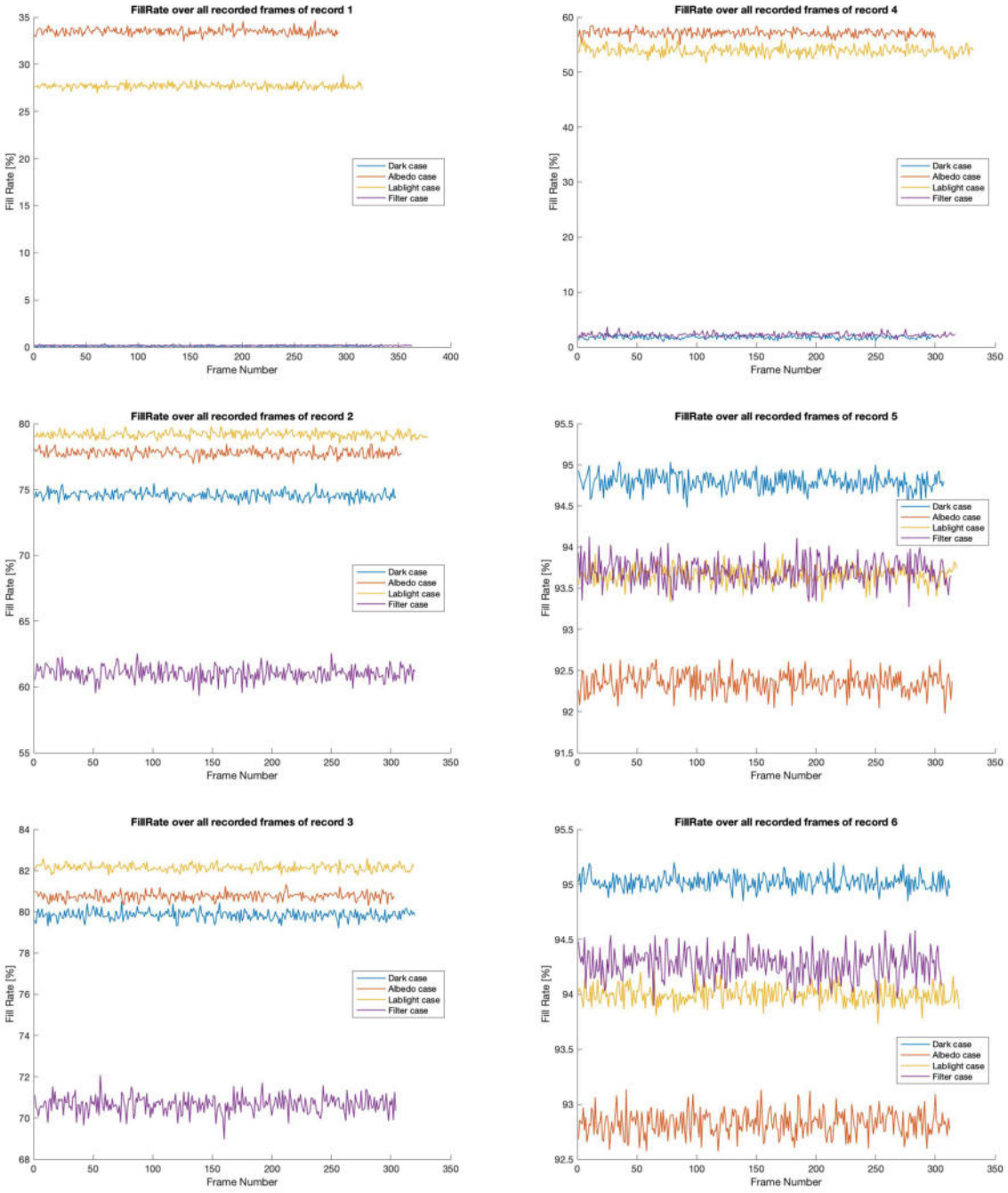

Fig. 5–2: Fill rates of the RealSense in records 1-6 over the time, in which the RealSense is operated alone. The left 3 figures show the records with the High Accuracy preset the ones on the right with the High Density preset active. The top row shows the figures with the laser projector of the RealSense working with 0 mW power, the middle the ones with 180 mW and the bottom the ones with 360 mW. Please note the different scale ranges on the y-axis.

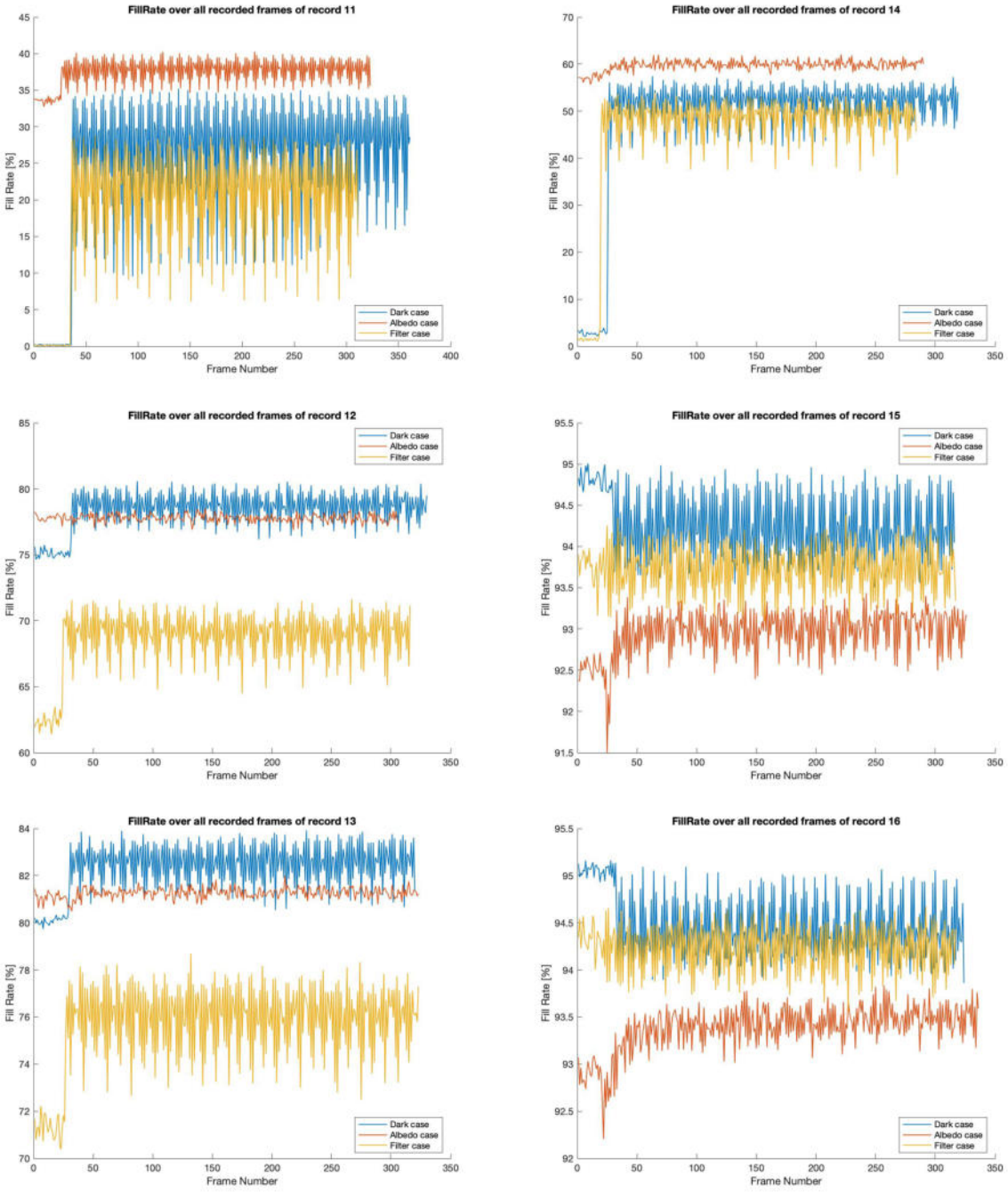

Fig. 5–3: Fill rates of the RealSense in records 11-16 over the time, in which the LiDAR is operated in the SUPER-HDR mode with 5 000 us and 4 combined frames. As before, on the left are the H.A. recordings and on the right the H.D. ones. At the top 0 mW, at the middle 180 mW and at the bottom 360 mW. Please note the different scale ranges on the y-axis.

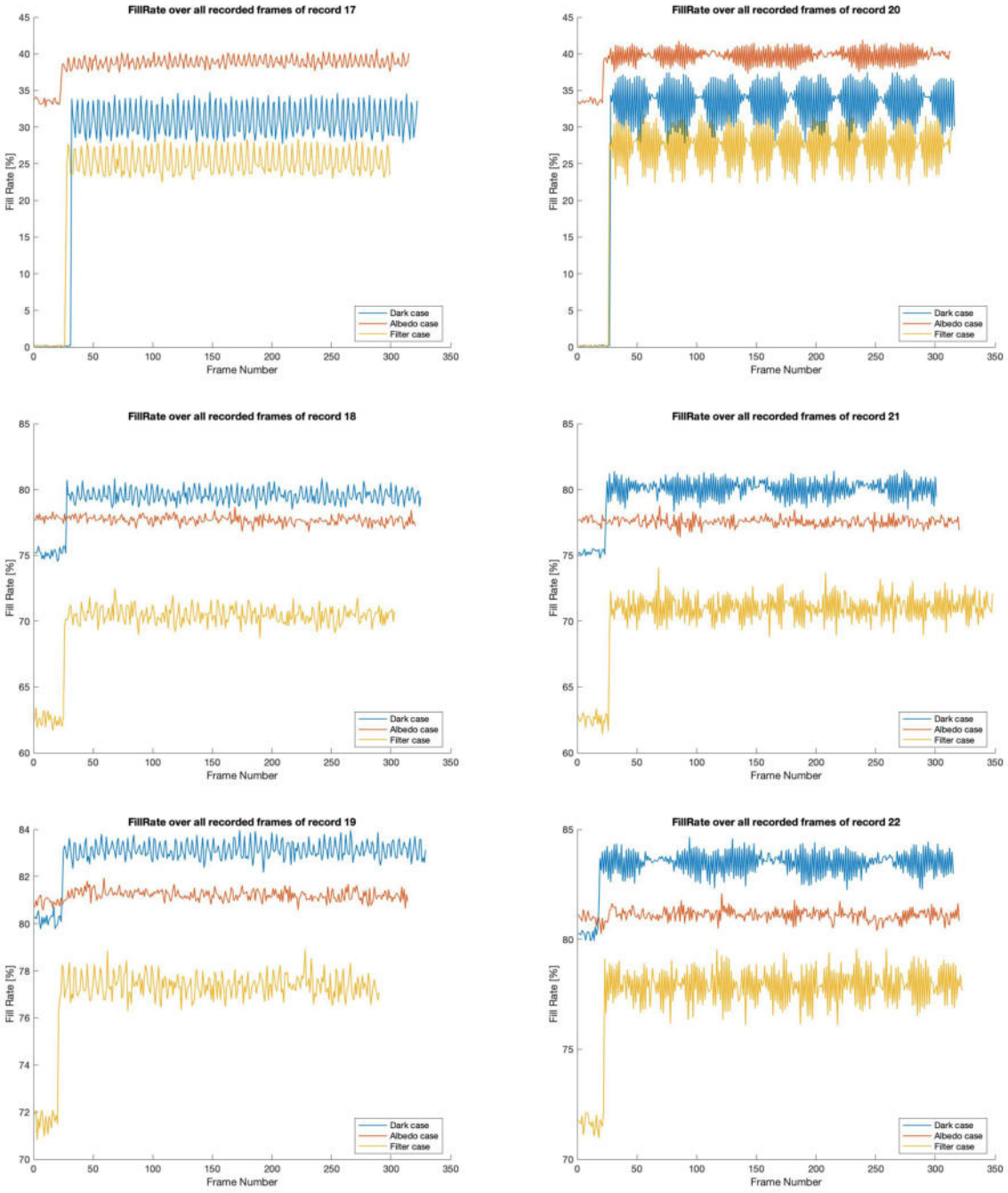

Fig. 5–4: Fill rates of the RealSense in records 17-22 over the time, in which the LiDAR is operated in the HDR Disabled mode. In contrast to the preceding figures, on the left side the maximum integration time of the LiDAR is 5 000 us and on the right 10 000 us. As before, at the top the laser power of the RealSense is 0 mW, at the middle 180 mW and at the bottom 360 mW. All figures are recorded with the H.A. preset. Please note the different scale ranges on the y-axis.

5.1.2 Standard Deviation

As the number of figures used to analyze the standard deviation of the different recordings is to big, all these figures can be found in appendix A. However to give a brief overview and analyze the general appearance of the data a selection of figures can be found in 5–5 and 5–6. The former shows 4 figures with the areas of occurrence. The latter shows how the magnitude of the deviations are distributed within each recording and therefore can give a good overview about the extent of deviation.

Some things can already be observed from the shown selection of figures. It can be seen that the magnitude of the deviation is in general significantly higher with the High Density preset. And the amount of pixels with deviations is higher for this preset as well. This observation is most distinctive for the case with the laser projector being inactive. With an increasing projector power the number of pixels with higher magnitudes of deviation is rising for the H.A. preset, for the H.D. one they are decreasing.

Both presets have a characteristic shape of the distribution, whereas the shape of the High Density one includes the one of the High Accuracy preset. But the H.D. recordings generally include higher magnitudes and the shape therefore looks slightly different. Generally speaking the shapes stay the same for every recording with H.A. or H.D. Variations only occur in the amount of pixels with deviation and the magnitudes.

The influence of the LiDAR is most significant for the recordings without the laser projector. Here the amount of pixels with deviations increases when the LiDAR is active for both presets, whereas the magnitude increases only slightly.

It is also interesting to see, that both the amount and magnitude of deviations for the Albedo and Lablight recordings without the LiDAR are already the same as the Dark and Albedo ones with LiDAR . This leads to the assumption that the amount of illumination has a big influence on the number of pixels with deviations. One has to keep in mind that deviations can only occur for valid pixels and are therefore connected to the fill rate.

For the H.A. cases most deviations stay below a value of 0.5 m, except the cases without the projector being active where they go up to a value of 1 m. Some pixels however have magnitudes of up to 2 meters or in the no-projector case up to 5. This can be seen on the left two figures in 5–6. In the H.D. recordings most pixels deviation stay under 2 m with some up to 5 m. Again the no-projector cases build an exception where the values reach magnitudes of up to 20 m.

The locations where the deviations occur are of interest as well. One observation is the fact, that most of the figures have a small stripe from the top to the bottom on their left side. Here one has to keep in mind the slightly different FOV of the two infrared sensors of the RealSense and the resulting non overlapping areas of the recorded pictures. As the depth picture is based on the left imager, the non overlapping part is seen on the left in the final frame. Besides that hardware based errors a lot of the deviations are located around the body of the satellite. This results in a shape around it on the figures. Especially on the left bottom side of the body, near to the solar panel a lot of deviations

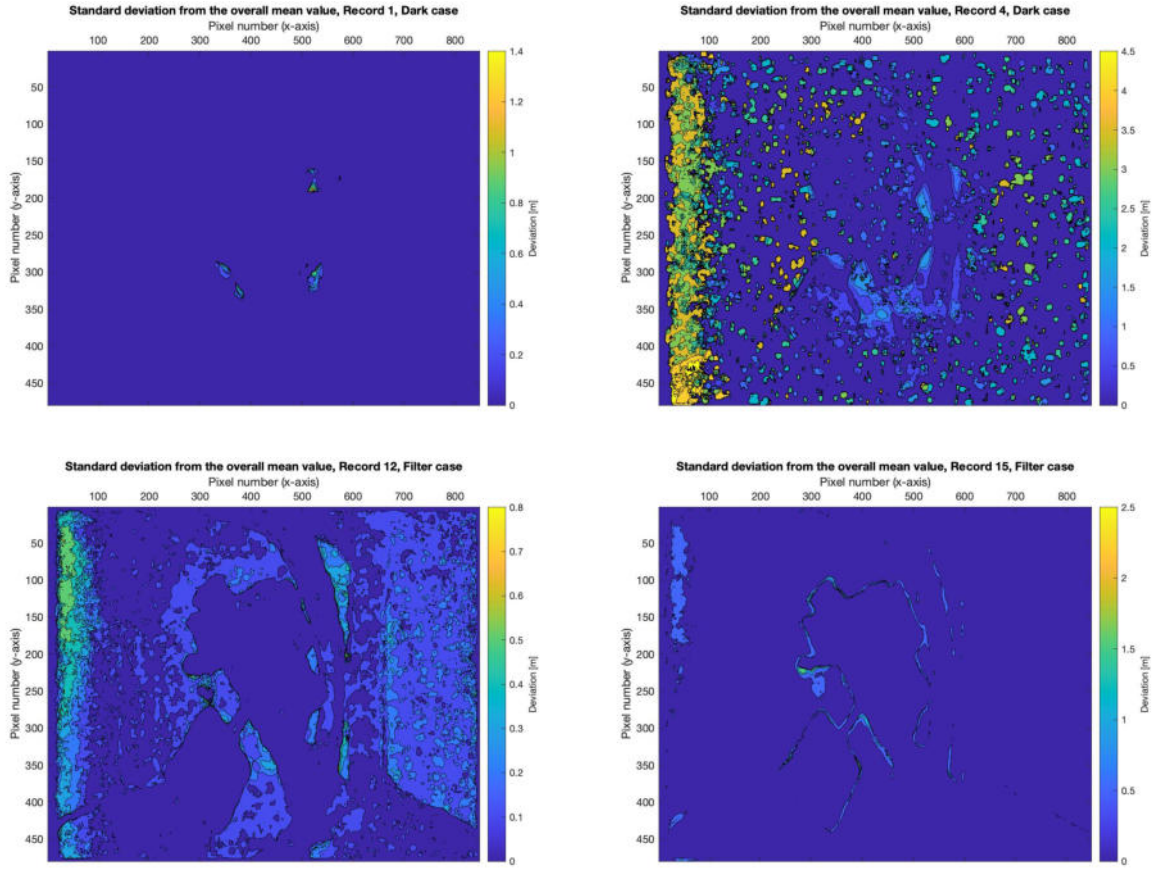

Fig. 5–5: Selected figures with the places of deviations for the RealSense. On the top are two figures from the dark case without the projector turned on. In the second row one can see figures from the filter case and 180 mW projector power and the HPS working in the SUPER-HDR mode. The left figures show recordings with the High Accuracy preset, on the right are High Density ones.

occur. This side can be identified in figure 4–1 as the side of the satellite with a flat and unstructured silver coating.

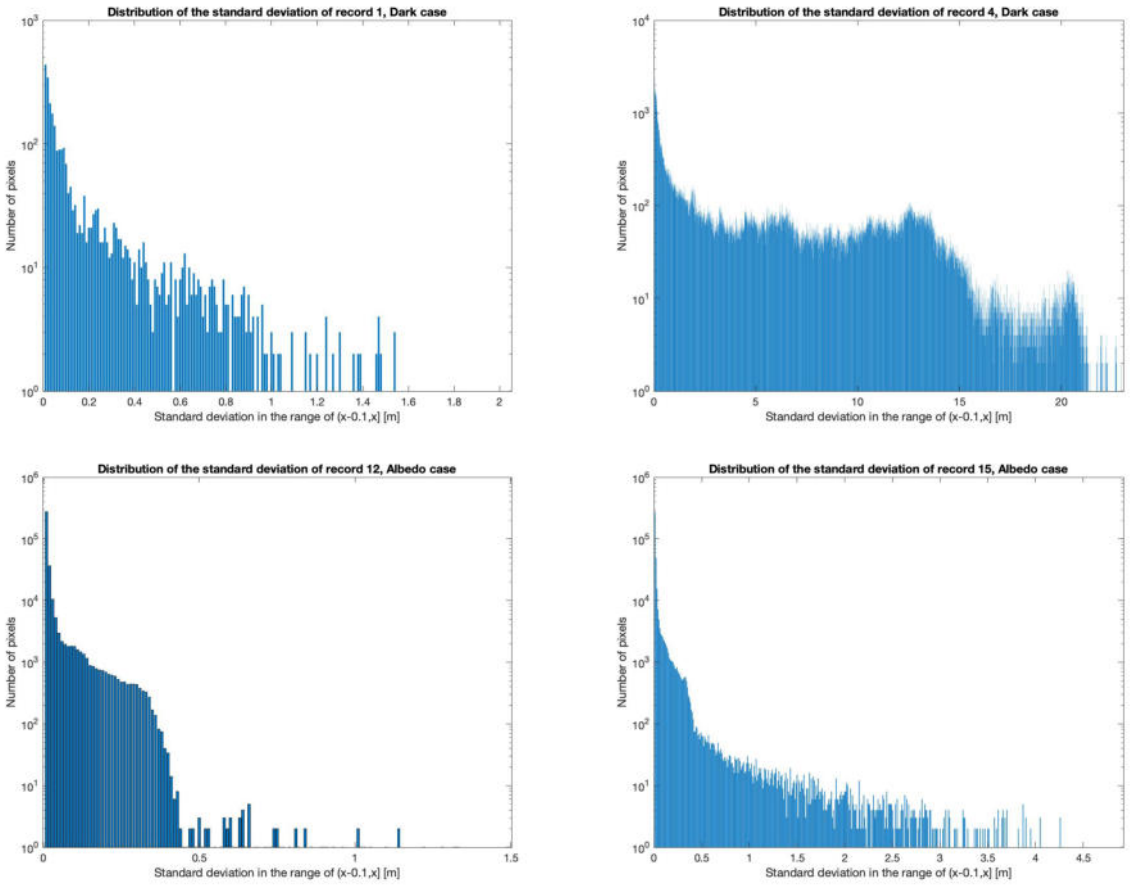

Fig. 5–6: Selected figures with the distribution of deviations for the RealSense. On the left are H.A. and on the right H.D. recordings. On the top are figures from the Dark case and without the laser projector, on the bottom the laser is active and the Albedo case is shown.

5.2 Influence on the LiDAR

5.2.1 Fill Rate

As for the RealSense, figure 5–7 gives a general overview over the influence of the RealSense on the fill rate of the LiDAR . Followed by the development over time in the figures 5–9, 5–10 and 5–11.

5.2.1.1 Mean fill rates

As can be seen, the influence of the LiDAR on the RealSense seems to be much higher than vice versa. However, a small influence is recognizable. For the HDR Disabled mode with an integration time of 10 000 μs and the SUPER-HDR mode with an integration time of 5 000 μs the fill rate increases slightly with the RealSense projector power. For the HDR Disabled mode the increase is about twice as much as for the SUPER-HDR mode. And for the Dark cases the increase is the highest, followed by the Albedo and then the Filter cases. The HDR Disabled mode recordings with an integration time of 5 000 μs in contrast show a slight decrease with increasing projector power. The decrease is significantly smaller than the increase of the others, but it is present in all three recording series.

Generally said, the fill rate is the highest for the HDR Disabled mode with an integration time of 10 000 μs, followed by the one with 5 000 μs and the SUPER-HDR mode with 5 000 μs. As can be seen in the following figures, the SUPER-HDR mode with an integration time of 10 000 μs is only slightly worse than the corresponding HDR Disabled mode.

5.2.1.2 Fill rates over time

The figure 5–9 shows the fill rate over time for the Dark, the Albedo and the Lablight case. The figures 5–10 and 5–11 for the Dark and Albedo case. The data for the Filter case is not included, as it is significantly lower for all recordings but has the same general shape as the other ones as can be seen in figure 5–8. By removing it the shape of the recorded data can be observed better.

The first observation is the very similar shape of all data in one sub figure. The different ambient conditions seem to have no influence on the shape of the graphs. They seem to only move the graph along the y-axis. Besides that it is remarkable, that almost all graphs have a short sequence where they approach a limit value. This could come from the algorithm of the camera, that first needs to adjust in the beginning of a recording. However this behavior is not present in recording 20-22 in figure 5–11. Here the graphs do not approach a limit value, but rise steadily. The rest of the observations are the same as for the mean fill rates before.

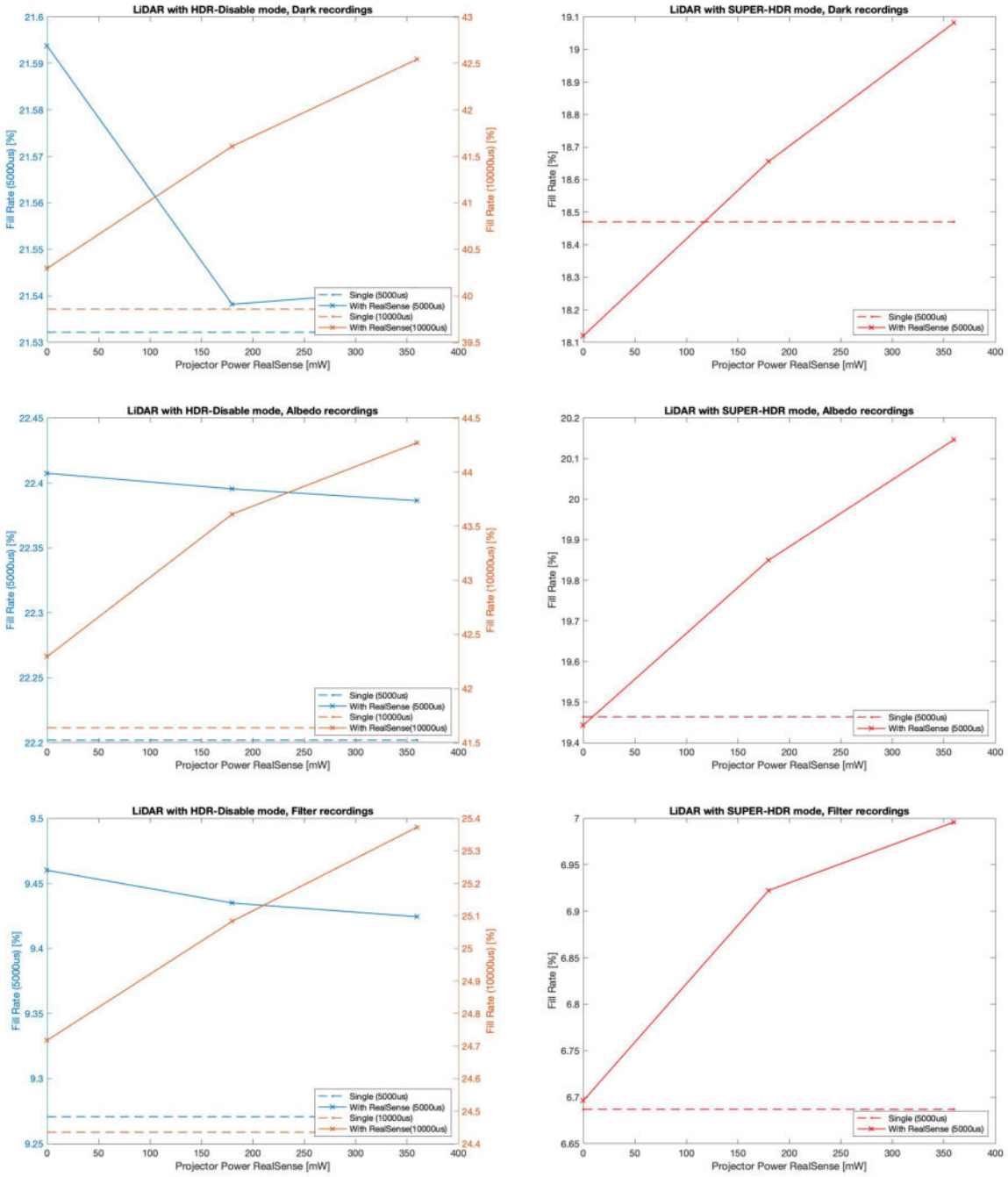

Fig. 5–7: Mean fill rates of the LiDAR . The figures on the left show the recordings with the HDR Disabled mode, on the right with the SUPER-HDR mode. The top row shows the recordings without light, the middle with albedo lightning and the bottom with attached polarizing filter. Each figure shows the development of the fill rate with increasing laser projector power of the RealSense. Please note the different scale ranges on the y-axis.

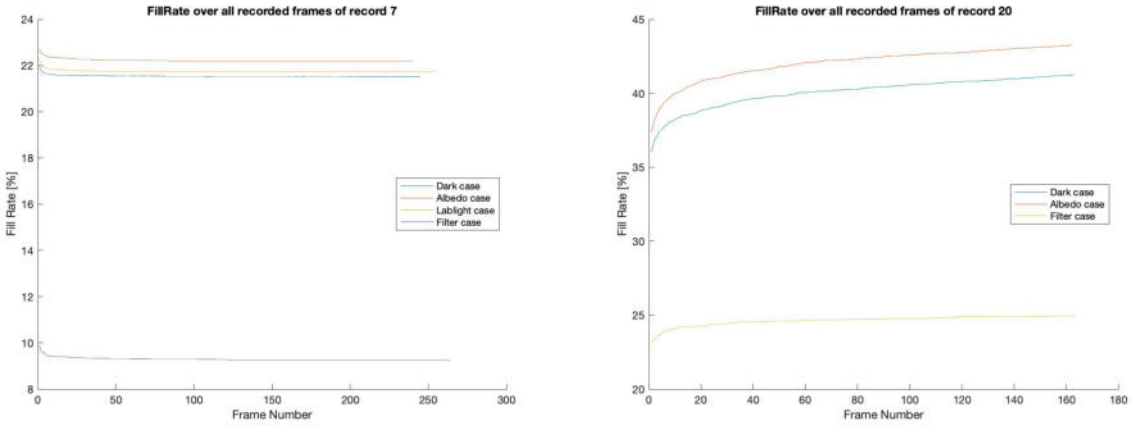

Fig. 5–8: Selected recordings over time of the LiDAR including the Filter case. As can be seen, the general shape of the filter graph is the same as for the others.

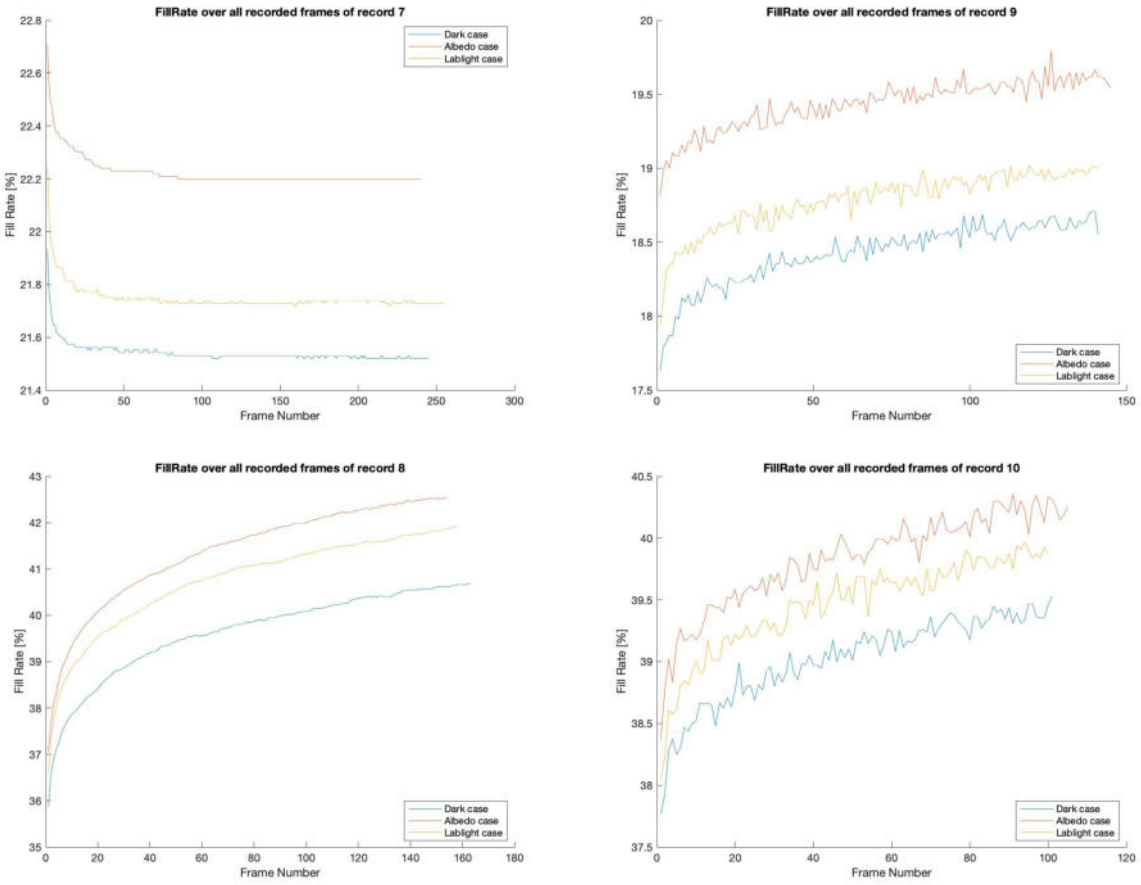

Fig. 5–9: Fill rates of the LiDAR in records 7-10 over time, in which the LiDAR is operated alone. The left figures show the records with the HDR Disabled mode, the ones on the right with the SUPER-HDR. The top row shows the figures with an integration time of 5 000 us and the bottom the ones with 10 000 us. Please note the different scale ranges on the y-axis.

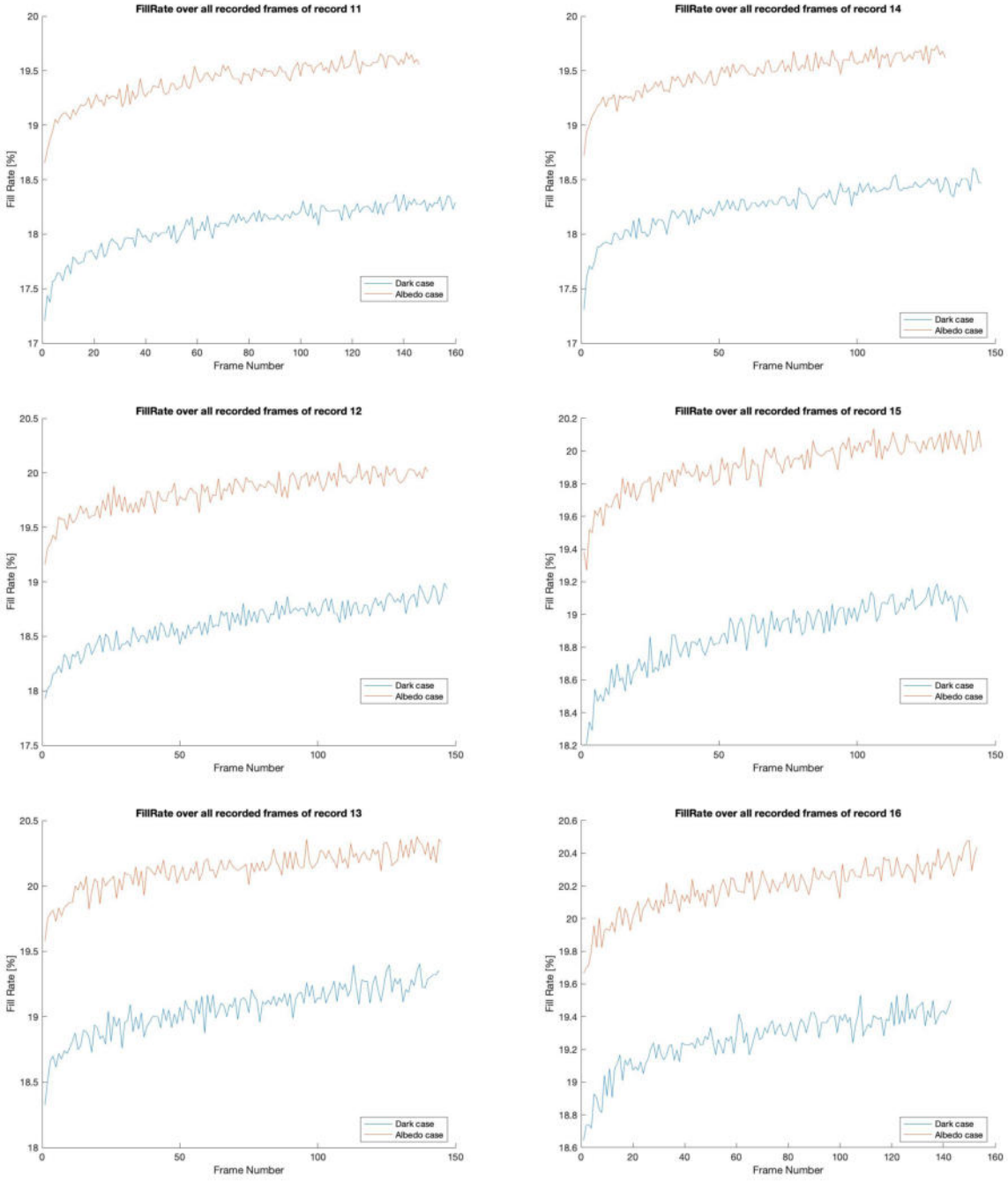

Fig. 5–10: Fill rates of the LiDAR in records 11-16 over the time, in which the LiDAR is operated in the SUPER-HDR mode with 5 000 us and 4 combined frames. On the left are the H.A. recordings and on the right the H.D. ones. At the top 0 mW, at the middle 180 mW and at the bottom 360 mW. Please note the different scale ranges on the y-axis.

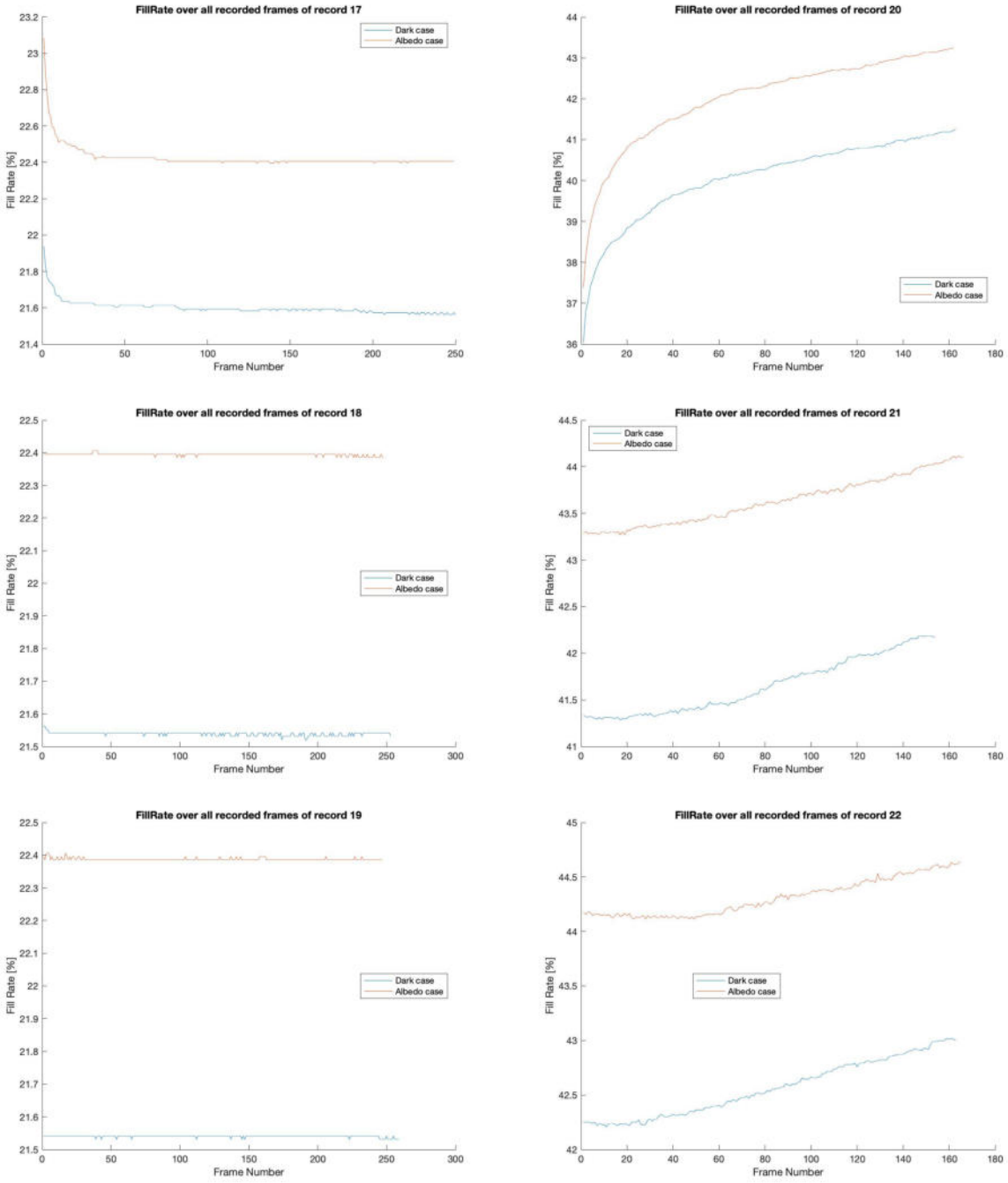

Fig. 5–11: Fill rates of the LiDAR in records 17-22 over the time, in which the LiDAR is operated in the HDR Disabled mode and the RealSense with the High Accuracy preset. On the left side the maximum integration time of the LiDAR is 5 000 us and on the right 10 000 us. As before, at the top the laser power of the RealSense is 0 mW, at the middle 180 mW and at the bottom 360 mW. All figures are recorded with the H.A. preset. Please note the different scale ranges on the y-axis

5.2.2 Standard Deviation

Regarding the figures for the standard deviation the complete set is again located in Appendix A, whereas a selection can be found in figure 5–12 and 5–13.

The deviations again are located mainly around the satellite and in the LiDAR recordings another spot is present in almost every figure. On the right a structure is visible which seems to be a part of the holding structure of the target. This can be also seen in figure 4–1. The deviations around the satellite are especially on the bottom left, silver coated surface of target, as they were on the RealSense as well. Additionally some are located in the area above the satellite.

The areas are about the same for both recording modes. It can be observed that they become less for some figures, especially in the Albedo recordings where the HDR Disabled mode with an integration time of 10 000 μs is used. It can be assumed though that the areas with small deviations stay the same but are not visible in the figures anymore. This would be due to the occurrence of larger magnitudes and therefore a change of the scale which doesn't show low magnitudes anymore.

Coming to the distribution, generally said the magnitude of the deviations for the LiDAR are much smaller than they are for the RealSense. Except some single outliers their magnitude stays under 5 cm. The amount of pixels with a deviations is higher, about twice as much, for the recordings with an integration time of 10 000 μs. In the Albedo and Lablight case there are some more pixels with deviations than for the Dark ones but also with small magnitudes. In the Filter recordings the number is in general lower than for the others.

The magnitude of some outliers is also higher for some recordings with an integration time of 10 000 μs, especially with the HDR Disabled mode.

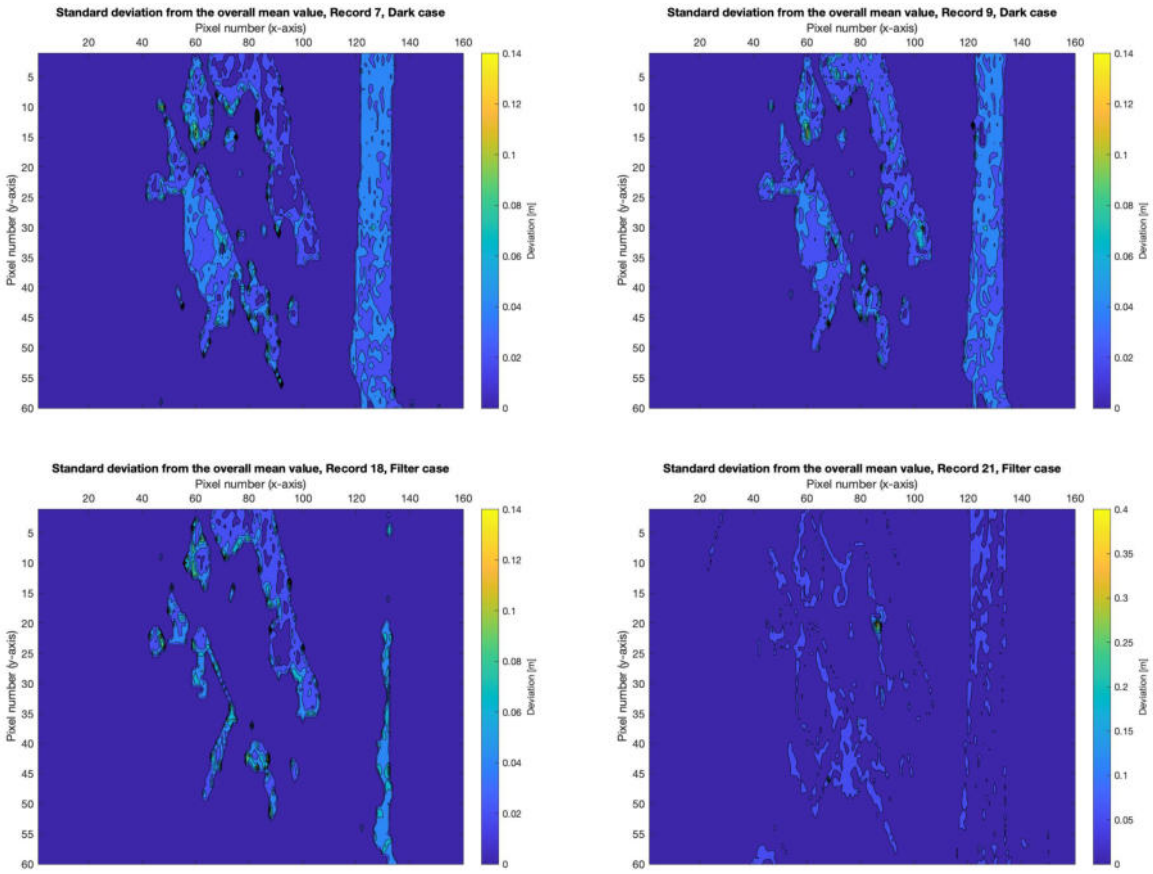

Fig. 5–12: Selected figures with the places of deviations for the LiDAR. On the top are two figures from the dark case without the RealSense being activated. On the left with the HDR Disabled mode and on the right the SUPER-HDR. In the second row one can see figures from the Filter case and the LiDAR working in the HDR Disabled mode.

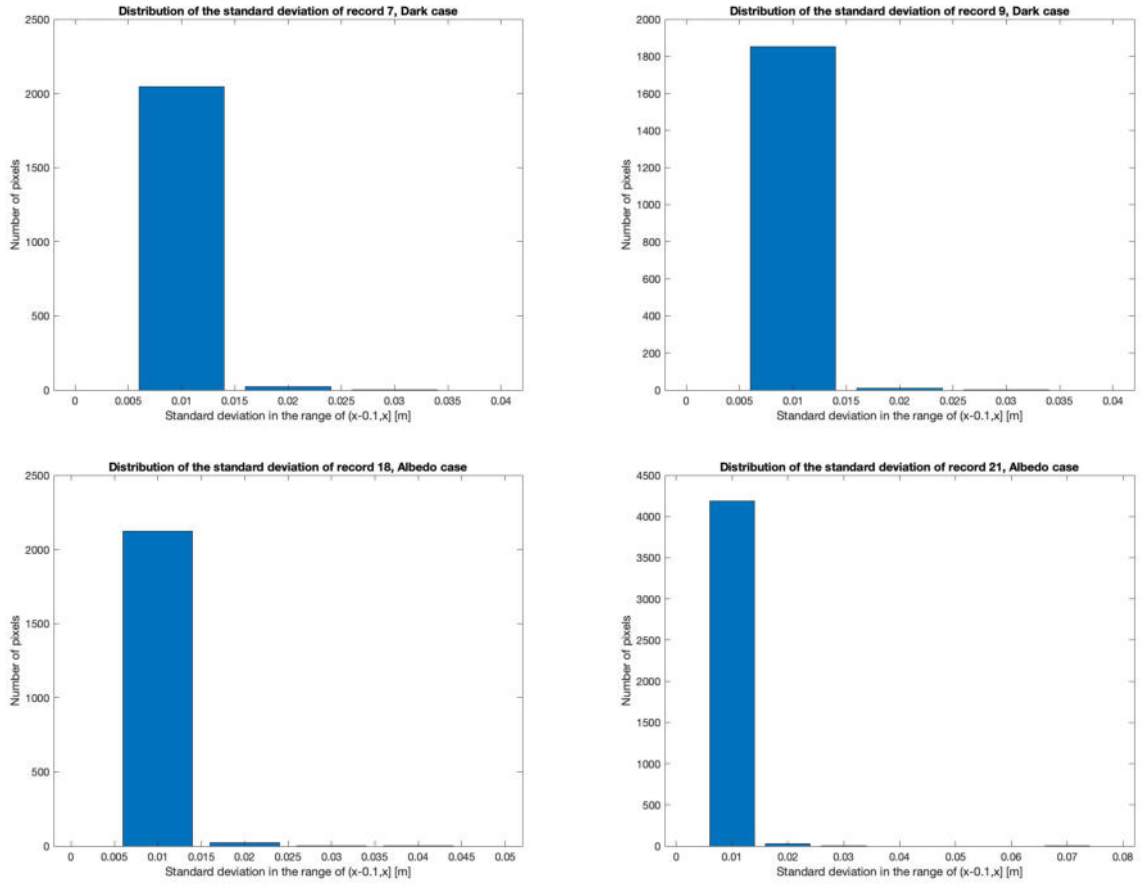

Fig. 5–13: Selected figures with the places of deviations for the LiDAR. On the top are two figures from the dark case without the RealSense being activated. On the left with the HDR Disabled mode and on the right the SUPER-HDR. In the second row one can see figures from the Filter case and the LiDAR working in the HDR Disabled mode.

6 Discussion

6.1 RealSense

Looking at as well the fill rate as the standard deviation the influence of the LiDAR on the RealSense seems to be much higher than vice versa. The fill rate is increasing with the illumination from the LiDAR . It could be shown that the increase of the fill rate correlates with the relative time the flash is active. Also the distribution graphs for the Albedo case without LiDAR show that the influence of the Albedo is the same as the LiDAR flashes in the Dark case. That all suits the hypothesis that the additional light from the LiDAR improves the performance of the RealSense. The influence of the LiDAR can especially be seen in the patterns of the fill rate over the time. They occur as soon as the LiDAR is turned on.

The selection of the preset for the RealSense has a big influence on the quality of the data as well. The High Density setting is providing a higher fill rate, though the standard deviation from the mean values is significantly higher for that preset. Especially the deviations in the recordings with both, no ambient light and inactivated pattern projector are high. The influence of the LiDAR again can be seen positive, as it seems to work as an illumination source and reduces the areas in the frames with high deviations. However, the use of the H.A. preset can be assumed to be more suited for this use case. It provides depth images with slightly lower fill rates but significantly lower variance. The influence of the LiDAR's integration time and therefore the percentage of the time its diodes are active is not clearly recognizable.

The improvements brought through the pattern projector seem to be independent from the flashes. Neither the fill rate nor the deviations improvements that are caused by it are somehow reduced with the LiDAR. That presumably is the case, as the intensity of the pattern is high enough to not be affected by the diffuse flashes of the LiDAR.

6.2 HPS-3D160

Coming to the LiDAR , an influence of the RealSense is more difficult to determine. As the RealSense projector power has an influence on the fill rate and deviations though, a slight interference can be assumed. The most promising and also the only theory is hypothesis 1a. The reflections of the pattern projector from the surface of the satellite are probably strong enough to be recognized by the CMOS of the LiDAR. These reflections would be constant inputs for the LiDAR, in contrast to the reflections of its own flashes. The result would be, that the sensor is not able to remove these inputs with its algorithm and therefore either ignores them and marks them as invalid or accepts their inputs as valid values. As the fill rate is increasing in two of the examined modes and decreases in the third a final conclusion is difficult to make. It seems that for the different modes the reaction is different. But as the amount of data is small it is not

possible to say if the HDR Disabled mode with an integration time of 5 000 μs is an exception or just a bad recording.

An interference is existing, though it is very small. One should keep this in mind when working with the camera, but in general no big restrictions should result from them.

As a side effect the results showed that the camera is also slightly influenced by ambient light. Regarding that the used light sources partly emit in the infrared spectrum of the camera, this influence is presumably of the same nature as the projector.

6.3 Polarizing filters

Coming to polarizing filters, their influence is visible in the generally reduced fill rate, as well as less deviations. As the influence on the RealSense however seems to be positive, the filters are rather unhelpful. The positive effects of the LiDAR are reduced. This can be seen in the fill rate that is generally the lowest in all recordings with the HDR Disabled mode and still below the dark cases for the SUPER-HDR mode. The main effect of the LiDAR on the RealSense is the illumination of the scene, which is restricted with the filter in front of the diodes. It is therefore considered as not helpful for the RealSense.

For the LiDAR the effect is even bigger. When the filter is applied the fill rate drops significantly for all recordings. In the figures showing the areas with deviation it can be seen that significantly less areas are affected, the distribution charts show a big drop of deviations. This however presumable is not the result of less deviations because of less interference caused by the filter. It is more likely the result of the lower percentage of valid pixels in general. The filter seems to strongly restrict the LiDAR and have a negative effect in the RealSense. It is therefore considered as unnecessary and should not be used. One has to keep in mind though, that the used filter was of a cheap quality and more professional versions could help in other use cases.

7 Conclusion

The main target of this thesis was to determine the occurrence of interferences between the Intel RealSense D435 and the Hypersen HPS-3D160. This general goal could be achieved. It was possible to find strong indicators for an influence between the two camera systems. These interference however has mainly an impact on the RealSense performance. The LiDAR is influenced but only slightly.

The presence of the LiDAR can be seen as supportive for the RealSense. Instead of having negative effects on the performance, the additional illumination is helpful especially in dark conditions. The assumption that the flashes would impair the functionality of the pattern could be rejected. Regarding the LiDAR the interferences are caused by the pattern projector which disturbs the LiDAR sensor.

Overall it can be recommended to use the sensors together in the examined configurations. Though one has to keep in mind that disturbances can occur that were not examined in this thesis.

The polarizing filter that was attached to the cameras for one recording series was found to be disturbing more than supporting. It could not fulfill its purpose to separate the two light emissions. Rather it had a bad influence especially on the LiDAR as its flashes were limited heavily.

7.1 Outlook

Regarding the bad documentation of the LiDAR it can be recommended to look for alternatives that provide more information. It could also be examined to what extend one can take advantage of the discovered effects.

Bibliography

[1] European Space Operations Center, “ESA’s Annual Space Environment Report,” Sep. 2020, rev. 4.0. [Online]. Available: https://www.sdo.esoc.esa.int/environment_report/Space_Environment_Report_latest.pdf

[2] ESA Space Debris Office, “Space debris by the numbers,” Jan. 2021. [Online]. Available: https://www.esa.int/Safety_Security/Space_Debris/Space_debris_by_the_numbers

[3] L. Franceschini, “Experimental Analysis of Pose Tracking Performance of Visual and Infrared Stereo Cameras under Low Orbital Light,” Master’s thesis, Technical University of Munich, 2019.

[4] D. Piatti, F. Remondino, and D. Stoppa, *TOF Range-Imaging Cameras*. Springer-Verlag Berlin Heidelberg, 2013, ch. State-of-the-Art of TOF Range-Imaging Sensors, pp. 1–9.

[5] L. Keselman, J. I. Woodfill, A. Grunnet-Jepsen, and A. Bhowmik, “Intel RealSense Stereoscopic Depth Cameras.” [Online]. Available: https://arxiv.org/pdf/1705.05548v2.pdf

[6] J. Langwald, “Stereo Vision,” Accessed: 06.6.2020. [Online]. Available: https://www.dlr.de/rm/en/desktopdefault.aspx/tabid-9389/

[7] S. Piatek and J. Li, “LiDAR: A photonics guide to the autonomous vehicle market,” Nov. 2018, Accessed: 6.6.2020. [Online]. Available: https://hub.hamamatsu.com/us/en/application-note/LiDAR-competing-technologies-automotive/index.html

[8] SICK AG, “Whitepaper lidar sensor functionality and variants,” Jul. 2018.

[9] A. Yaacobi, J. Sun, M. Moresco, G. Leake, D. Coolbaugh, and M. R. Watts, “Integrated phased array for wide-angle beam steering,” *Optics Letters*, vol. 39, no. 15, p. 4575, jul 2014.

[10] B. Behroozpour, P. A. M. Sandborn, M. C. Wu, and B. E. Boser, “Lidar System Architectures and Circuits,” *IEEE Communications Magazine*, vol. 55, no. 10, pp. 135–142, oct 2017.

[11] C. V. Poulton, M. J. Byrd, P. Russo, E. Timurdogan, M. Khandaker, D. Vermeulen, and M. R. Watts, “Long-Range LiDAR and Free-Space Data Communication With High-Performance Optical Phased Arrays,” *IEEE Journal of Selected Topics in Quantum Electronics*, vol. 25, no. 5, pp. 1–8, sep 2019.

[12] Y. Wang, G. Zhou, X. Zhang, K. Kwon, P.-A. Blanche, N. Triesault, K. sik Yu, and M. C. Wu, “2D broadband beamsteering with large-scale MEMS optical phased array,” *Optica*, vol. 6, no. 5, p. 557, apr 2019.

[13] N. Reichenbach, “Entwicklung und Integration eines Erdalbedosimulators zum Testen von Sensoren fur die Nahbereichsnavigation von Satelliten im Erdorbit,” 2017, Semester’s thesis, RT-SA 2017/02.

[14] A. Ciadamidaro, “Auslegung und Konstruktion eines Sonnensimulators für eine Simulationsumgebung zur Nahbereichsnavigation von Satelliten,” 2016, Bachelor’s thesis, RT-BA 2016/07.

[15] Chair of Astronautics, “The RACOON Lab - Technologies for operating robots in space,” accessed: 10.6.2020. [Online]. Available: https://www.lrg.tum.de/fileadmin/w00bzj/lrt/Forschung/Racoon/Racoon_Info_Deck_2017.pdf

[16] Intel, *Datasheet Intel RealSense D400 Series Product Family*, Jun. 2020, rev. 002. [Online]. Available: https://www.intelrealsense.com/wp-content/uploads/2020/06/Intel-RealSense-D400-Series-Datasheet-June-2020.pdf

[17] A. Grunnet-Jepsen, J. N. Sweetser, and J. Woodfill, *Best-Known-Methods for Tuning Intel RealSense D400 Depth Cameras for Best Performance*, rev. 1.7 ed., Accessed: 23.6.2020; Rev. 2.0. [Online]. Available: https://www.intel.com/content/dam/support/us/en/documents/emerging-technologies/intel-realsense-technology/BKMs_Tuning_RealSense_D4xx_Cam.pdf

[18] “Depth Camera D435,” Accessed: 2.6.2020. [Online]. Available: https://www.intelrealsense.com/depth-camera-d435/

[19] A. Grunnet-Jepsen, P. Winer, A. Takagi, J. Sweetser, K. Zhao, T. Khuong, D. Nie, and J. Woodfill, “Using the Intel® RealSense Depth cameras D4xx in Multi-Camera Configurations.”

[20] Hypersen, *Datasheet HPS-3D160*, Jul. 2019, rev. 1.4.

[21] *Hypersen Technologies Co., Ltd. LiDAR PC software User Manual*, Rev. 1.8.

[22] “3D Solid-state LiDAR HPS-3D160,” Accessed: 4.6.2020. [Online]. Available: https://en.hypersen.com/product/detail/10.html

[23] A. OrRiordan, T. Newe, G. Dooly, and D. Toal, “Stereo Vision Sensing: Review of existing systems,” in *2018 12th International Conference on Sensing Technology (ICST)*. IEEE, dec 2018.

[24] A. Pacala, “How Multi-Beam Flash Lidar Works,” Nov. 2018, accessed: 12.6.2020. [Online]. Available: https://ouster.com/blog/how-multi-beam-flash-lidar-works/

[25] Intel, *Datasheet Intel RealSense LiDAR Camera L515*, Jan. 2021, rev. 003.

[26] R. Martin-Martin, M. Lorbach, and O. Brock, “Deterioration of depth measurements due to interference of multiple RGB-D sensors,” in *2014 IEEE/RSJ International Conference on Intelligent Robots and Systems*. IEEE, sep 2014.

[27] K. Berger, K. Ruhl, Y. Schroeder, C. Bruemmer, A. Scholz, and M. Magnor, “Markerless motion capture using multiple color-depth sensors,” pp. and Visualization (2011)–, 2011.

[28] D. Vakhshoori, “Symmetry considerations in vertical-cavity surface-emitting lasers: Prediction of removal of polarization isotropicity on (001) substrates,” *Applied Physics Letters*, vol. 65, no. 3, pp. 259–261, jul 1994.

[29] A. Grunnet-Jepsen, J. N. Sweetser, P. Winer, A. Takagi, and J. Woodfill, *Projectors for Intel RealSense Depth Cameras D4xx*, rev. 1.0. [Online]. Available: https://www.intelrealsense.com/wp-content/uploads/2019/03/WhitePaper_on_Projectors_for_RealSense_D4xx_1.0.pdf

[30] Y. Hsu, A. Grunnet-Jepsen, J. Sweetser, and S. Brook, "D400 Series Visual Presets." [Online]. Available: https://dev.intelrealsense.com/docs/d400-series-visual-presets

[31] "YI 4K Action Camera," Accessed: 15.8.2020. [Online]. Available: https://www2.yitechnology.com/yi-4k-action-camera

A Deviation Figures

A.1 RealSense

A.2 HPS-3D160

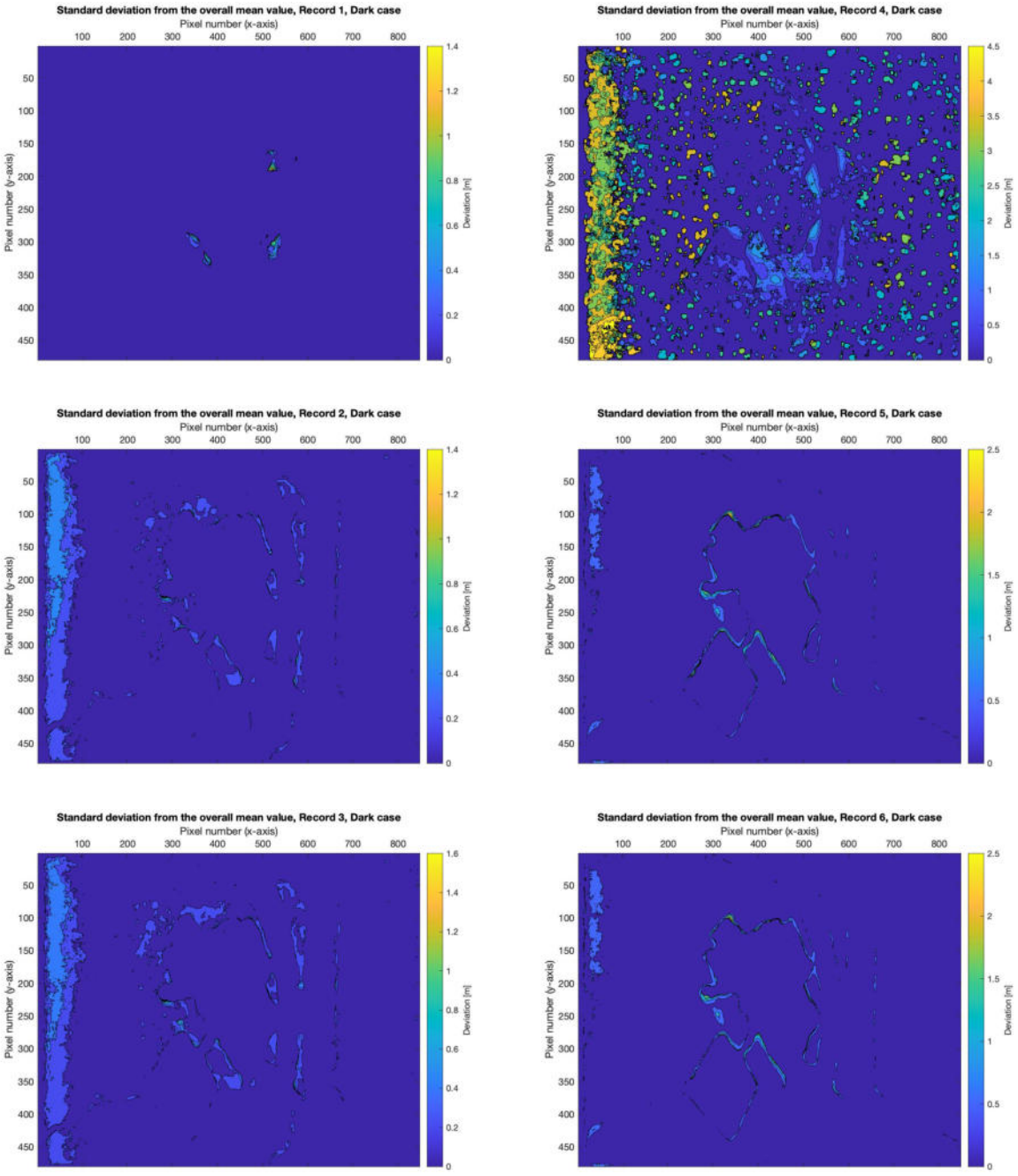

Fig. A–1: Standard Deviation for recording 1-6, Dark case, RealSense

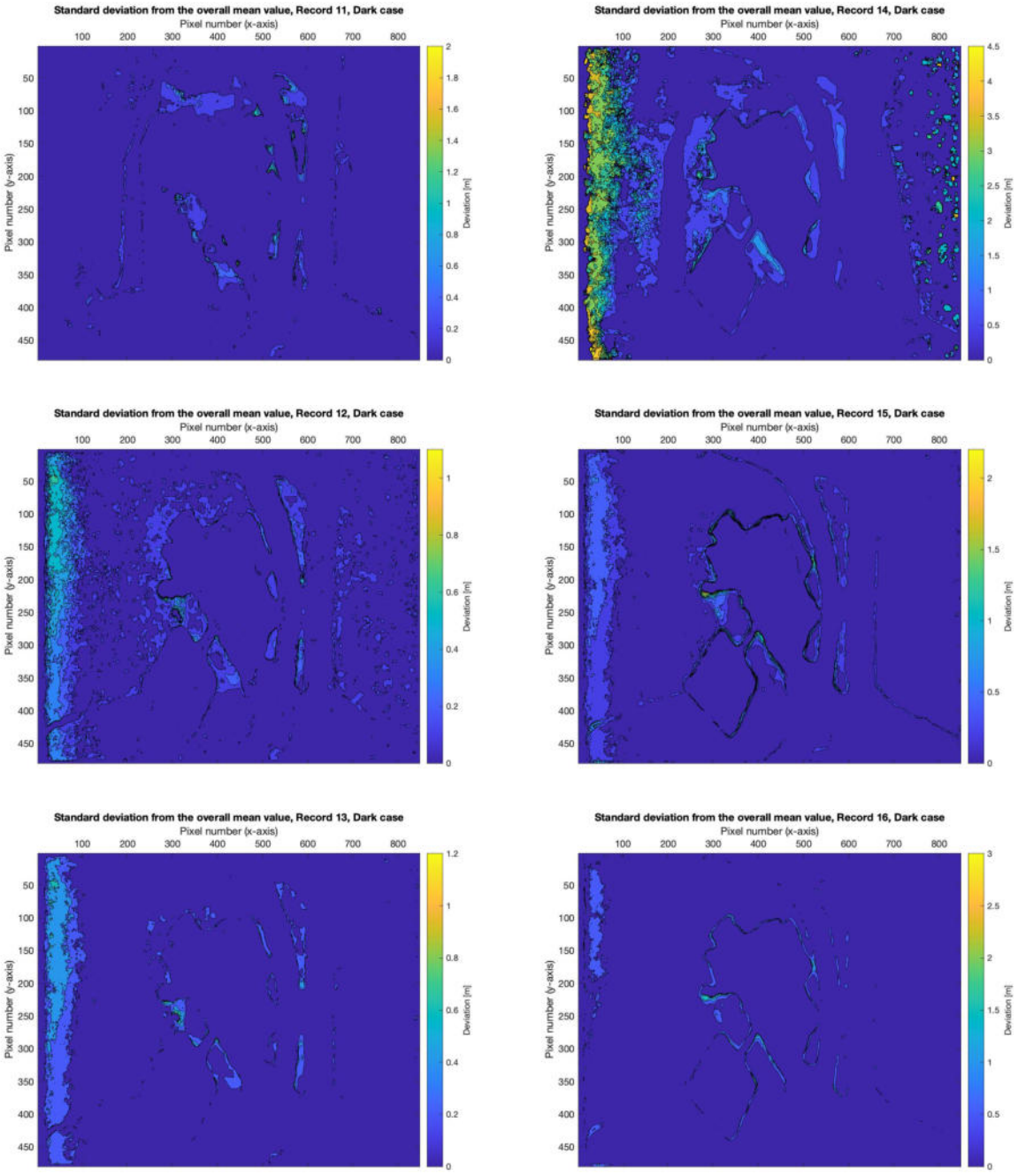

Fig. A–2: Standard Deviation for recording 11-16, Dark case, RealSense

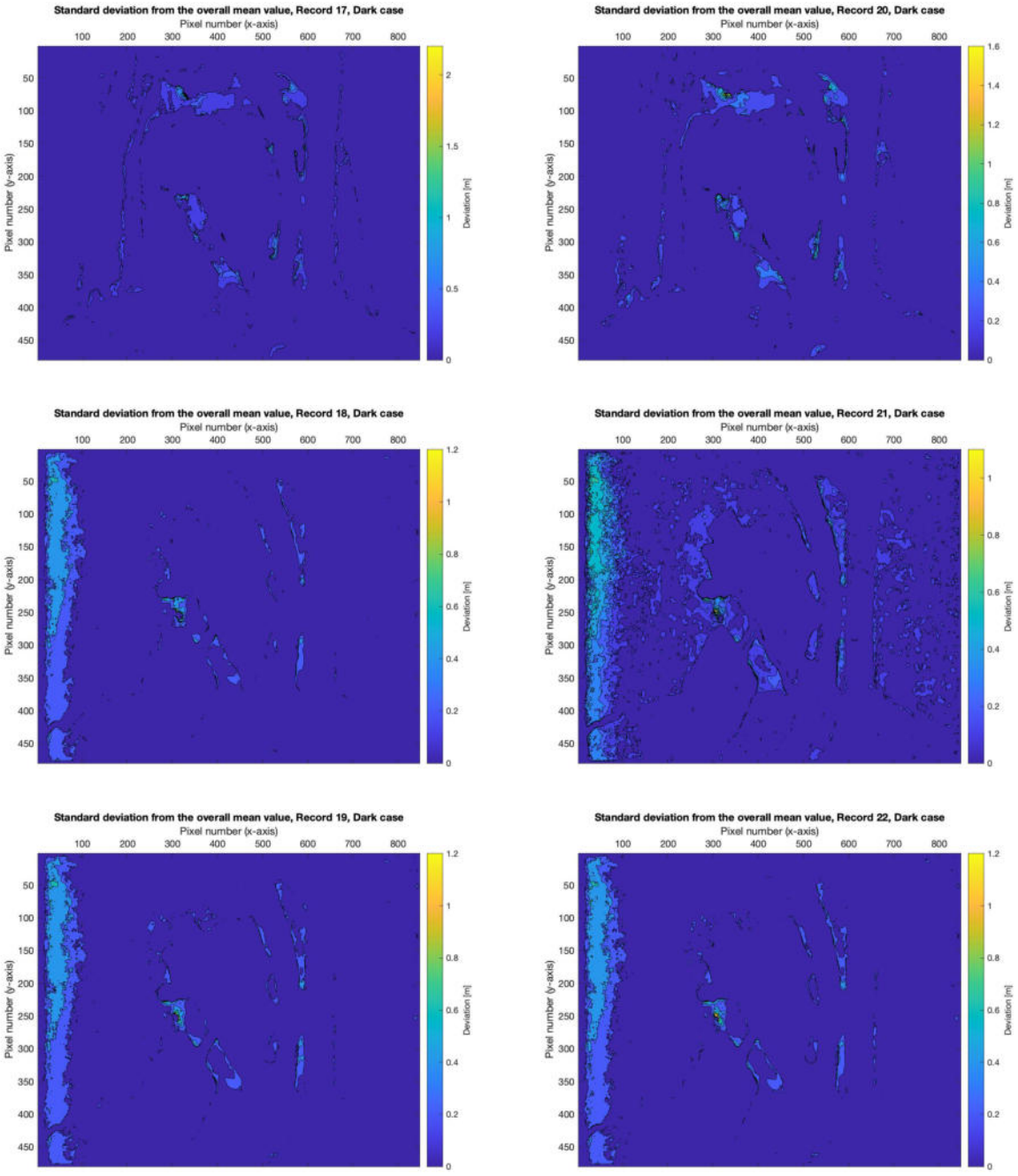

Fig. A–3: Standard Deviation for recording 17-22, Dark case, RealSense

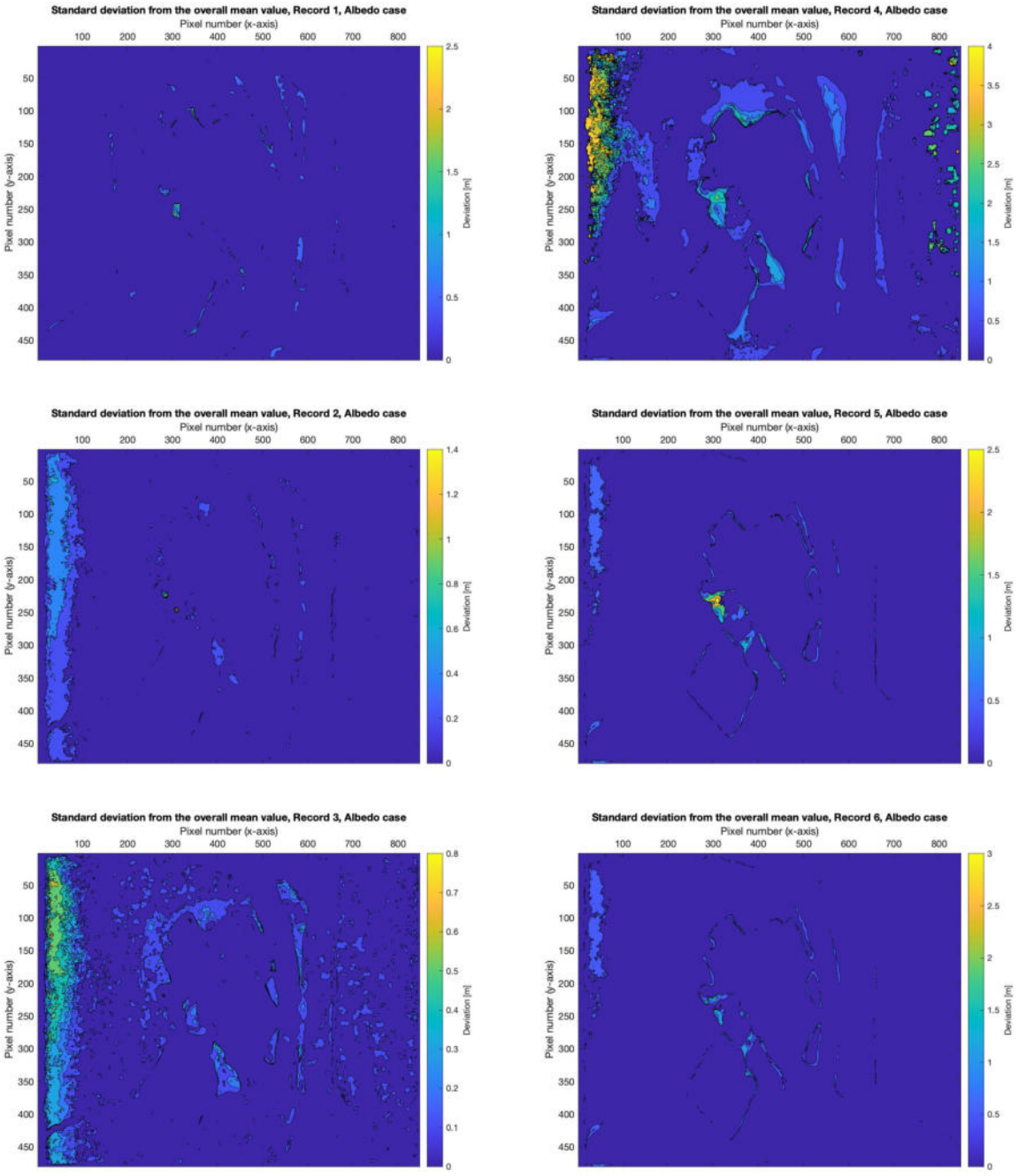

Fig. A–4: Standard Deviation for recording 1-6, Albedo case, RealSense

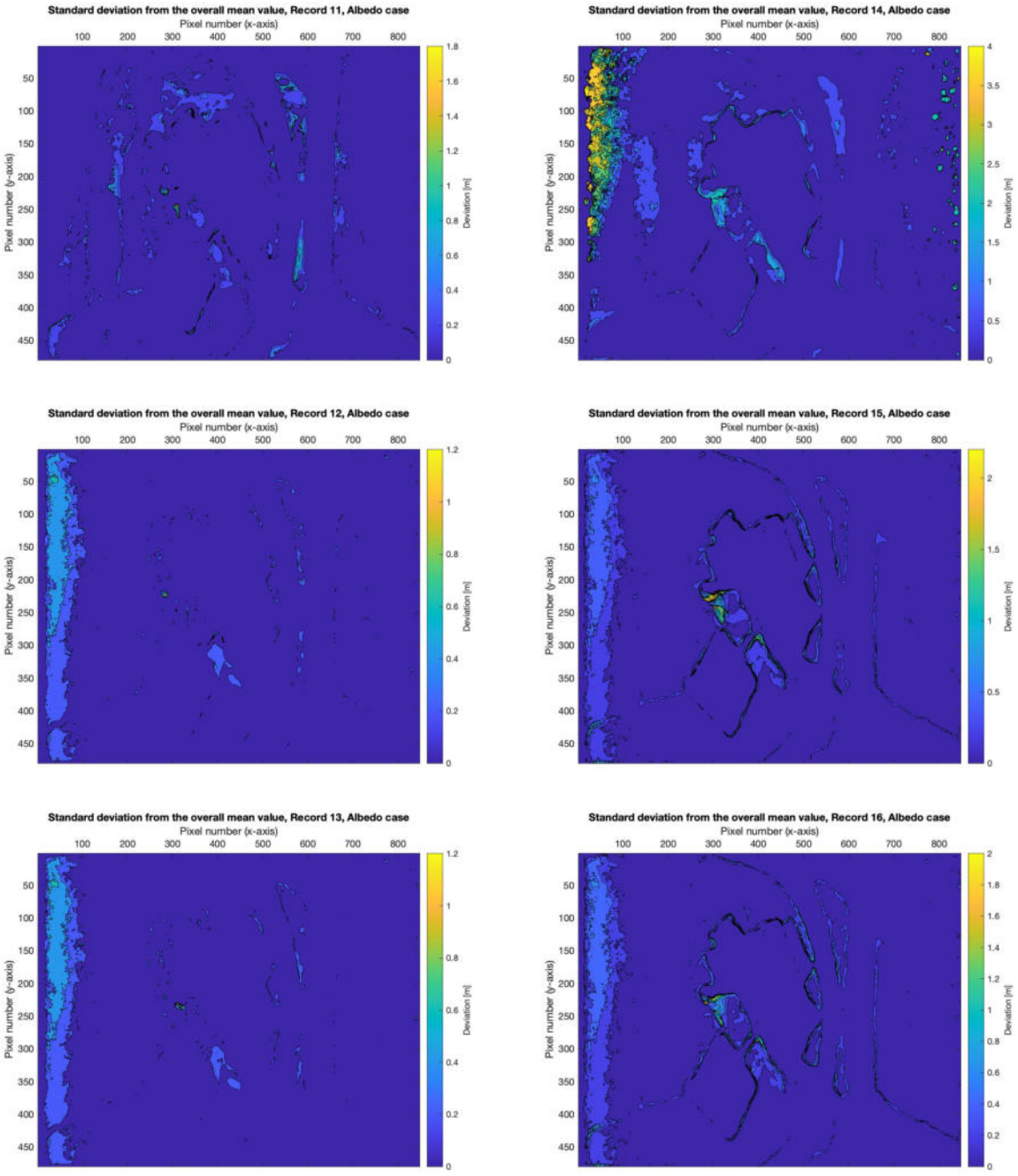

Fig. A–5: Standard Deviation for recording 11-16, Albedo case, RealSense

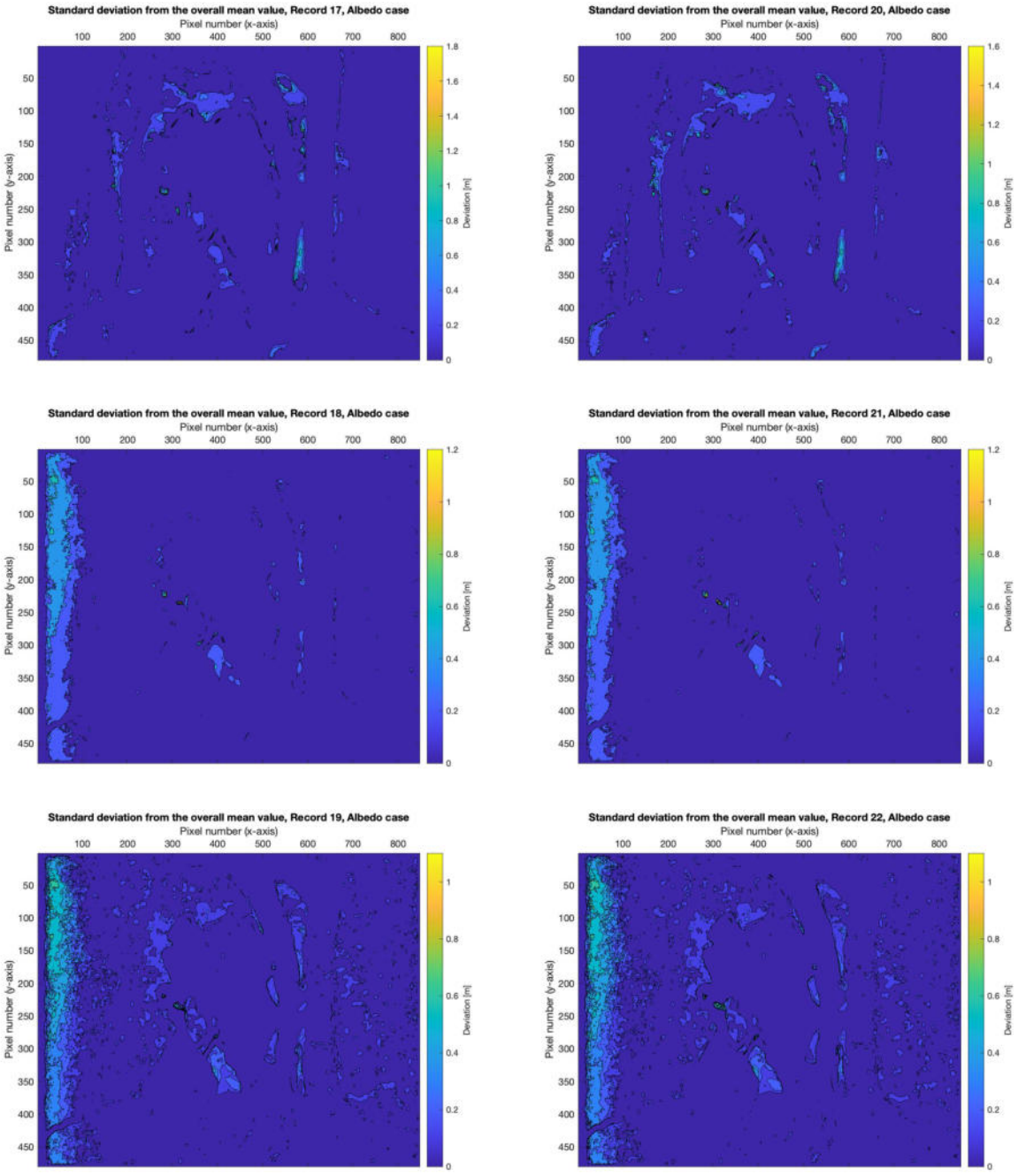

Fig. A–6: Standard Deviation for recording 17-22, Albedo case, RealSense

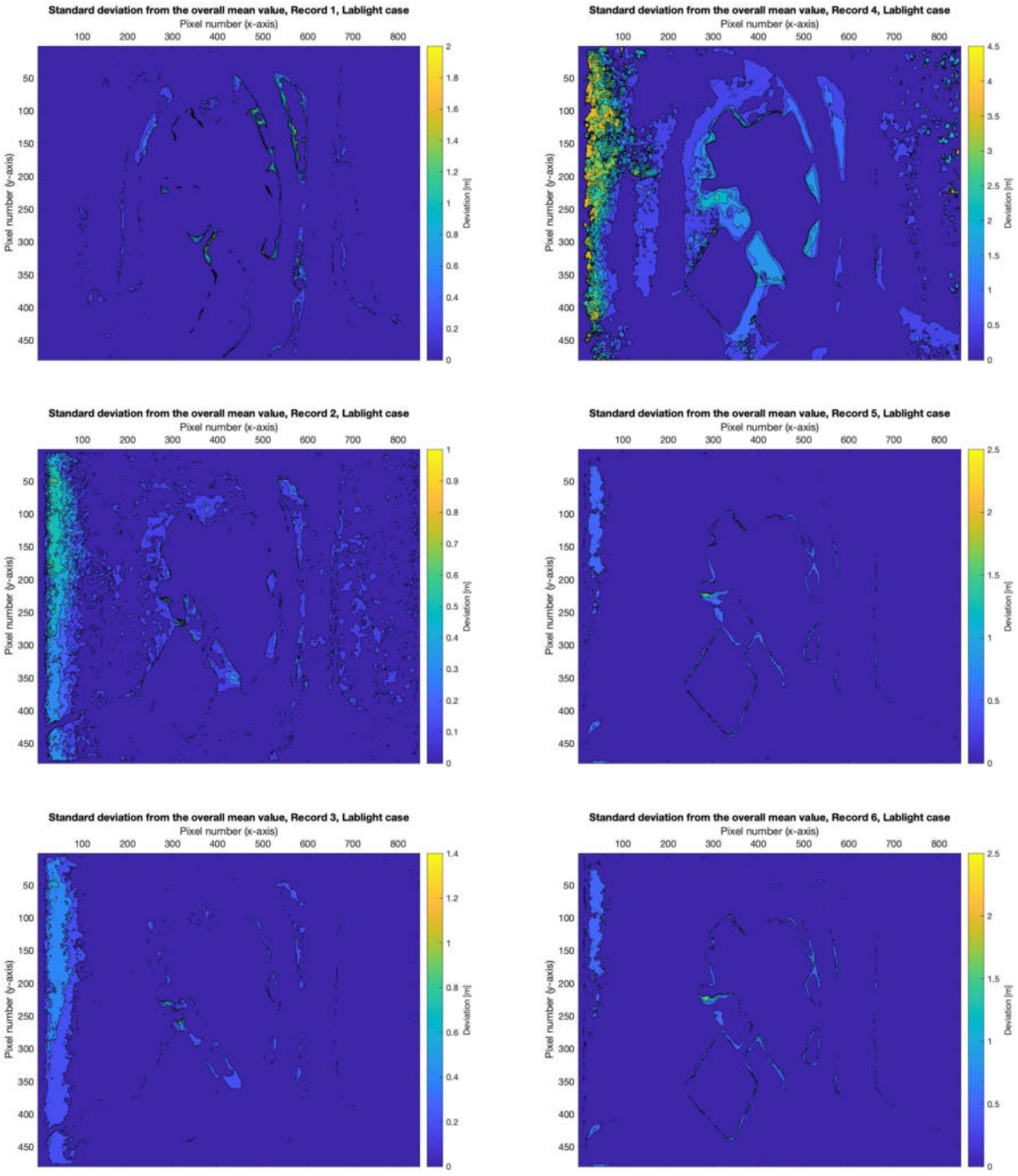

Fig. A–7: Standard Deviation for recording 1-6, Lablight case, RealSense

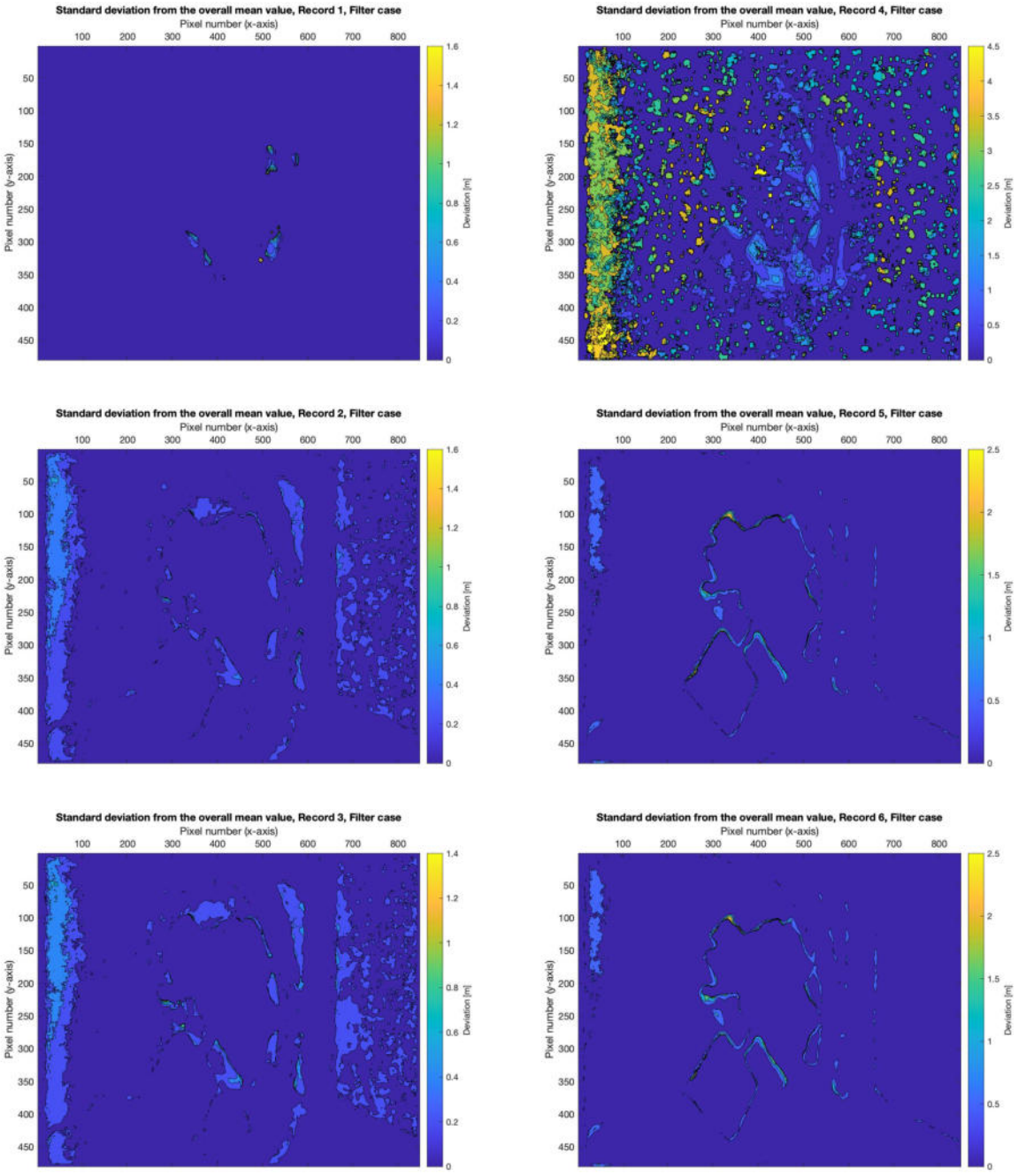

Fig. A–8: Standard Deviation for recording 1-6, Filter case, RealSense

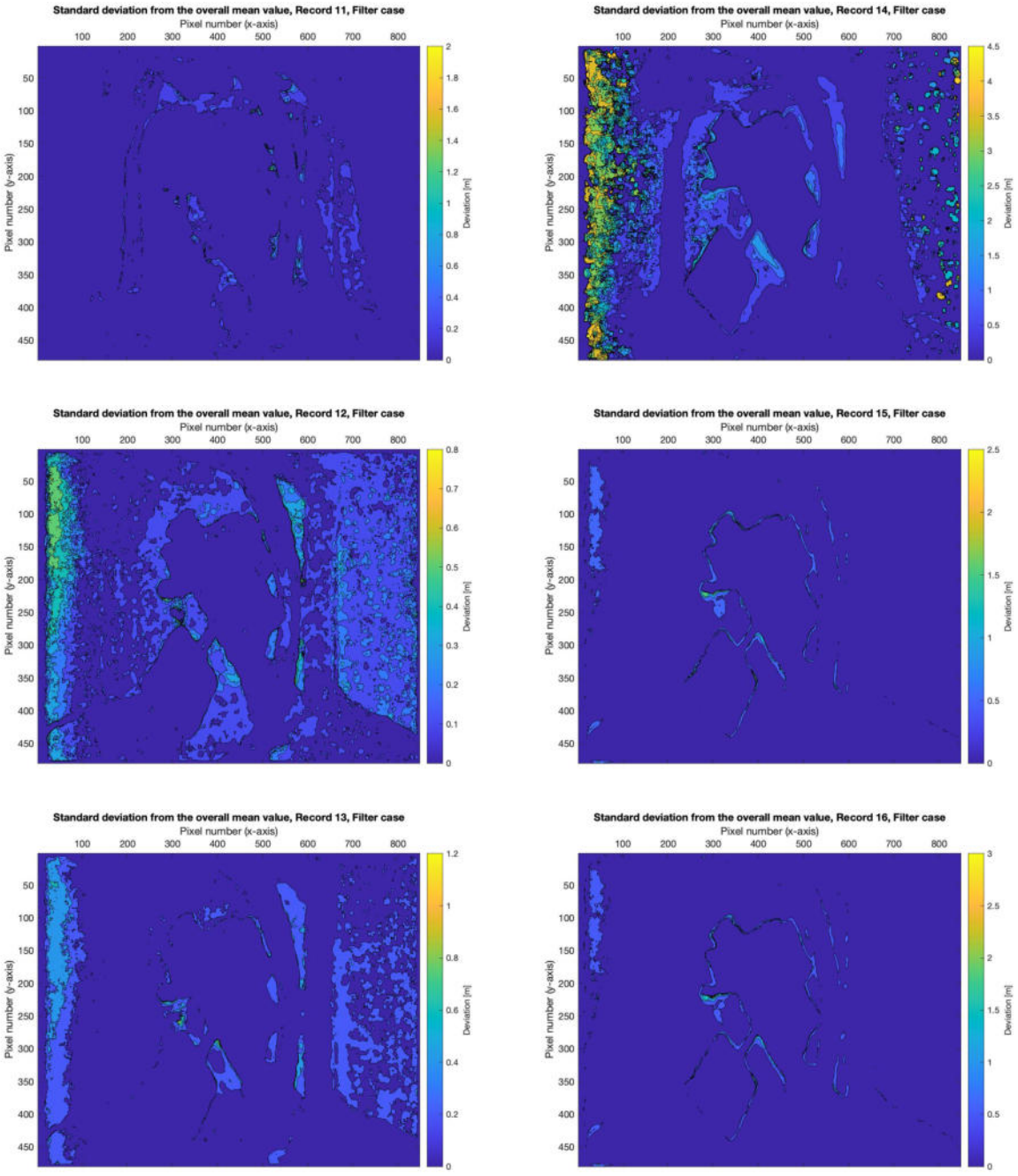

Fig. A–9: Standard Deviation for recording 11-16, Filter case, RealSense

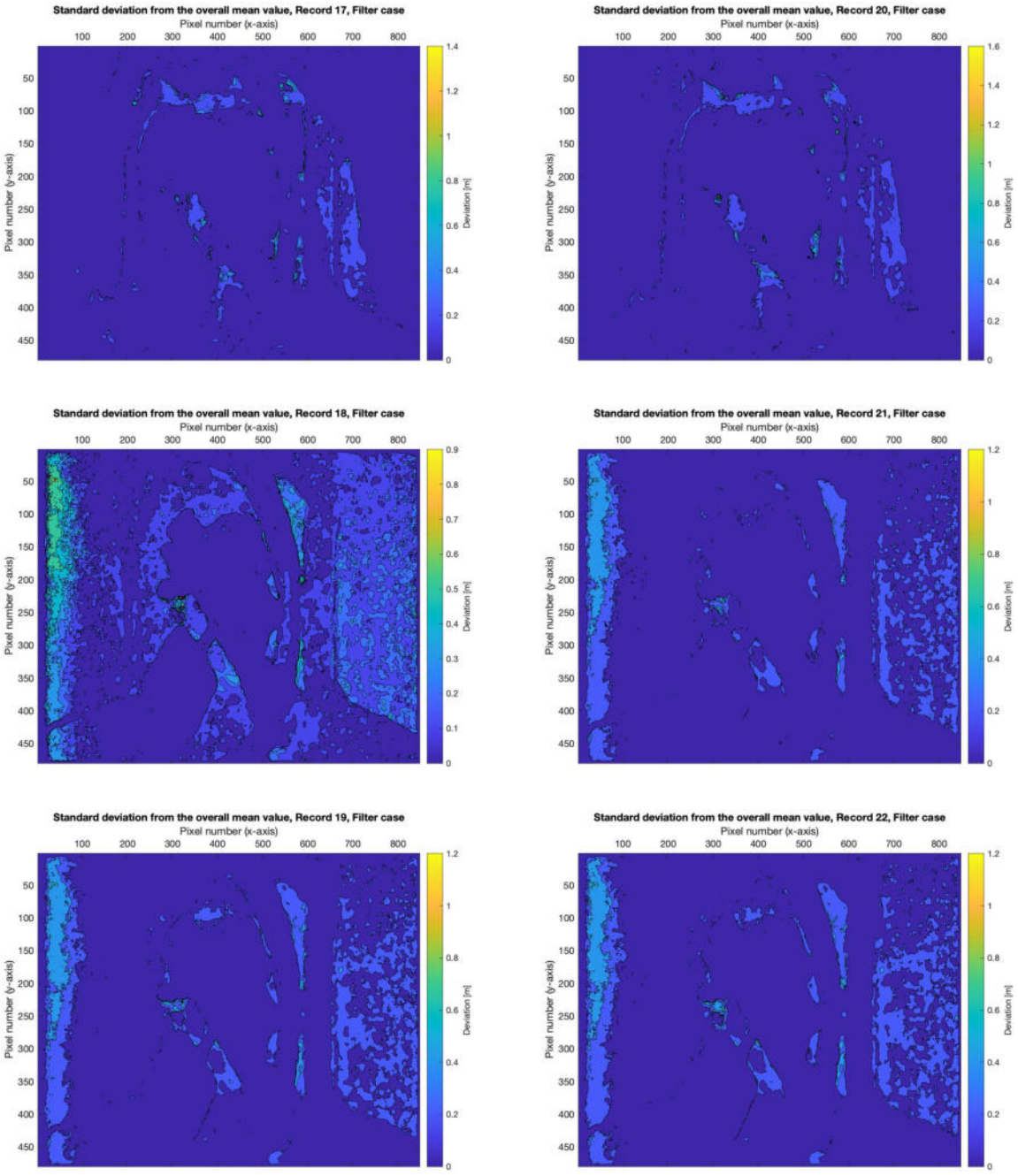

Fig. A–10: Standard Deviation for recording 17-22, Filter case, RealSense

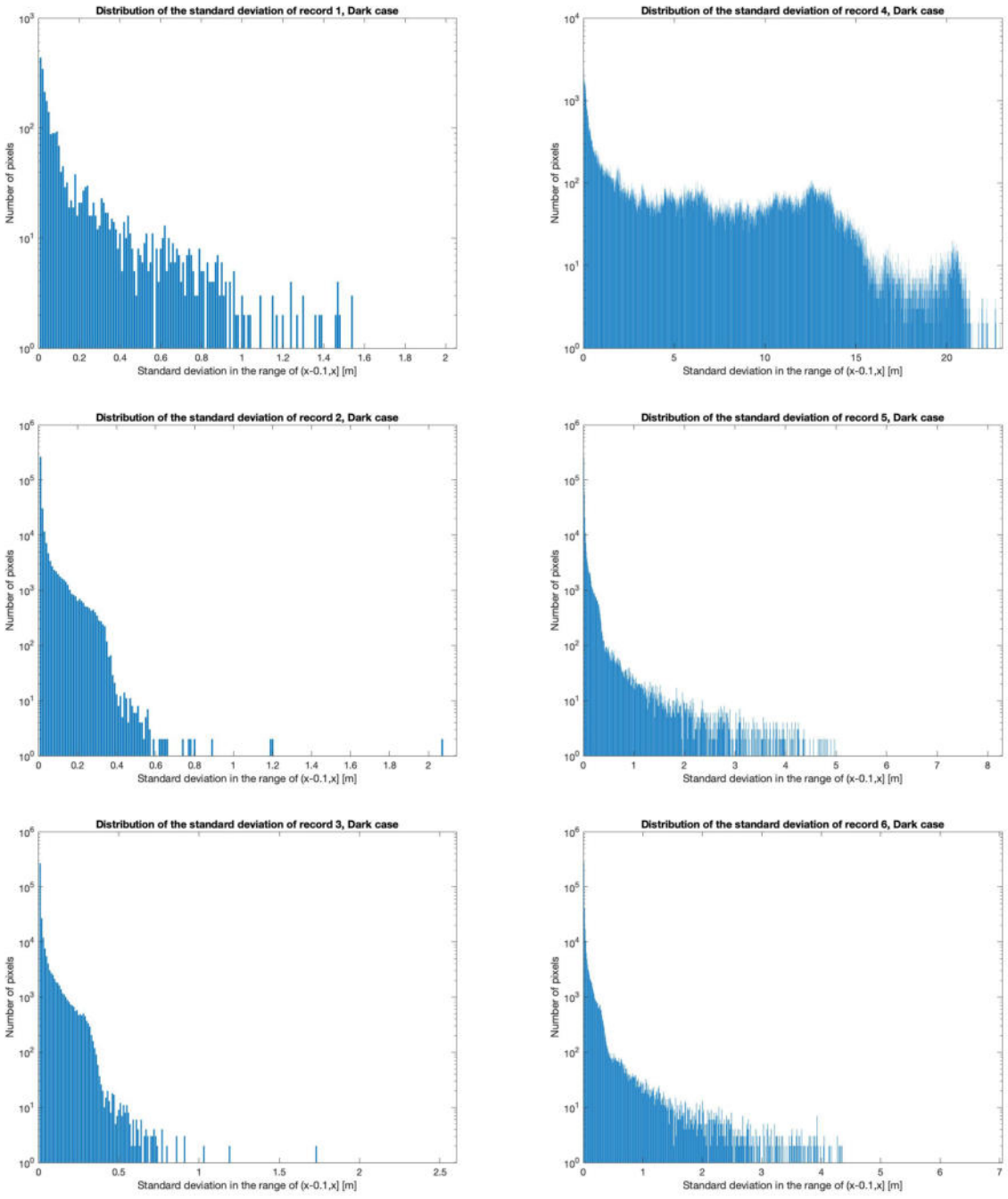

Fig. A–11: Distribution of the standard deviation for recording 1-6, Dark case, RealSense

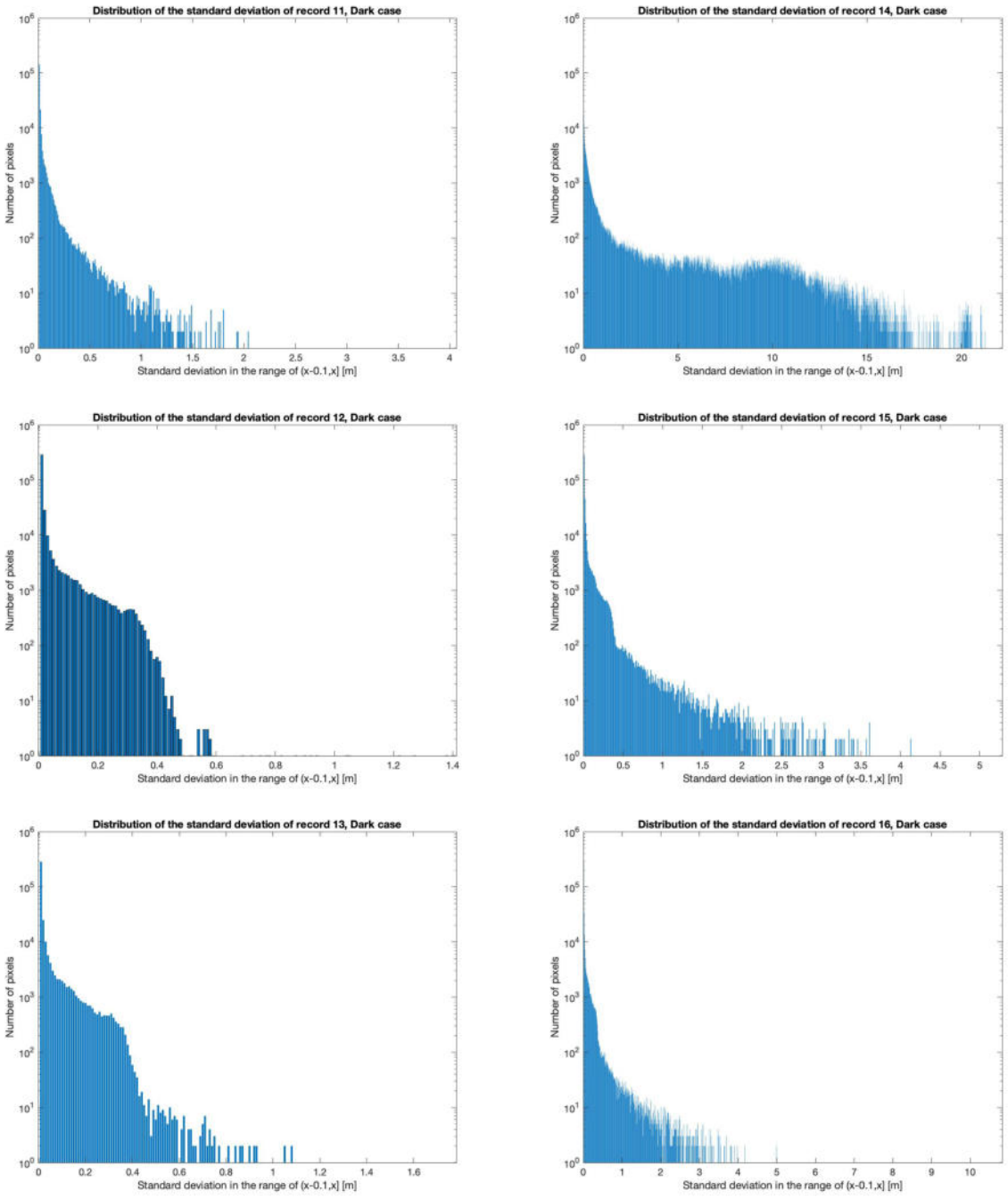

Fig. A–12: Distribution of the standard deviation for recording 11-16, Dark case, RealSense

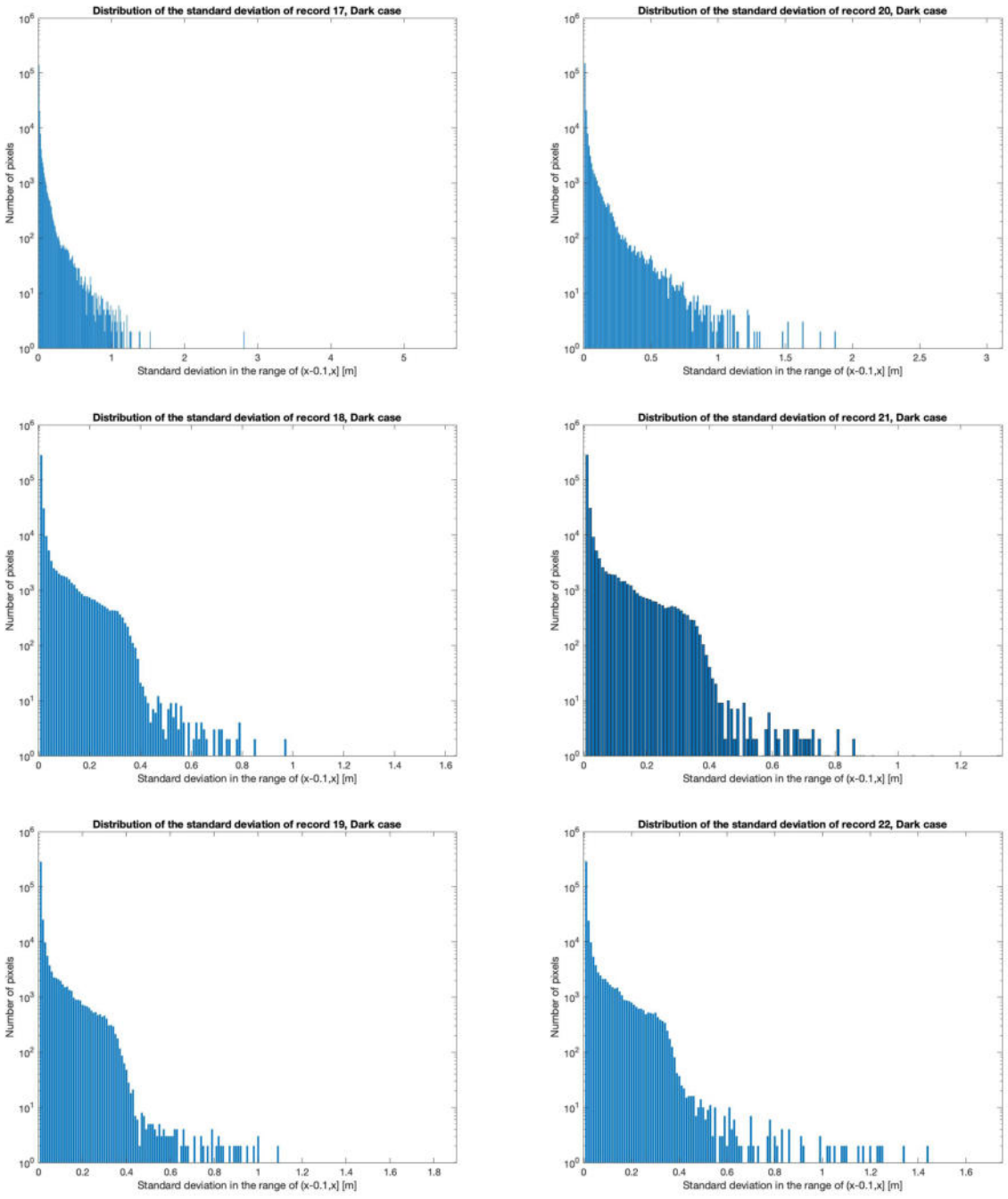

Fig. A–13: Distribution of the standard deviation for recording 17-22, Dark case, RealSense

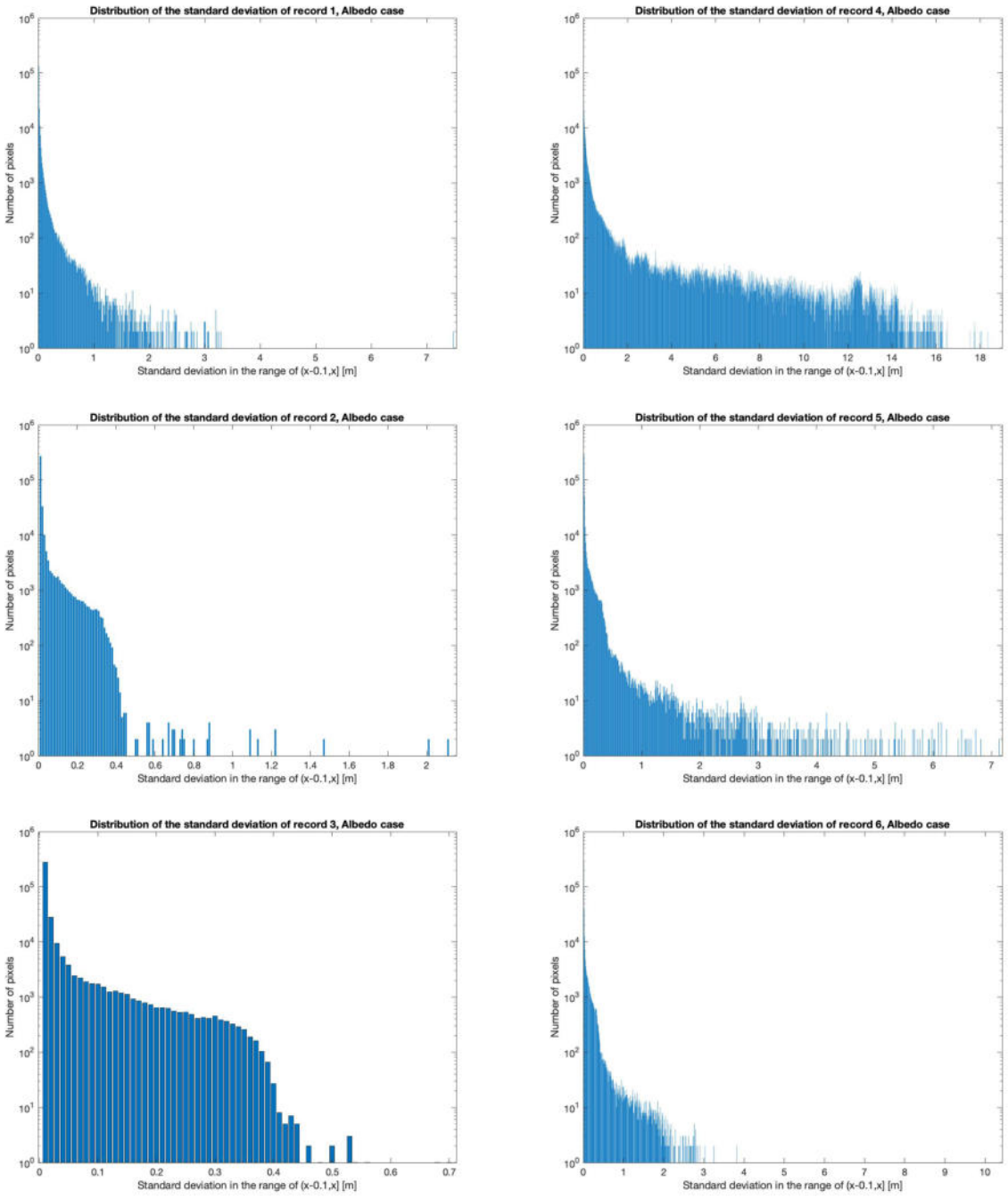

Fig. A–14: Distribution of the standard deviation for recording 1-6, Albedo case, RealSense

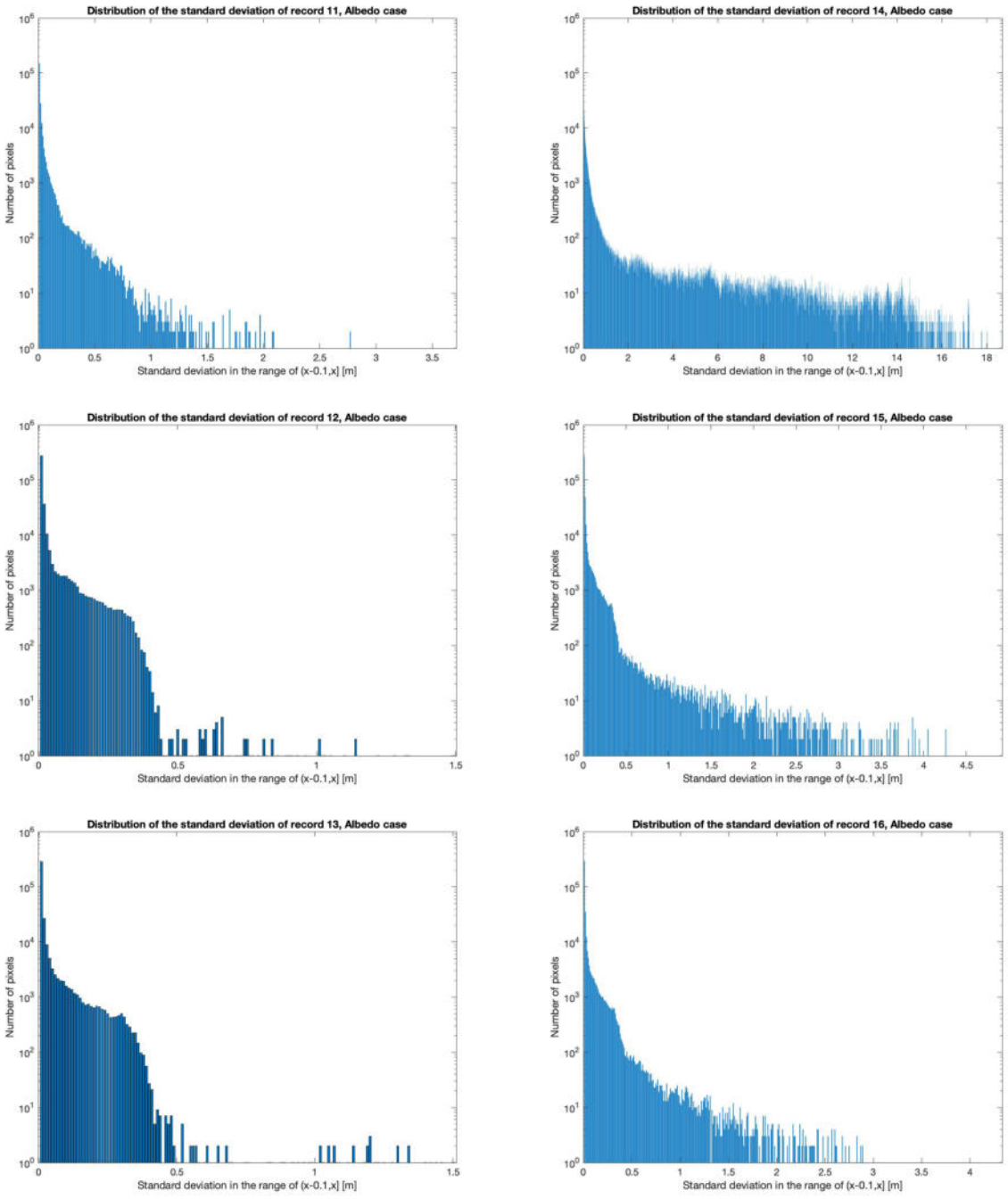

Fig. A–15: Distribution of the standard deviation for recording 11-16, Albedo case, RealSense

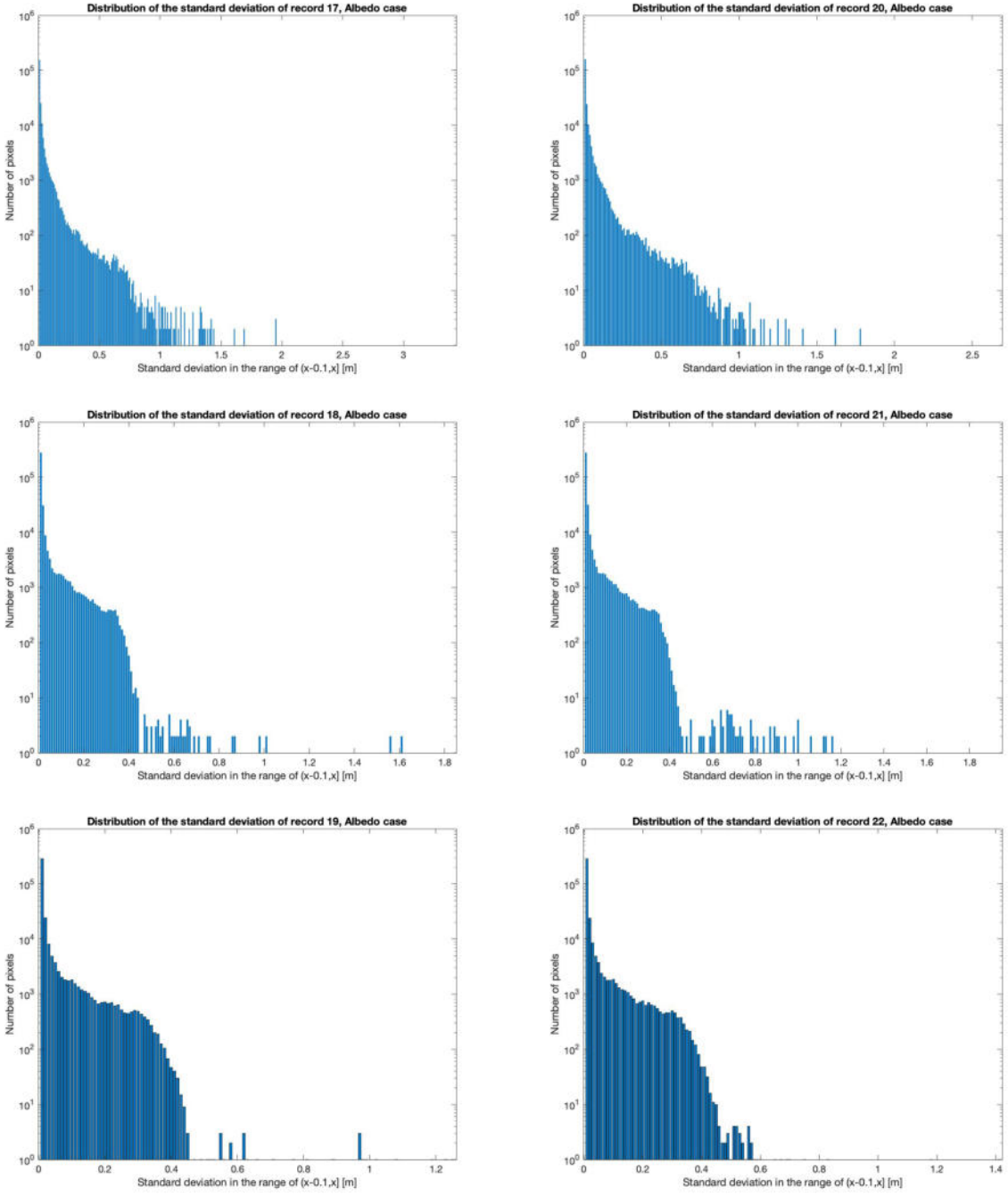

Fig. A–16: Distribution of the standard deviation for recording 17-22, Albedo case, RealSense

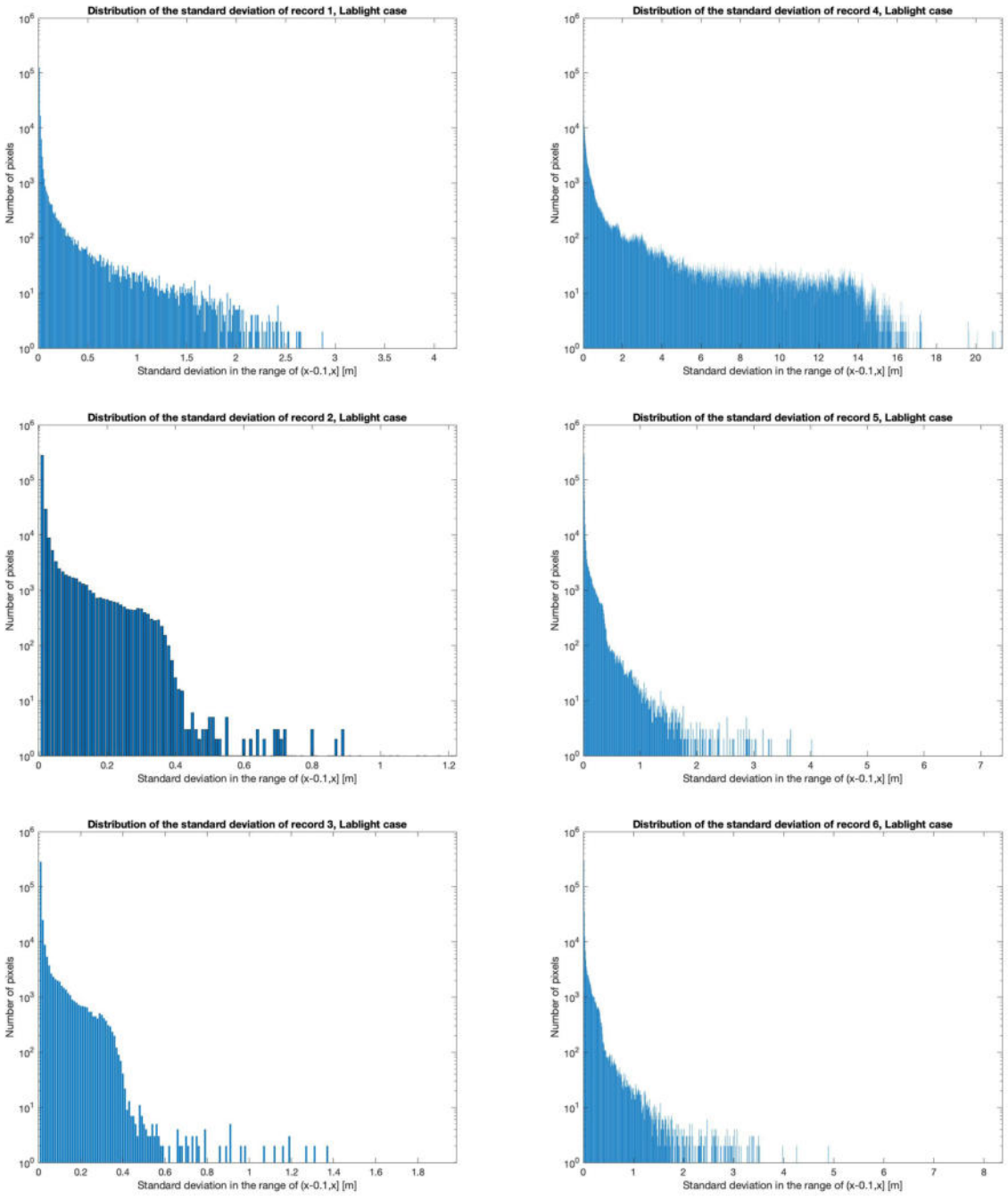

Fig. A–17: Distribution of the standard deviation for recording 1-6, Lablight case, RealSense

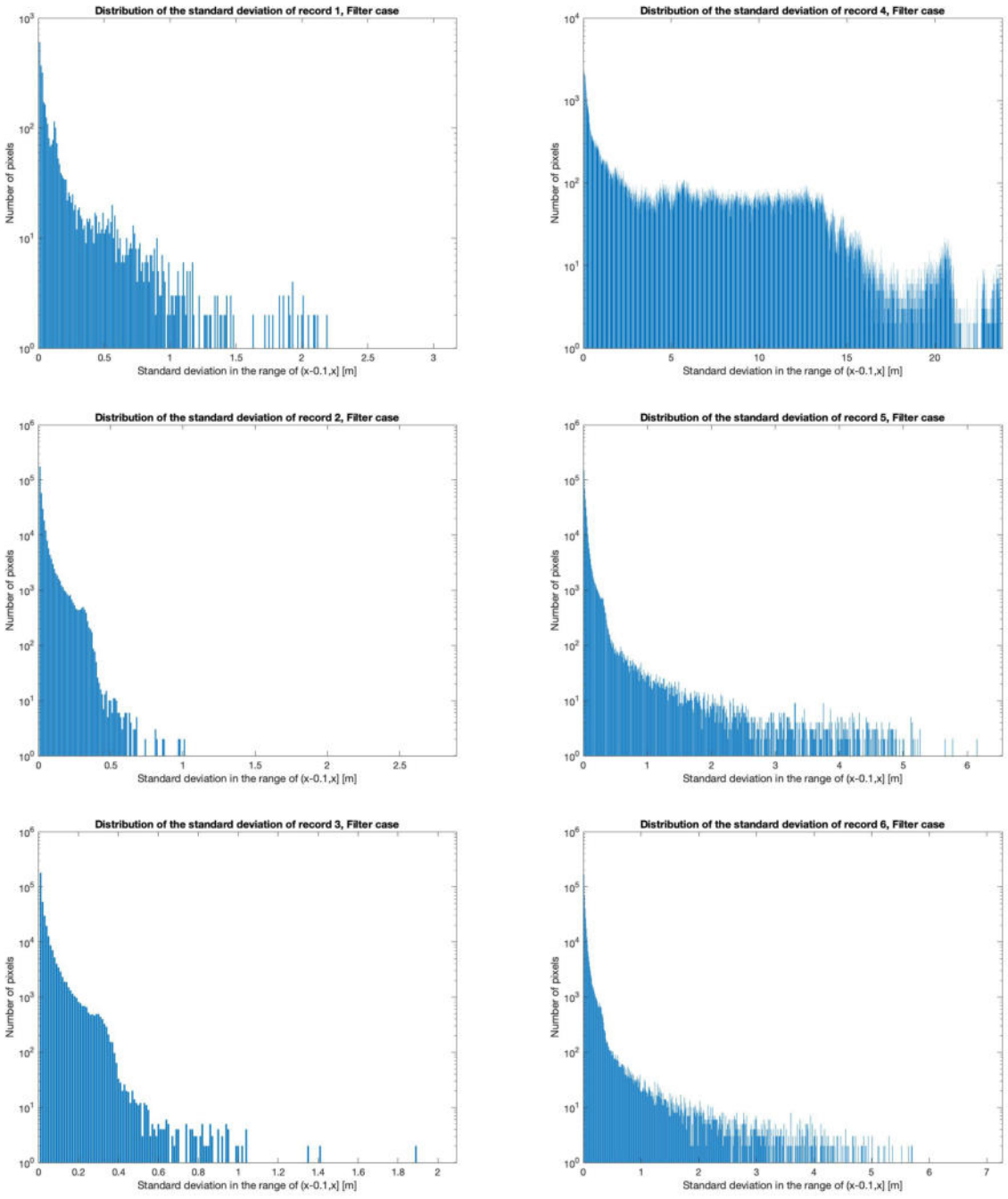

Fig. A–18: Distribution of the standard deviation for recording 1-6, Filter case, RealSense

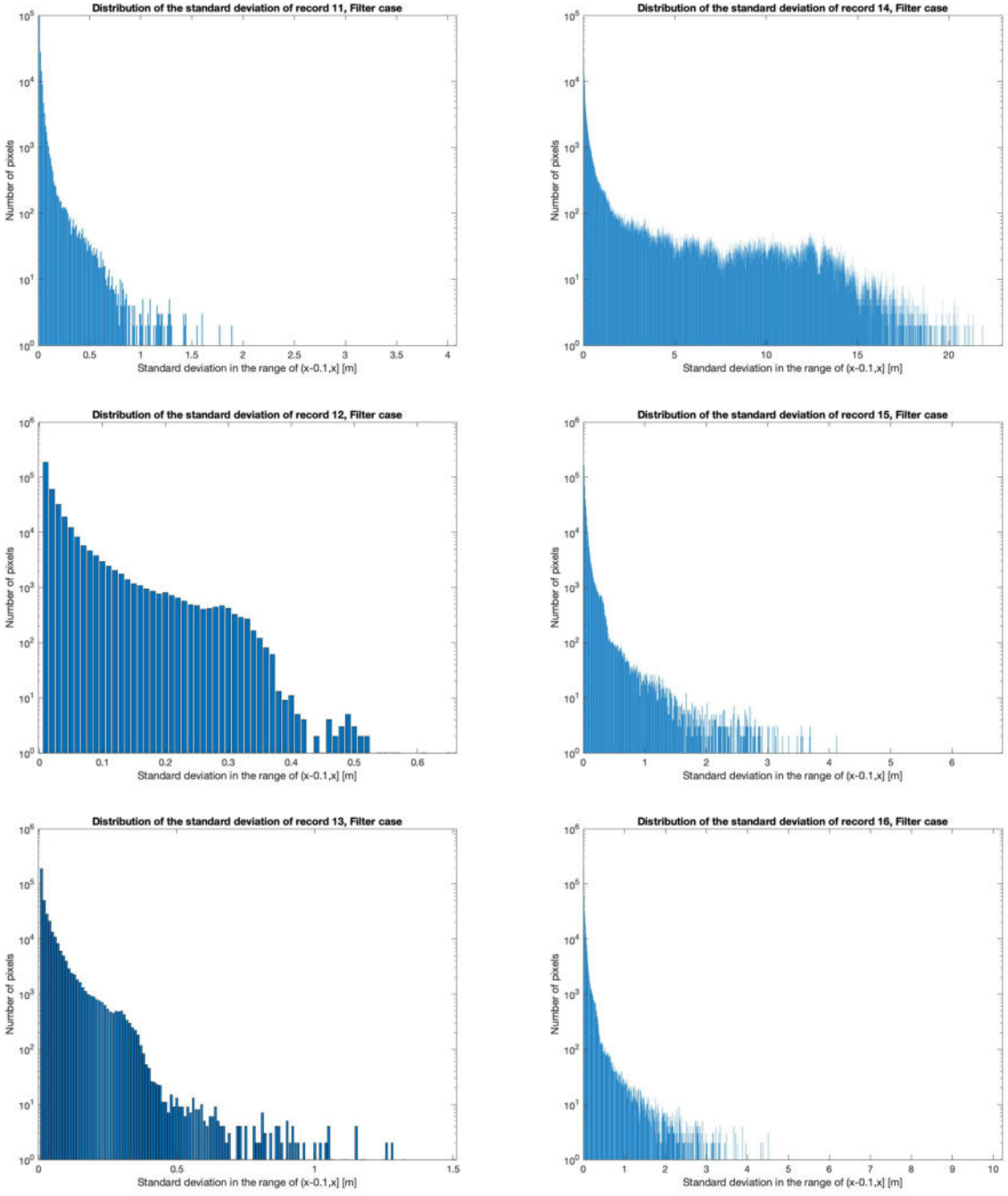

Fig. A–19: Distribution of the standard deviation for recording 11-16, Filter case, RealSense

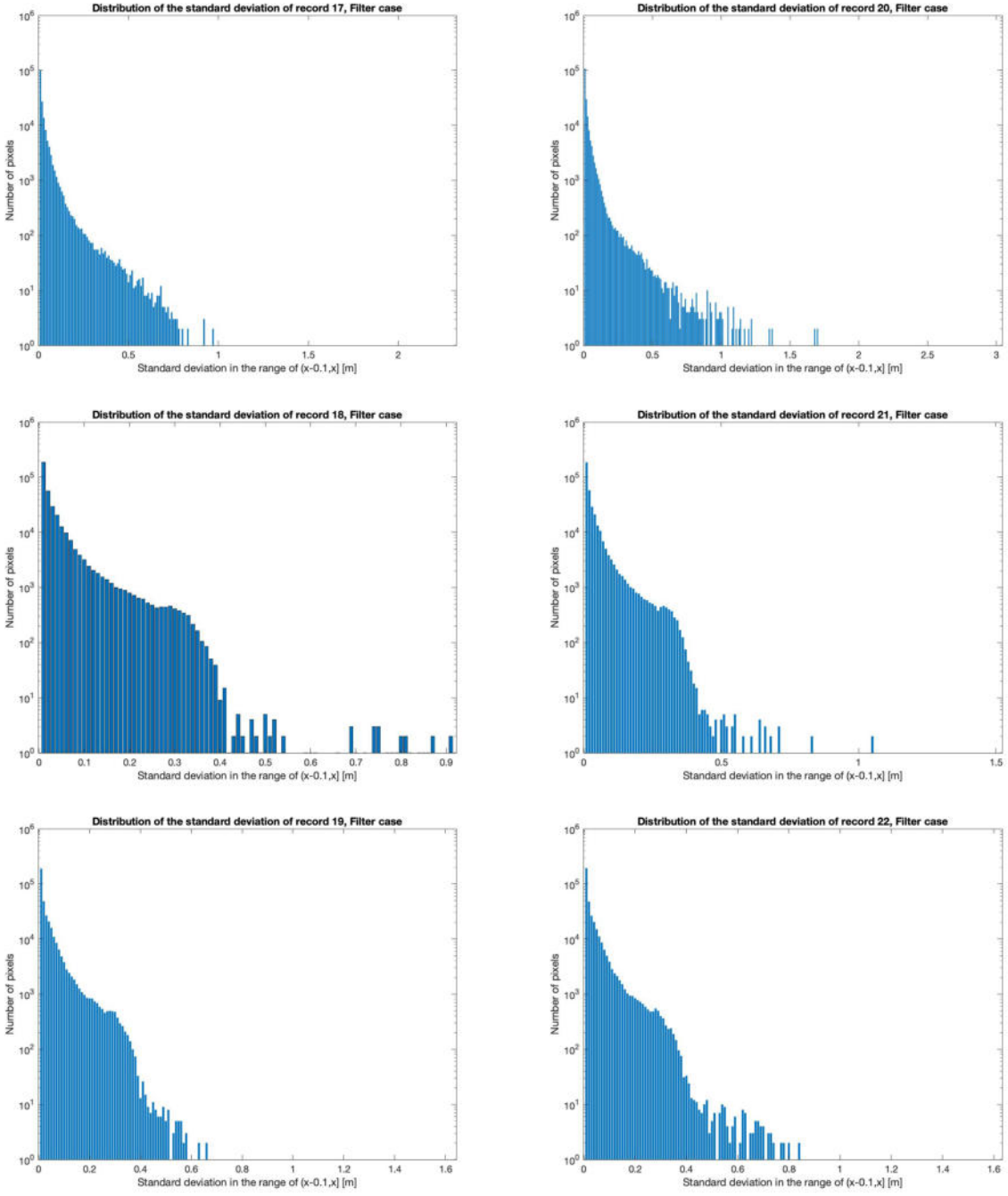

Fig. A–20: Distribution of the standard deviation for recording 17-22, Filter case, RealSense

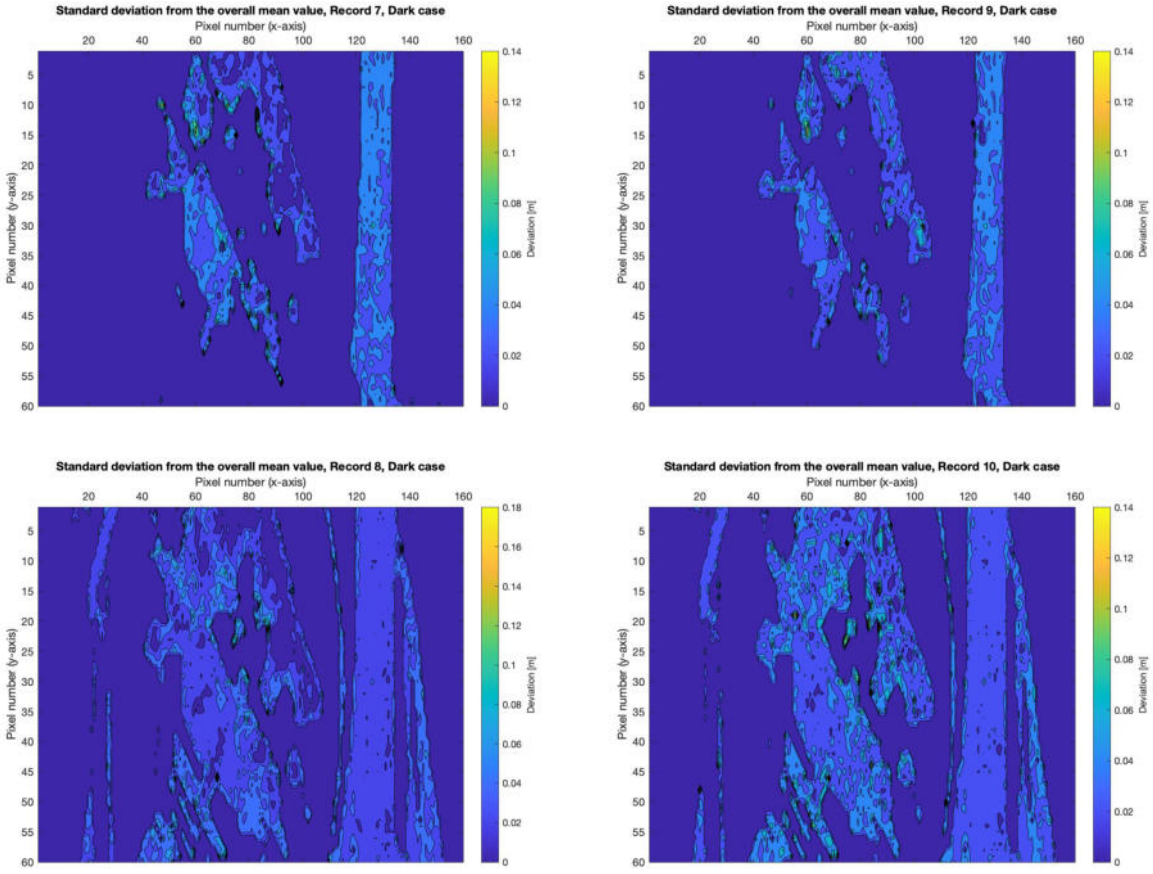

Fig. A–21: Standard Deviation for recording 7-10, Dark case, HPS-3D160

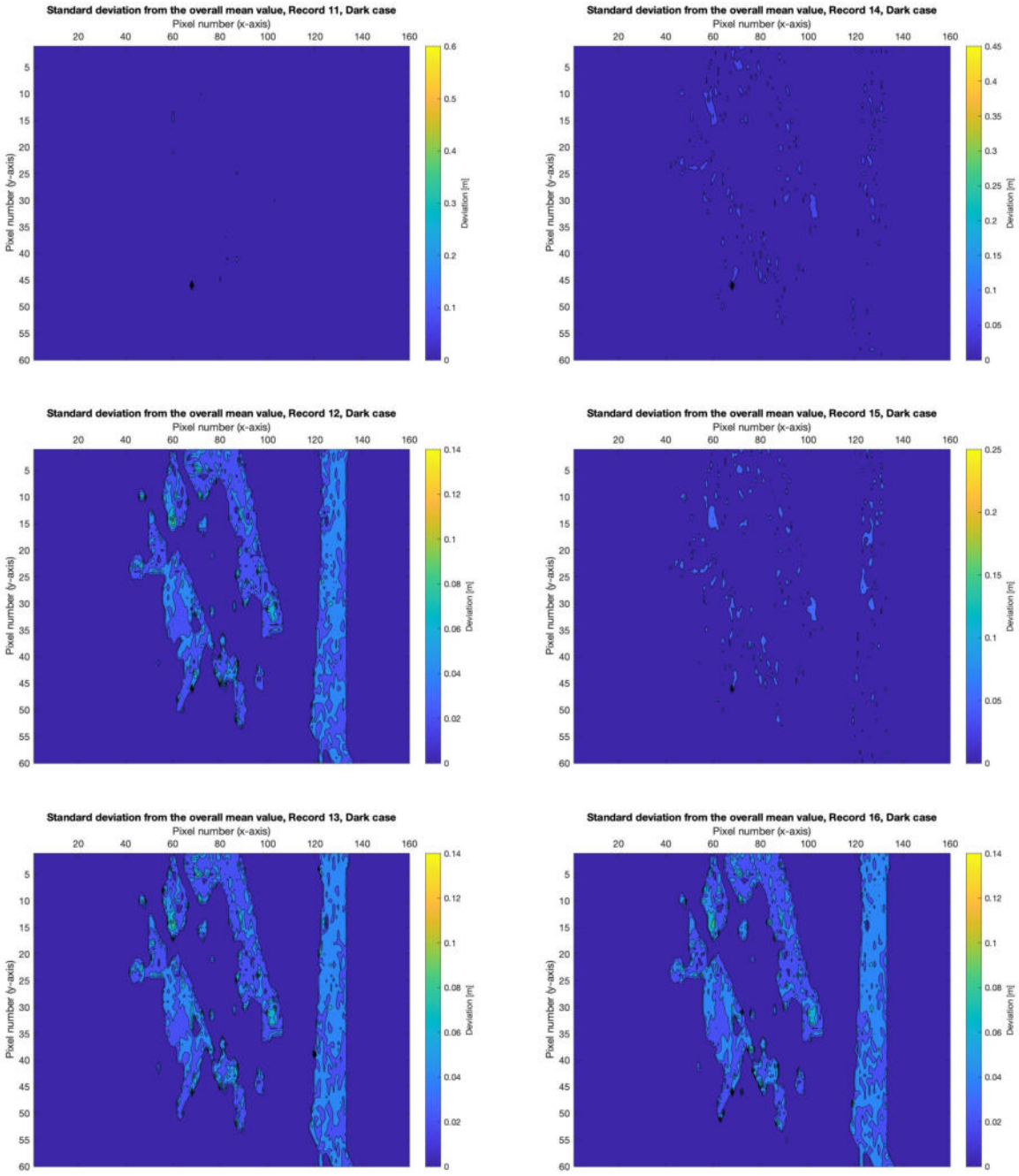

Fig. A–22: Standard Deviation for recording 11-16, Dark case, HPS-3D160

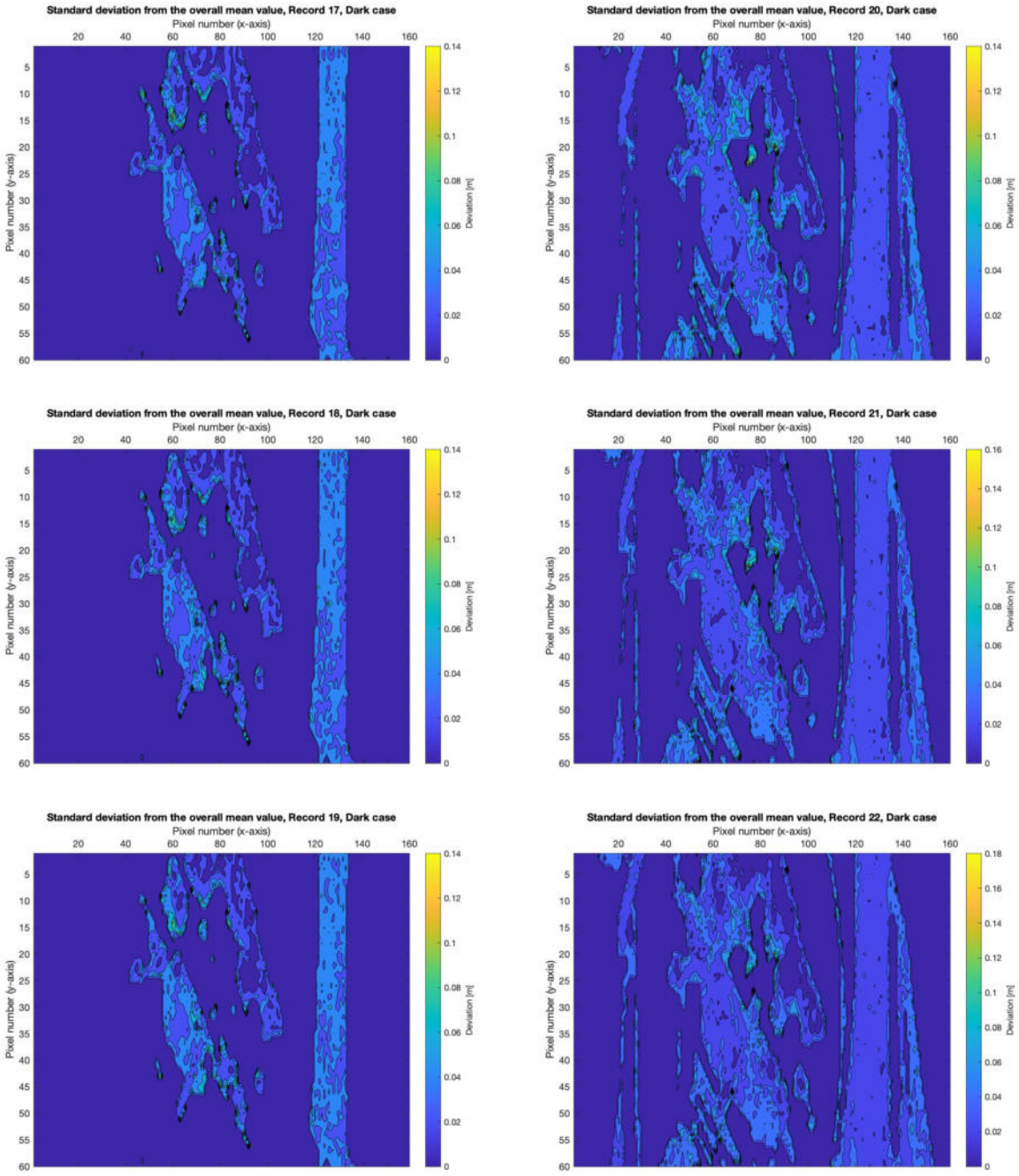

Fig. A–23: Standard Deviation for recording 17-22, Dark case, HPS-3D160

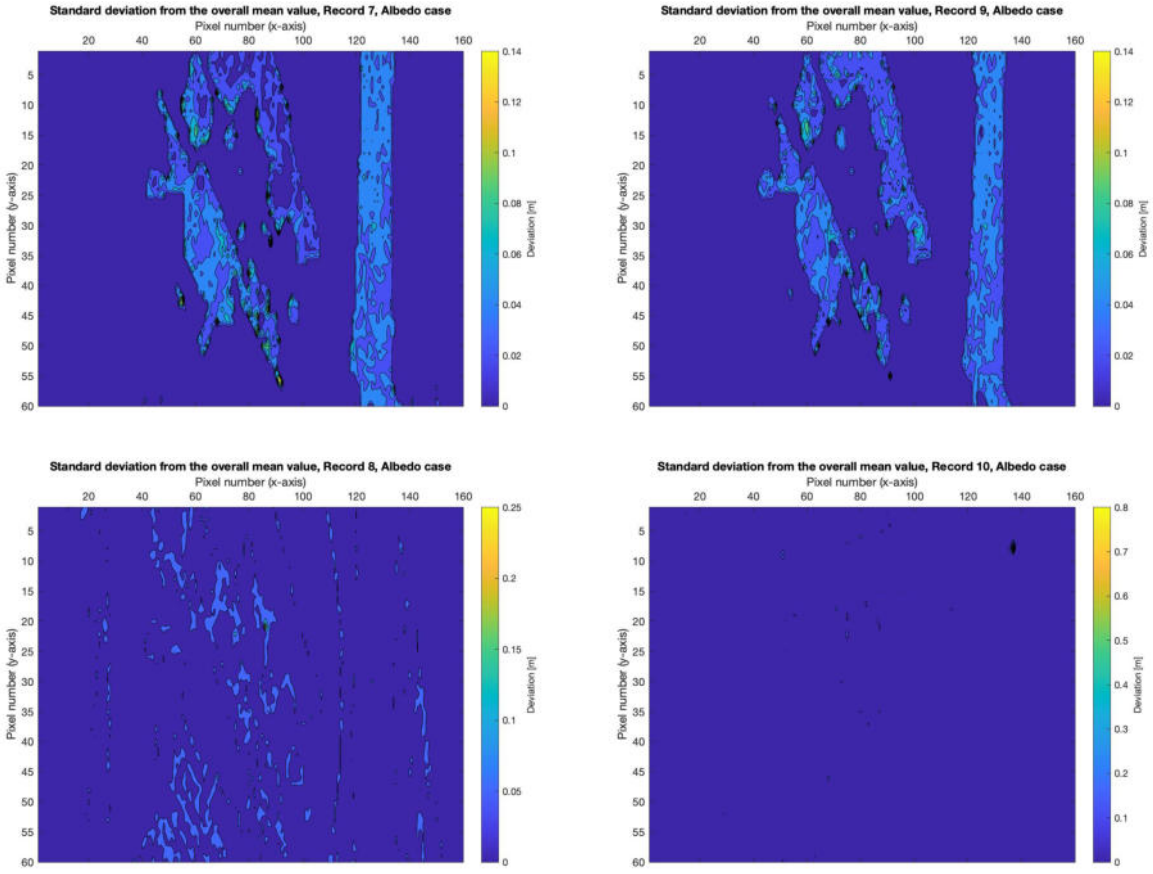

Fig. A–24: Standard Deviation for recording 7-10, Albedo case, HPS-3D160

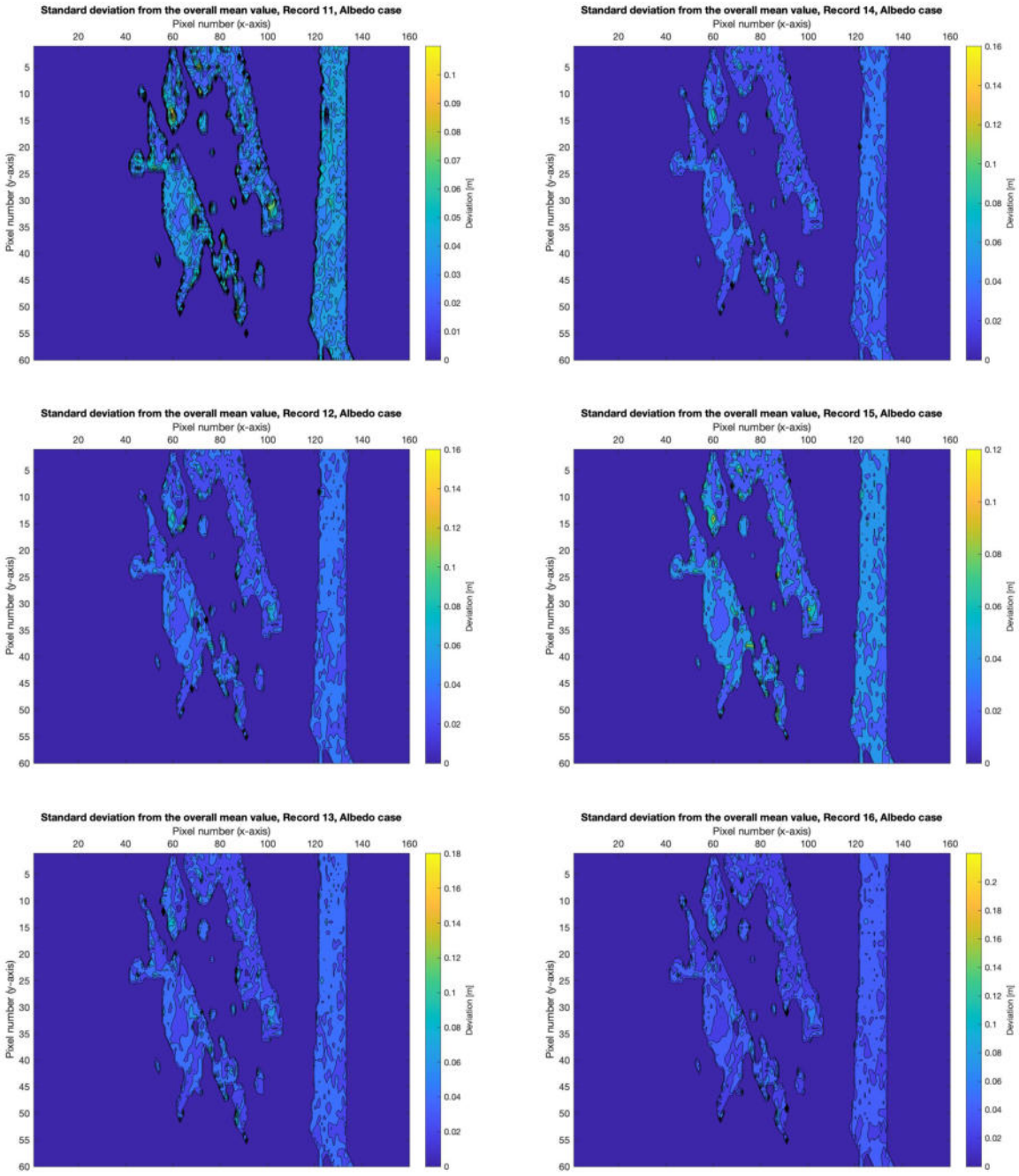

Fig. A–25: Standard Deviation for recording 11-16, Albedo case, HPS-3D160

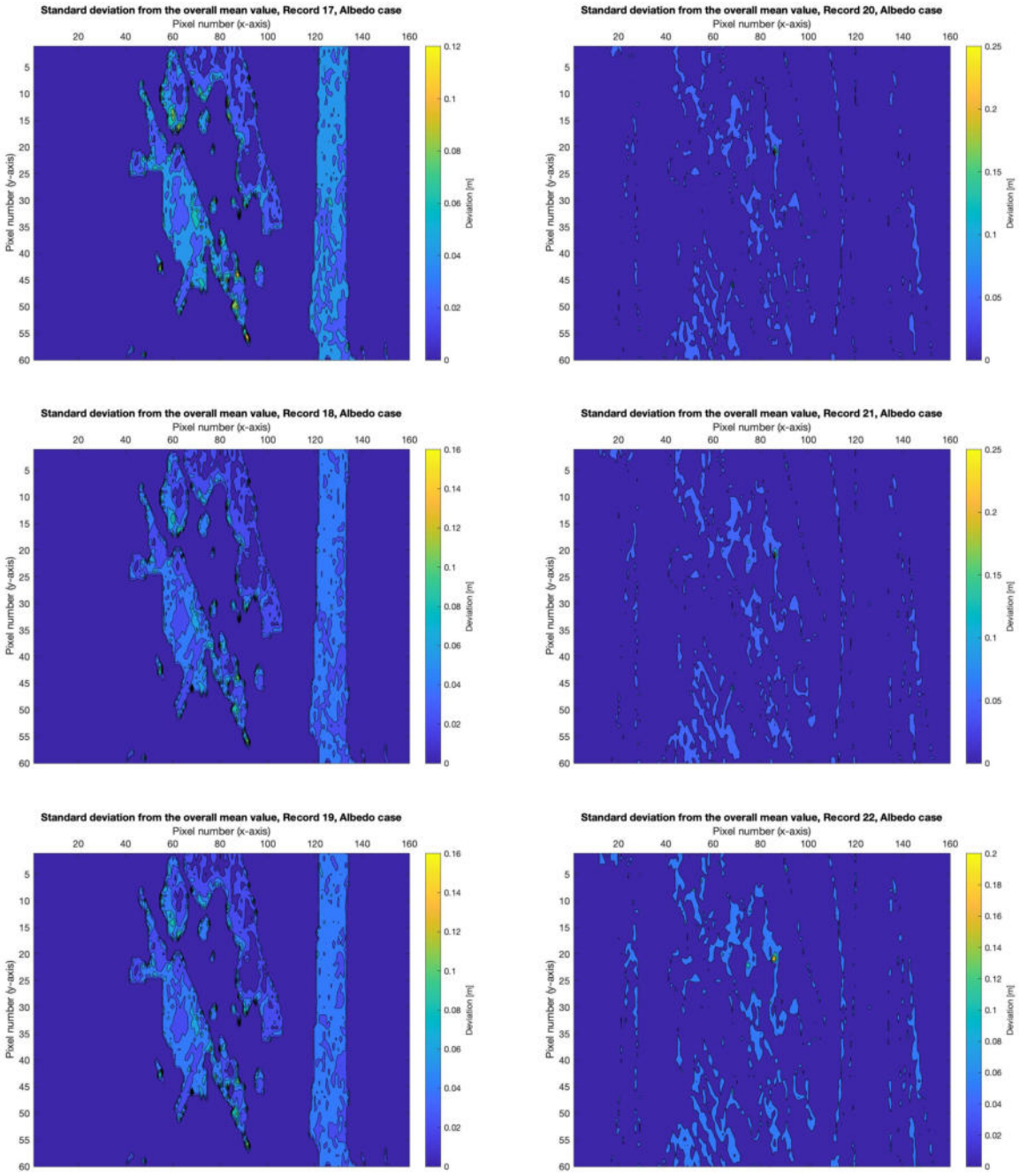

Fig. A–26: Standard Deviation for recording 17-22, Albedo case, HPS-3D160

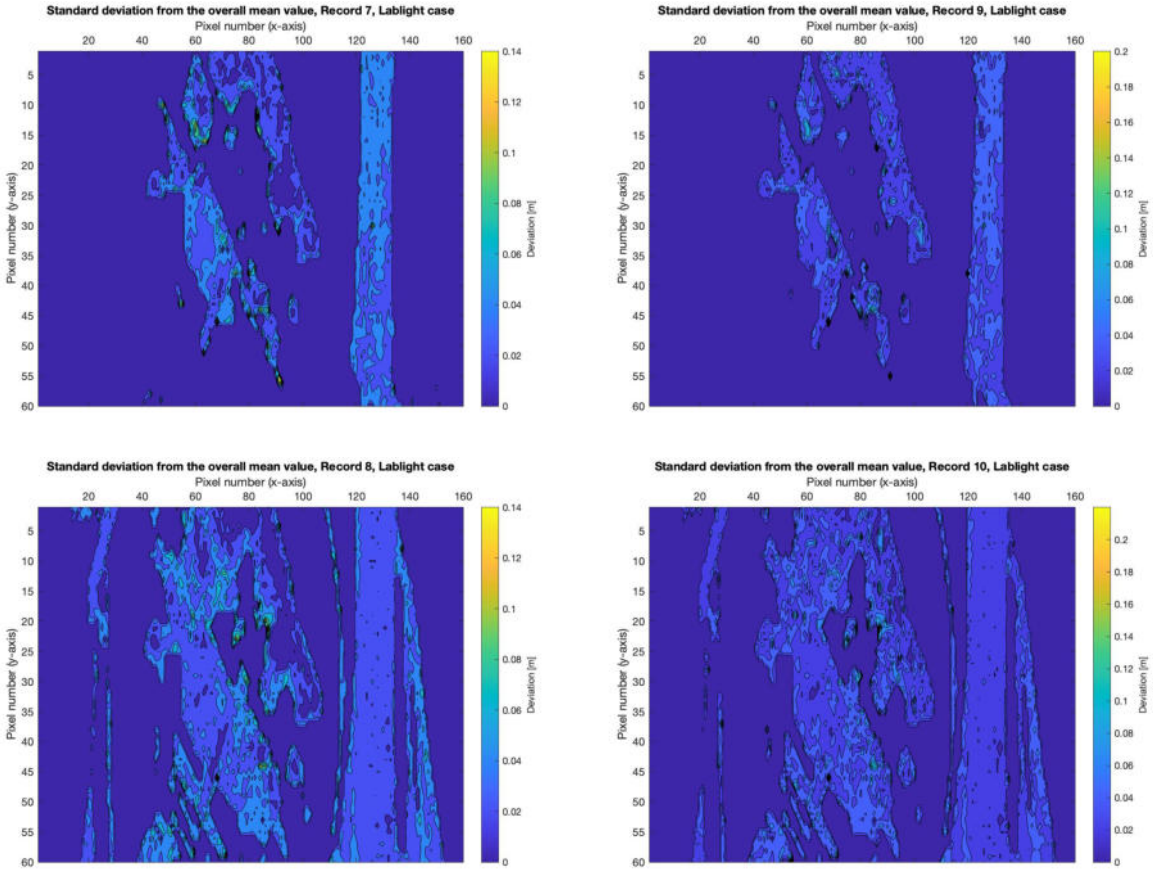

Fig. A–27: Standard Deviation for recording 7-10, Lablight case, HPS-3D160

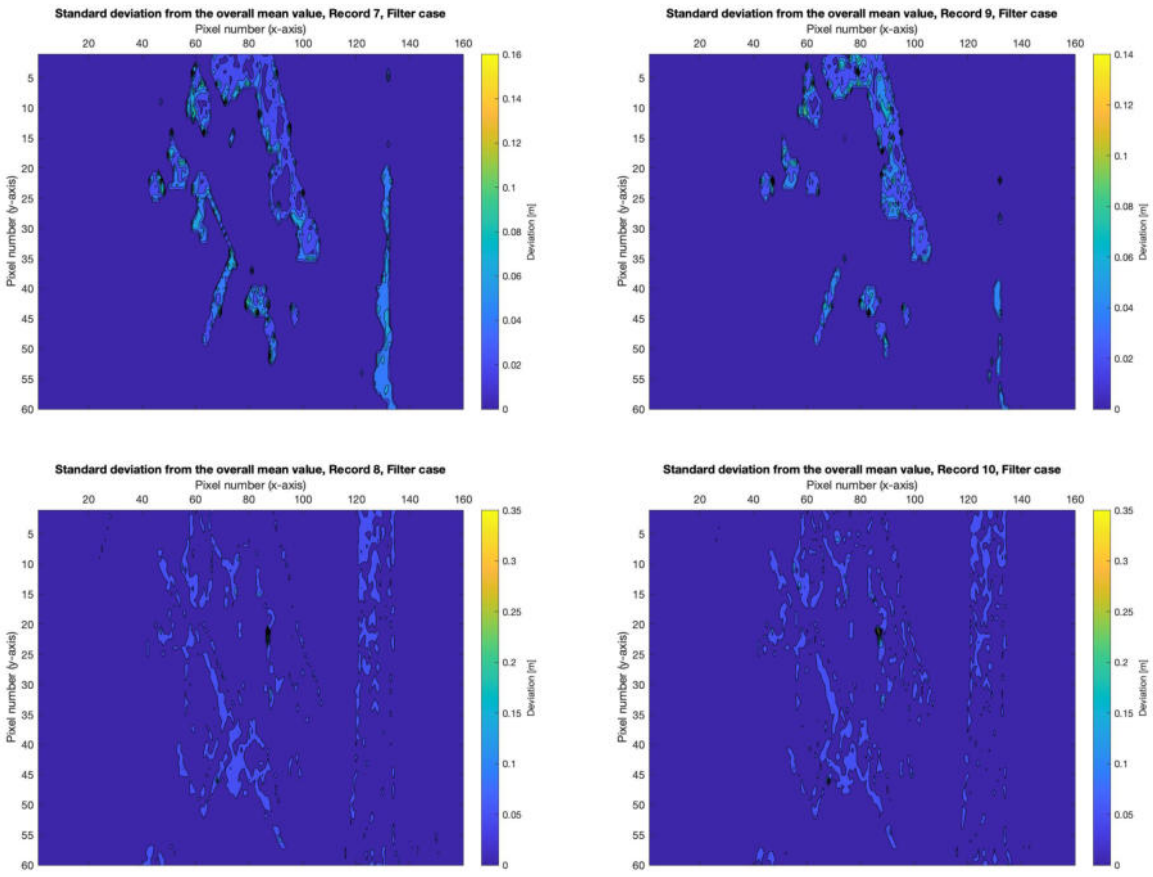

Fig. A–28: Standard Deviation for recording 7-10, Filter case, HPS-3D160

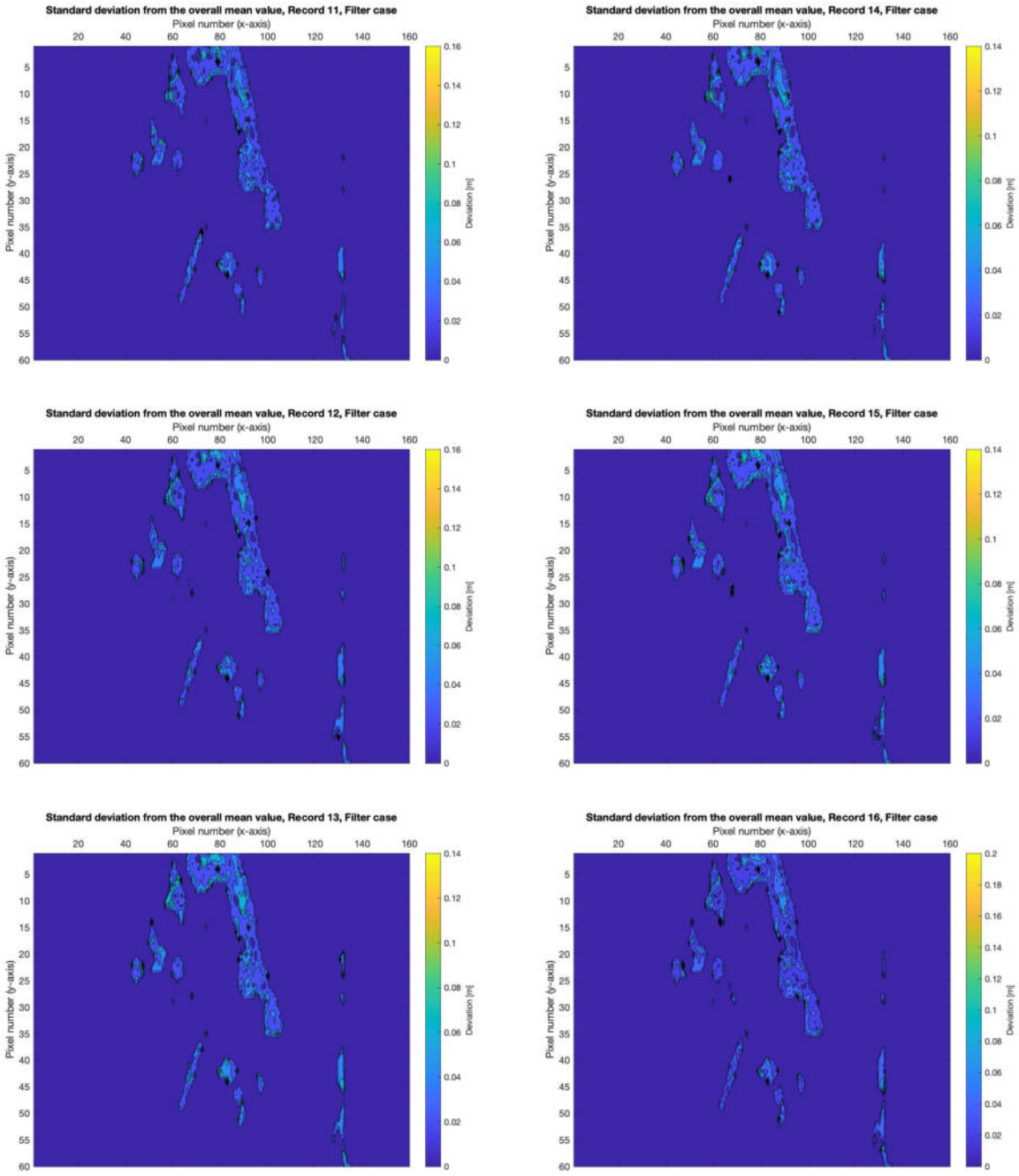

Fig. A–29: Standard Deviation for recording 11-16, Filter case, HPS-3D160

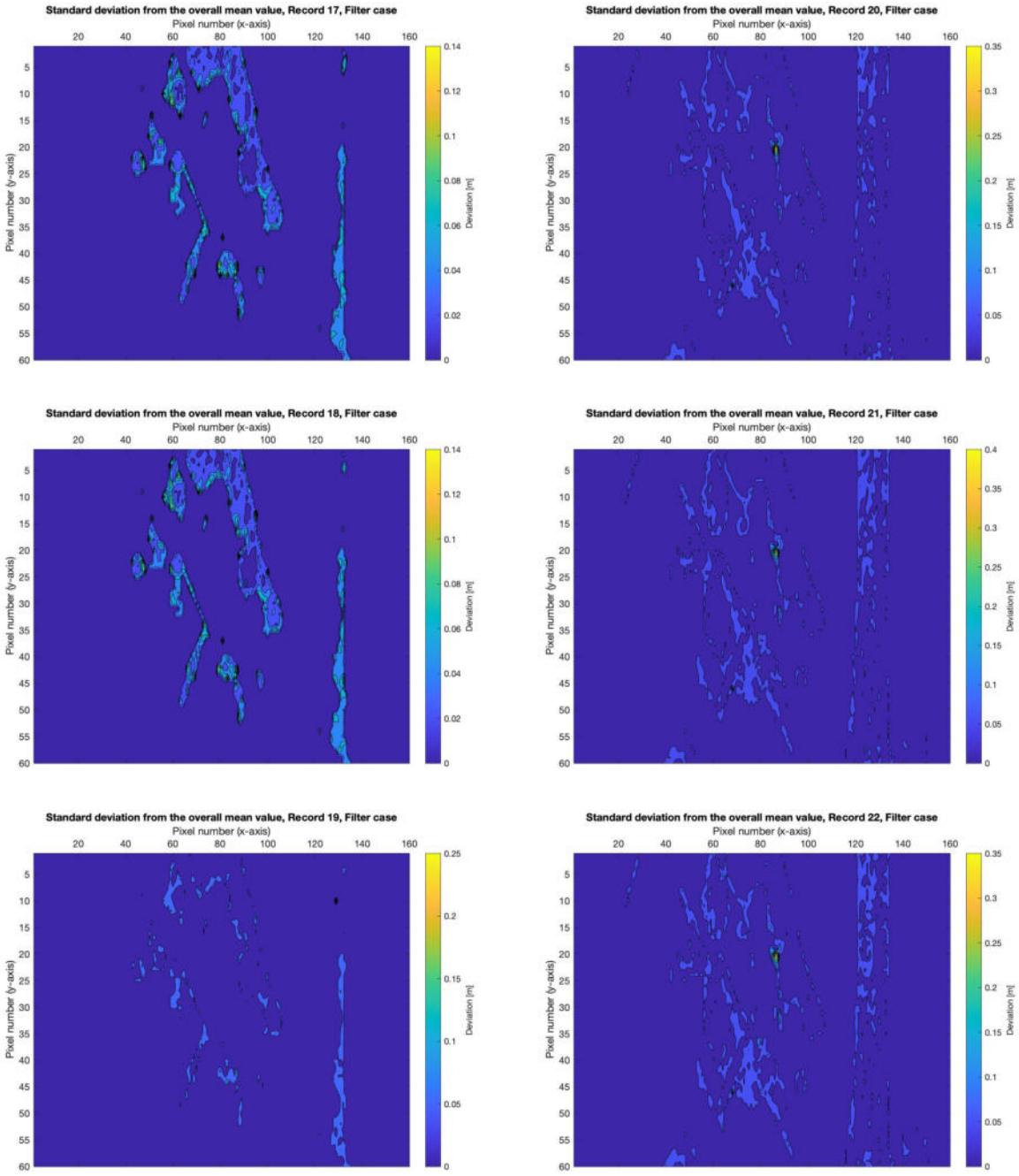

Fig. A–30: Standard Deviation for recording 17-22, Filter case, HPS-3D160

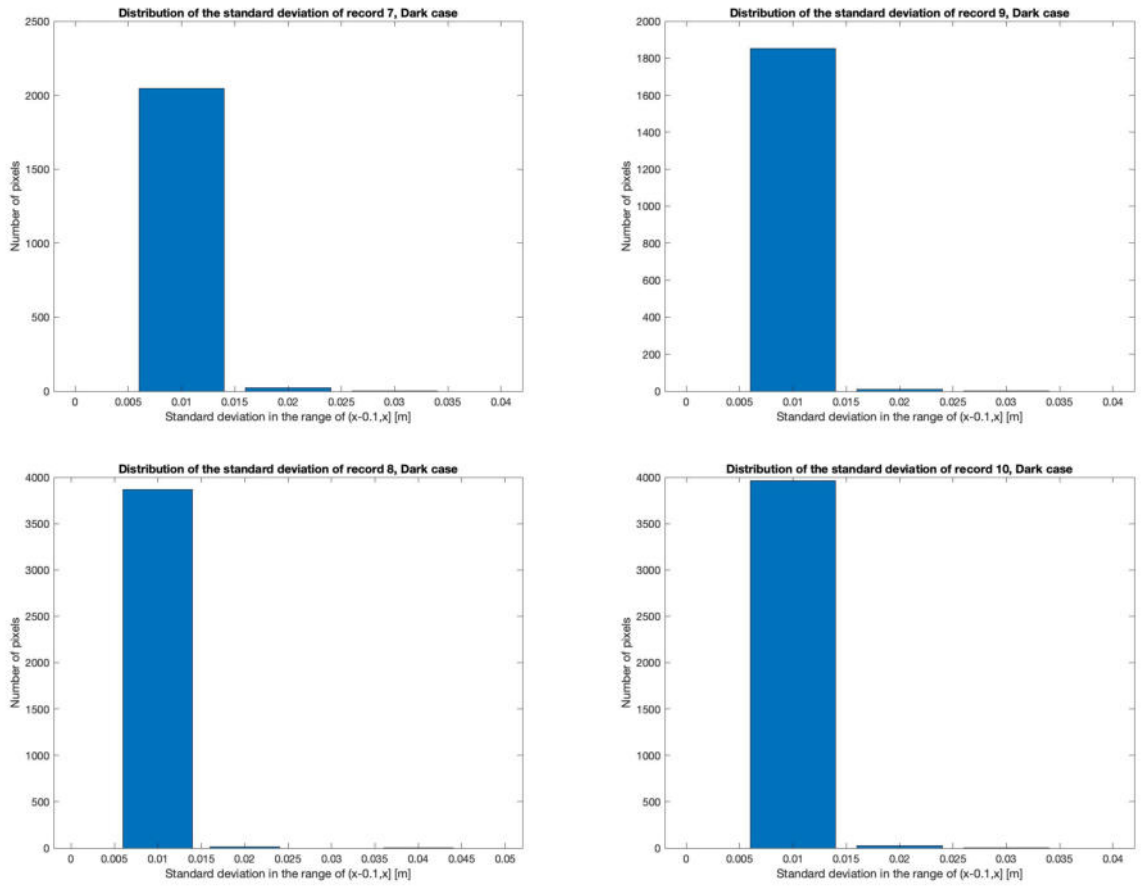

Fig. A–31: Distribution of the standard deviation for recording 7-10, Dark case, HPS-3D160

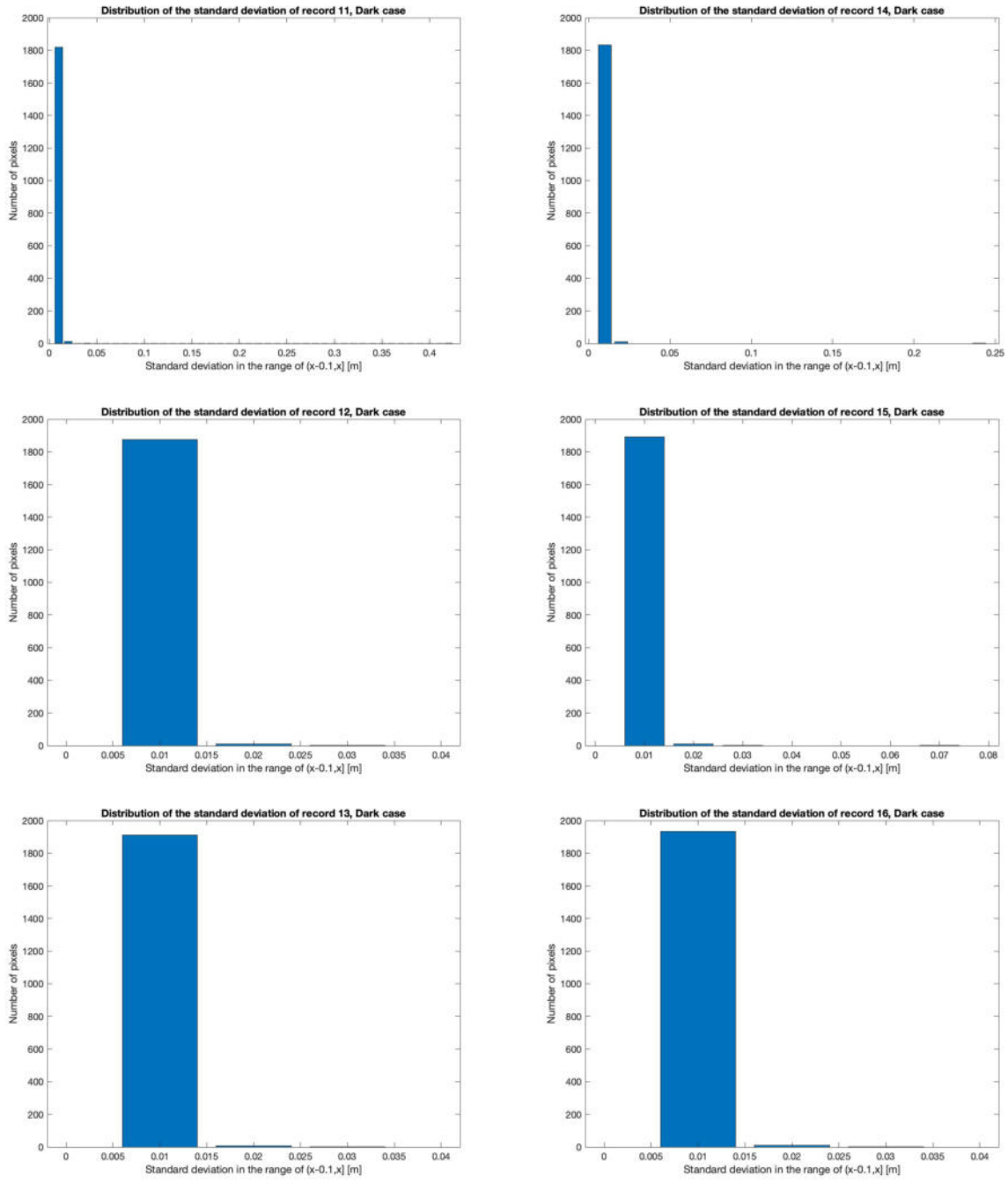

Fig. A–32: Distribution of the standard deviation for recording 11-16, Dark case, HPS-3D160

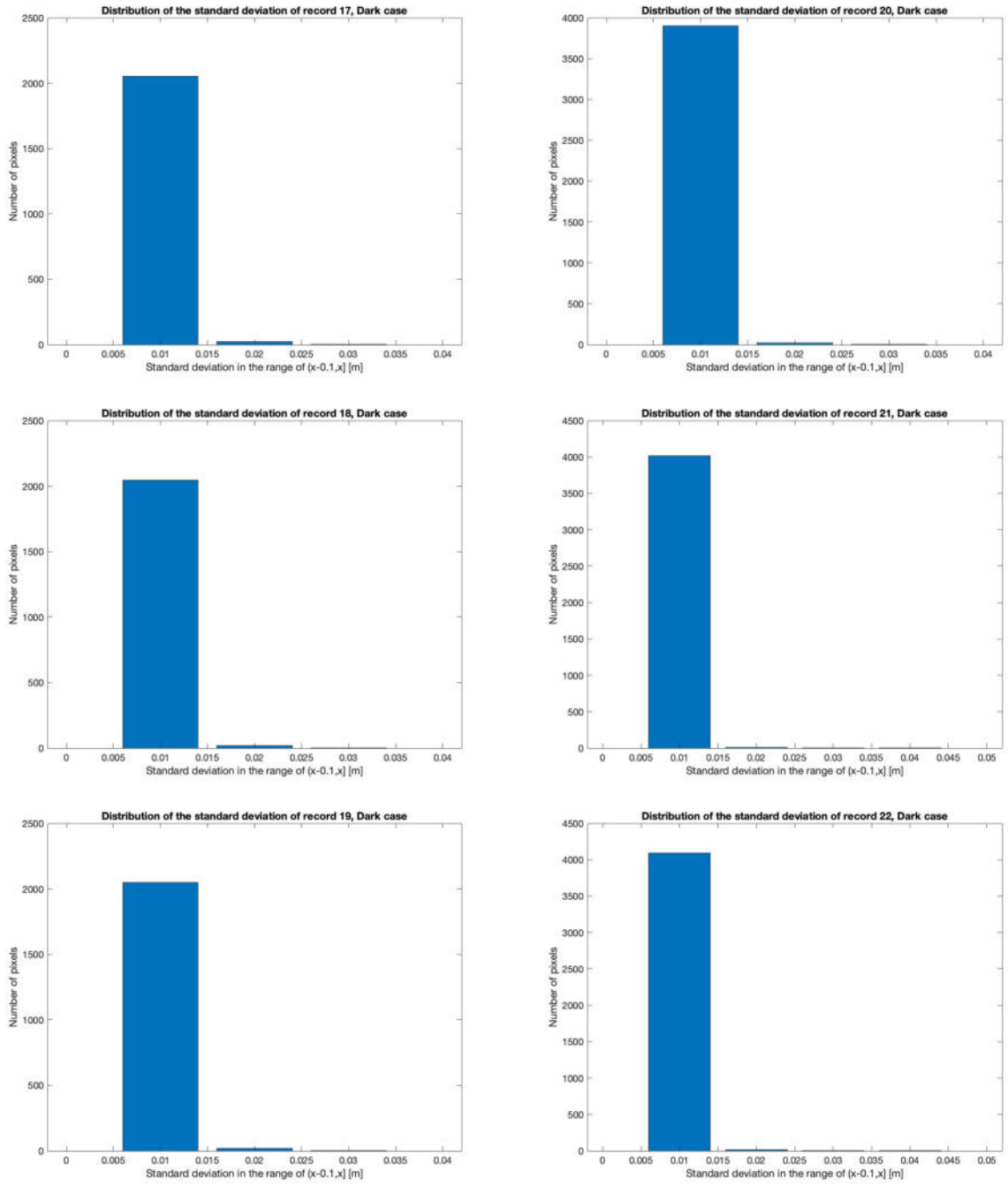

Fig. A–33: Distribution of the standard deviation for recording 17-22, Dark case, HPS-3D160

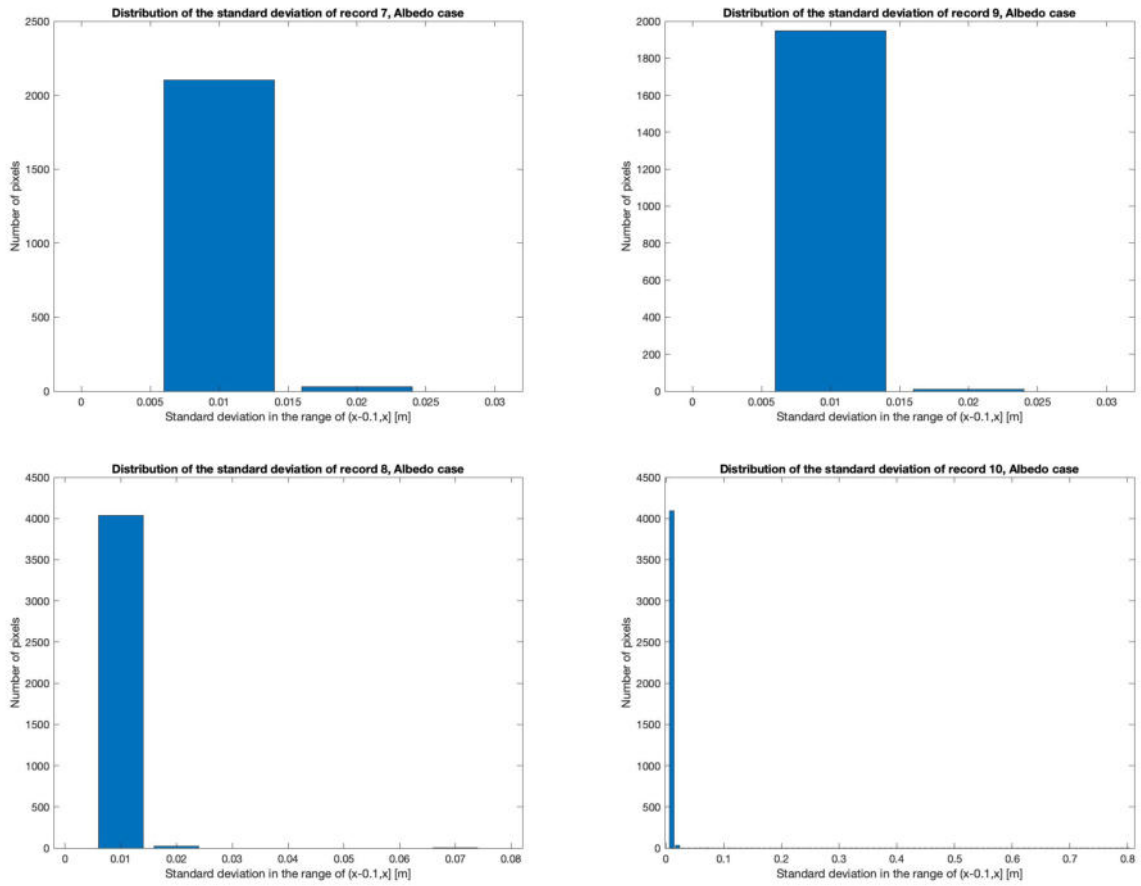

Fig. A–34: Distribution of the standard deviation for recording 7-10, Albedo case, HPS-3D160

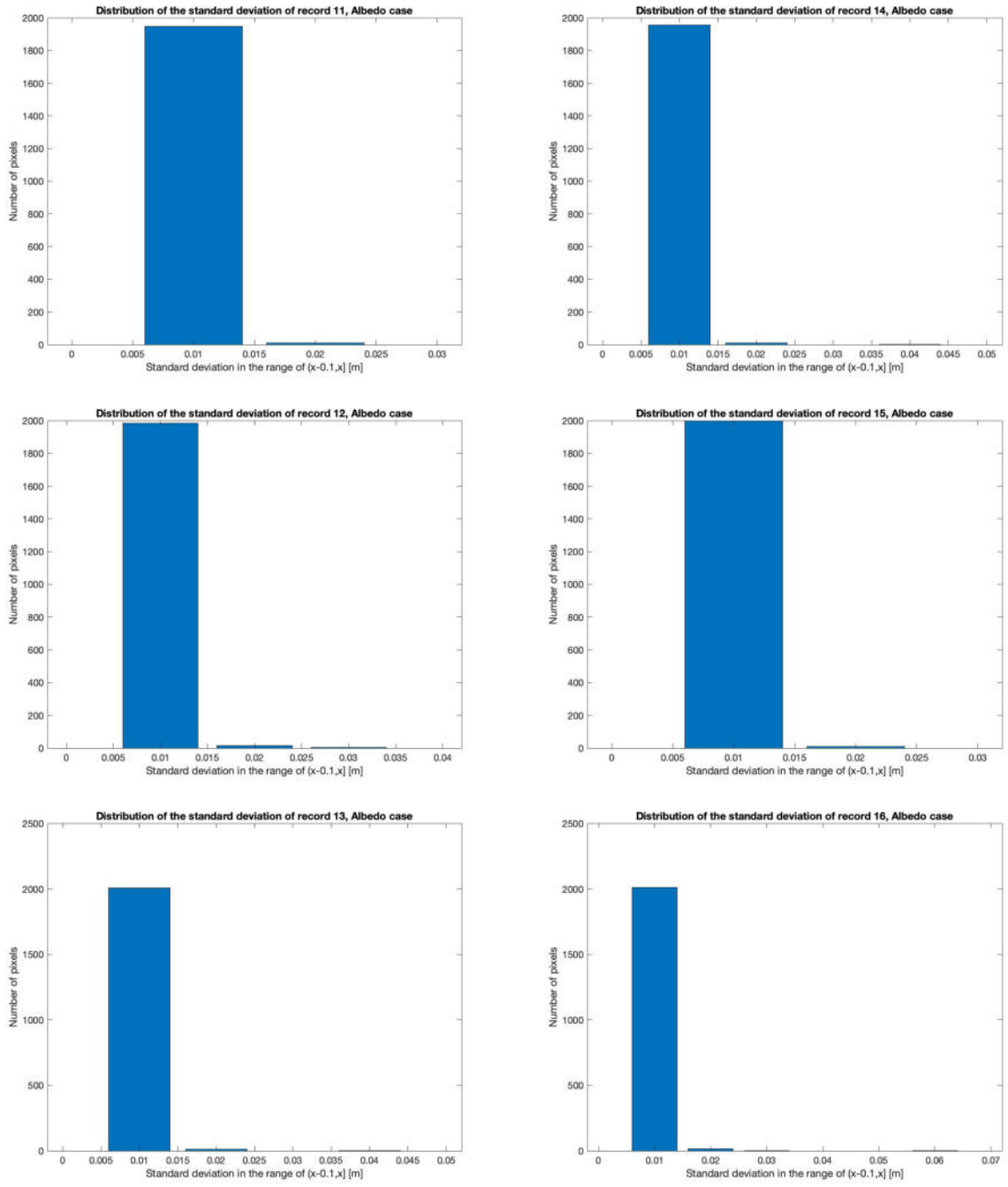

Fig. A–35: Distribution of the standard deviation for recording 11-16, Albedo case, HPS-3D160

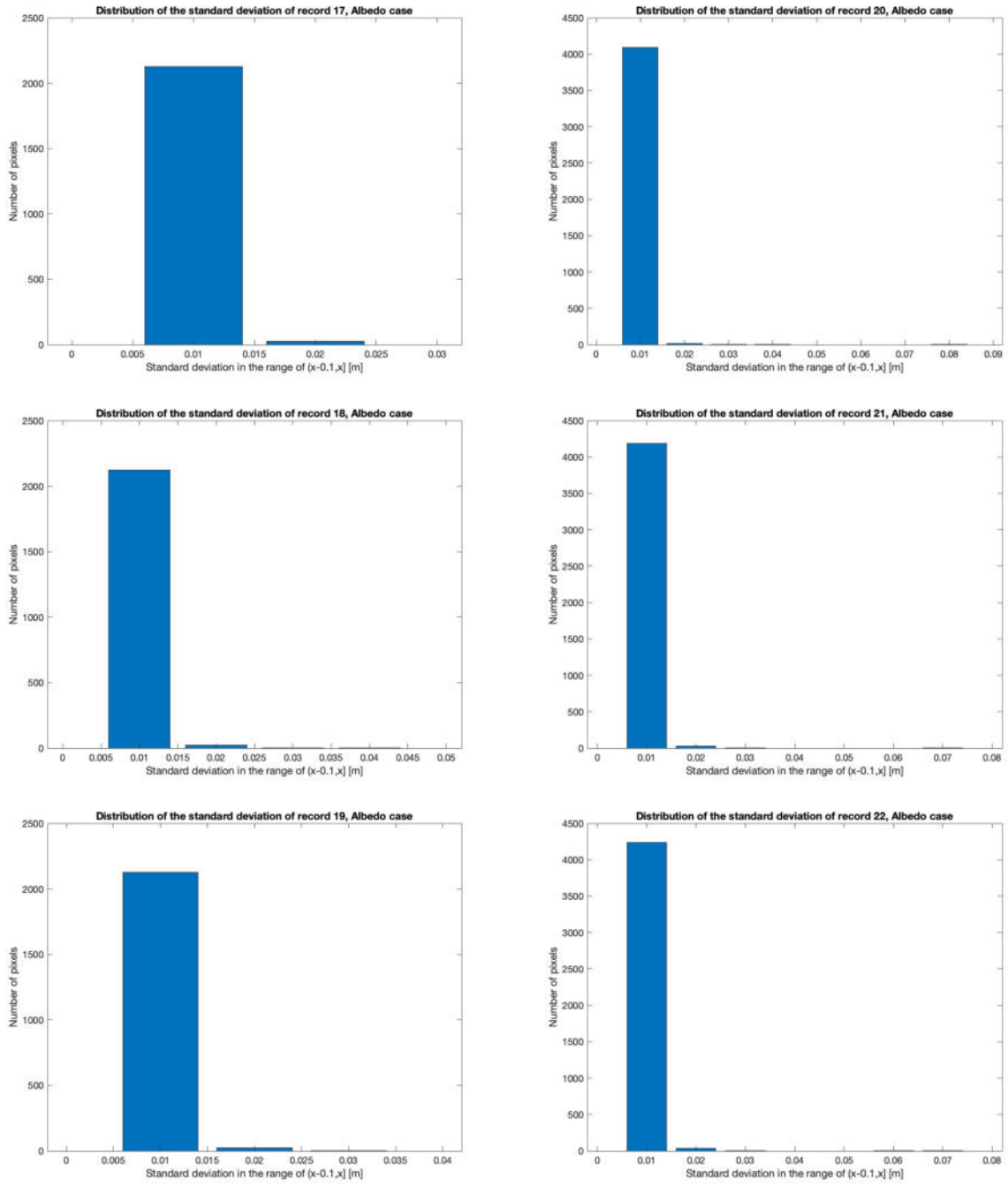

Fig. A–36: Distribution of the standard deviation for recording 17-22, Albedo case, HPS-3D160

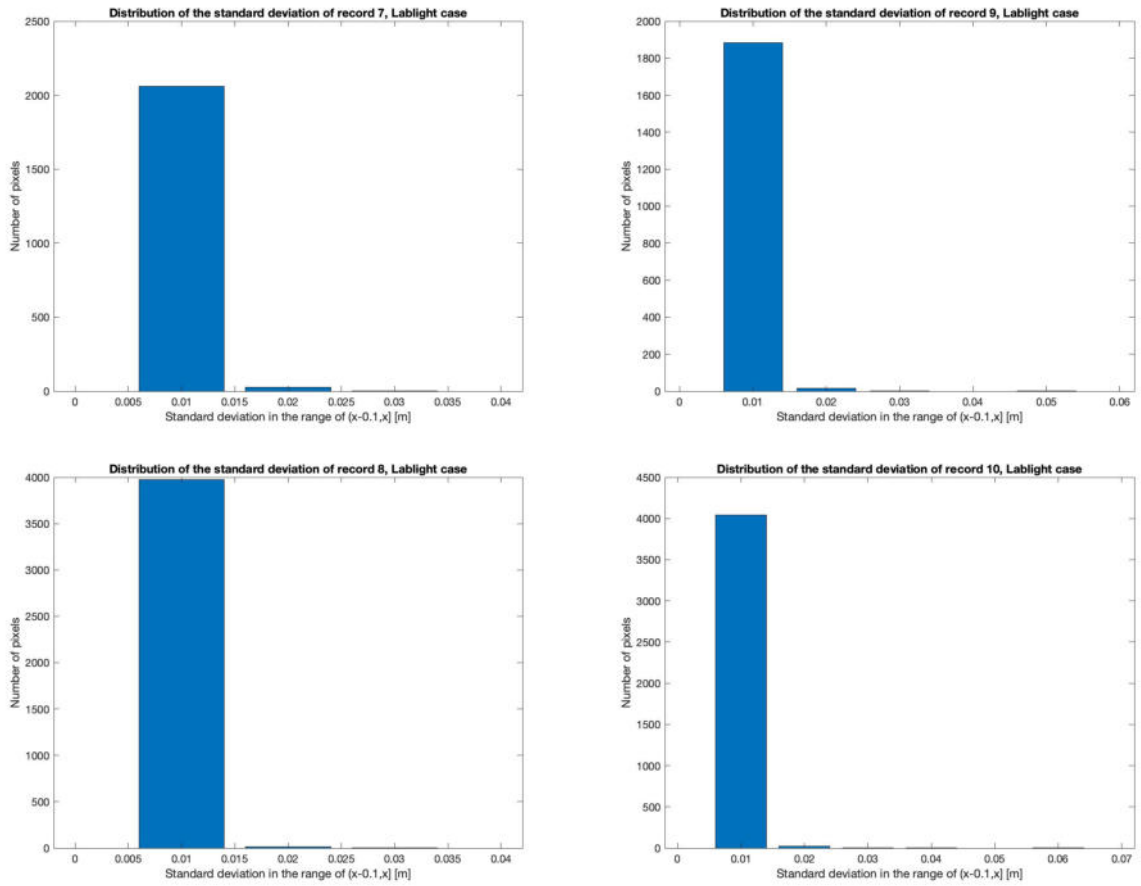

Fig. A–37: Distribution of the standard deviation for recording 7-10, Lablight case, HPS-3D160

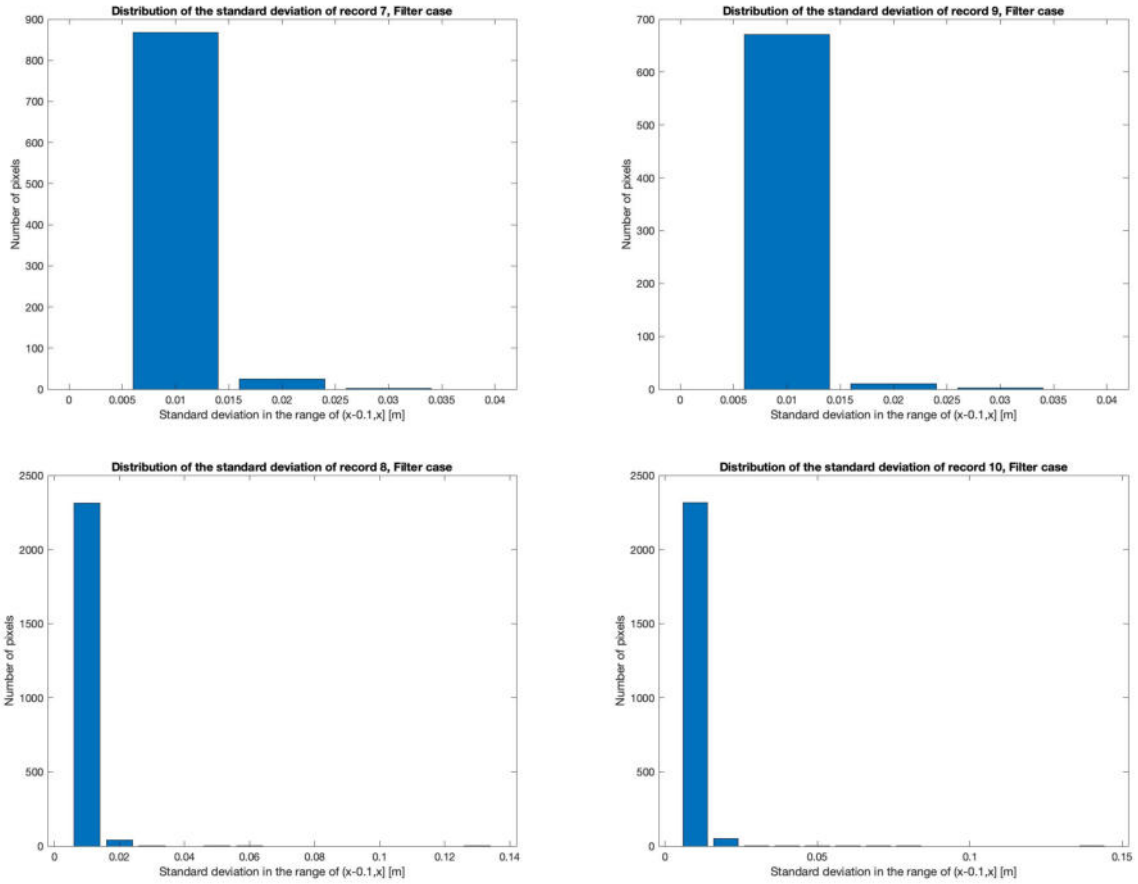

Fig. A–38: Distribution of the standard deviation for recording 7-10, Filter case, HPS-3D160

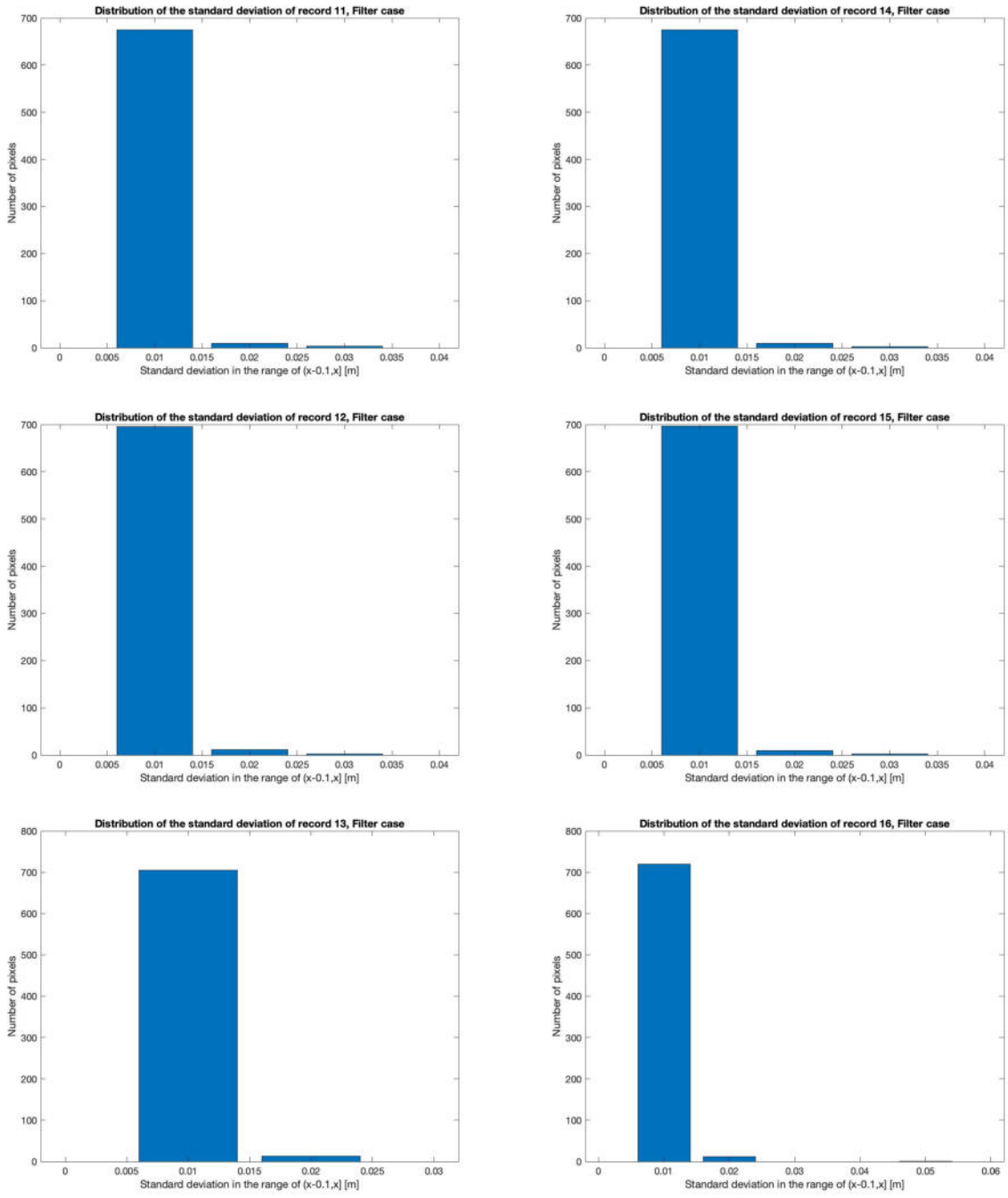

Fig. A–39: Distribution of the standard deviation for recording 11-16, Filter case, HPS-3D160

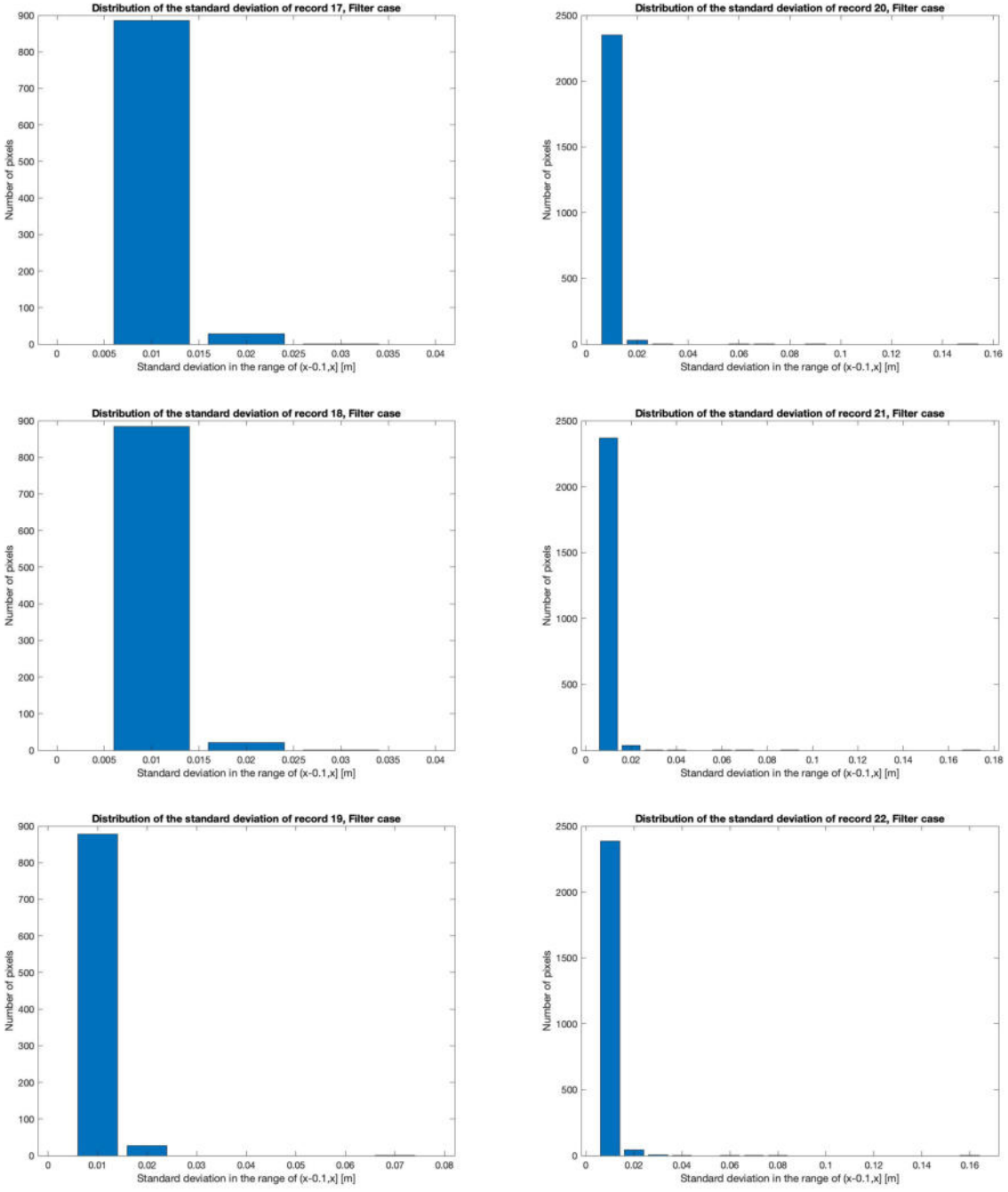

Fig. A–40: Distribution of the standard deviation for recording 17-22, Filter case, HPS-3D160